2466
- S

Theorems belonging to the thesis

Process-based modelling of aeolian bedforms

J.M.T. Stam

1. Considering the possible influence of the non-symmetrical character of the large-scale permeability tensor on transport phenomena (Zijl et al. 1993), it seems advisable to develop fluid-flow simulators that account for the off-diagonal terms of the permeability tensor.

   Zijl, W. and Stam, J.M.T., (1993). Anisotropic block-scale permeability and generalized principal directions: a correction to the direction of advective transport. Proceedings of the Ground Quality Management 93 conference, Tallinn, Estonia, September 1993. Ed. K. Kovar and J. Soveri. IAHS Publication no. 220, pp.281-289.

2. Sand roses as defined by Fryberger (1979) do not give a good indication of the sand transport within an area. It is preferable to use detailed wind roses that include the wind force.

   Fryberger, S.G., (1979). Dune forms and wind regime, in E.D. McKee , (Ed.), A study of global sand seas, Geological Survey Professional Paper 1052, Washington 1979, p. 137-169.

3. Wilson's graph relating grain size and wave-length (Wislon, 1972) is often unjustly interpreted as a universal proof that dune-spacing is controlled by grain size, for example by Lancaster (1988).

   Wilson, I.G., (1972), Aeolian Bedforms - Their development and origins, Sedimentology, v. 19, p.173-210.
   Lancaster, N., (1988). Controls of eolian dune size and spacing. Geology, v. 16, p. 972-975.

4. Before the sand transport of an area can be calculated with an empirical or semi-empirical formula, a formula has to be chosen that either was developed in an area with analogous climatic, humidity and vegetation conditions, or else the coefficients of the formula should be recalibrated.

5. Convective wind acceleration is more important with respect to the processes of dune formation than local wind acceleration.

6. The concept of stratification is used in different scientific disciplines. It is interesting, however, to observe that in sedimentology this generally refers to layers with a thickness of the order of centimetres to metres, while in the physics of magnetism (Stam et al., 1988) this refers to layers with a thickness of the order of nanometres.

   Stam, M.T.H.C.W., Gerritsma, G.J., Lodder, J.C., and Popma, Th.J.A., (1988). FMR Measurements on CoCr/NiFe Double Layers, IEEE Transactions on Magnetics, vol. 24, no.2, p.1799-1801.

7. Considering the effects of the impact of the Shoemaker-Levi 9 comet on Jupiter, it seems reasonable to assume that the impact of a comet of smaller mass on the Earth, could have caused the extinction of many species of the dinosaurs.

8. The period of time known in climatology as the "little ice age" has its repercussions in contemporary Dutch and Flemish painting. This can be seen by the number of winter landscapes where popular ice-activities form the main subject.

9. The zarzuela evolved in Spain as a genre of operetta whose thematic and musical inspiration is almost exclusively to be found in the national culture. A clear indication of this is the reworking of fragments of older zarzuelas that reappear as popular songs in modern zarzuelas.

10. Theresa of Avila is best known for her mystical experiences and visions. It was however, through use of her realism and organizing talent, evident in her many letters, that she was able to successfully reform the order of Carmel.

11. There is an apparent contradiction between the politico-economic goal of a unified Europe and local nationalistic aspirations. This, however, fits the concept of a Europe in dynamic equilibrium the existance of which is due to its own plurality (Ortega y Gasset, 1937).

    Ortega y Gasset, J. (1937). La rebelion de las masas, in Revista de Occidente en Alianza Editorial, 1990, Ed. Paulino Gerragorri.

12. Although the development of electric sabre fencing considerably simplifies the task of judging, it has also resulted in a loss of playfulness and a reduction in the variety of applied techniques.

13. Besides familiarity with European history and culture, it is advisable to have a good knowledge of French language and literature to be able to fully appreciate the adventures of Asterix.

Stellingen behorende bij het proefschrift

Process-based modelling of aeolian bedforms

J.M.T. Stam

1. Gezien de mogelijke invloed die het niet-symmetrische karakter van de grootschalige permeabiliteitstensor heeft op transportverschijnselen (Zijl et al., 1993), verdient het aanbeveling om vloeistofstromingssimulatoren te ontwikkelen die rekening houden met de niet-diagonale termen van de permeabiliteitstensor.

   Zijl, W. and Stam, J.M.T., (1993). Anisotropic block-scale permeability and generalized principal directions: a correction to the direction of advective transport. Proceedings of the Ground Quality Management 93 conference, Tallinn, Estonia, Sept. 1993. Ed. K. Kovar and J. Soveri. IAHS Publication no. 220, p.281-289.

2. Zandrozen zoals gedefinieerd door Fryberger (1979) geven geen juiste weergave van het zandtransport binnen een gebied. Het is beter hiervoor gedetailleerde windrozen te gebruiken waarin ook de windkracht wordt aangegeven.

   Fryberger, S.G., (1979). Dune forms and wind regime, in E.D. McKee , (Ed.), A study of global sand seas, Geological Survey Professional Paper 1052, Washington 1979, p. 137-169.

3. Wilson's (1972) grafiek waarin een relatie wordt gelegd tussen korreldiameter en golflengte wordt vaak ten onrechte geinterpreteerd als een universeel bewijs dat spatiëring van duinen afhankelijk is van de korreldiameter, zoals bij voorbeeld door Lancaster (1988).

   Wilson, I.G., (1972), Aeolian Bedforms - Their development and origins, Sedimentology, v. 19, p.173-210.
   Lancaster, N., (1988). Controls of eolian dune size and spacing. Geology, v. 16, p. 972-975.

4. Voordat het zandtransport van een gebied met behulp van een empirische of semi-empirische transportformule berekend kan worden dient men: ofwel een formule te nemen die in een analoog gebied qua klimaatsomstandigheden, vochtigheid en vegetatie is ontwikkeld; ofwel de coëfficiënten van de transportformule opnieuw te kalibreren.

5. De convectieve windversnelling is belangrijker ten aanzien van duinvormingsprocessen dan de lokale windversnelling.

6. Het begrip stratificatie wordt in verschillende wetenschappen gebruikt. Het is echter opmerkelijk dat in de sedimentologie dit begrip in het algemeen betrekking heeft op lagen met een dikte van centimeters tot meters terwijl het in de magnetische fysica (Stam et al., 1988) om een orde van nanometers gaat.

   Stam, M.T.H.C.W., Gerritsma, G.J., Lodder, J.C., and Popma, Th.J.A., (1988). FMR Measurements on CoCr/NiFe Double Layers, IEEE Transactions on Magnetics, vol. 24, no.2, p.1799-1801.

7. Gezien de gevolgen van de inslag van de komeet Shoemaker-Levi 9 op Jupiter, is het goed denkbaar dat de inslag van een komeet van beduidend mindere massa op Aarde het uitsterven van vele soorten dinosauriërs heeft veroorzaakt.

8. Het tijdperk dat in de klimatologie bekend staat als "de kleine ijstijd" vindt zijn weergave in de contemporaine nederlandse en vlaamse schilderkunst. Dit is te zien aan de hoeveelheid winterlandschappen waarin ijspret het hoofdonderwerp is.

9. De zarzuela ontwikkelde zich in Spanje als een genre van operette dat zijn thematische en muzikale inspiratie bijna uitsluitend in de nationale cultuur vindt. Een aanwijzing hiervoor zijn de fragmenten van oudere zarzuelas die in de moderne zarzuelas als gangbare liedjes terugkomen.

10. Theresia van Avila staat vooral bekend om haar mystieke belevenissen en visioenen. Het is echter dankzij haar nuchterheid en organisatorisch talent, die vooral blijken uit haar talrijke brieven, dat zij een hervorming van de orde van de Carmel met succes kon doorvoeren.

11. Er is een schijnbaar contrast tussen het politiek economisch streven naar een verenigd Europa en de lokale nationalistische ontwikkelingen. Dit past echter volkomen in het begrip van Europa als een dynamisch evenwicht dat bestaat dankzij zijn pluraliteit (Ortega y Gasset, 1937).

    Ortega y Gasset, J. (1937). La rebelion de las masas, in Revista de Occidente en Alianza Editorial, 1990, Ed. Paulino Gerragorri.

12. Ofschoon de ontwikkeling van het elektrische sabelschermen het jureren aanzienlijk vergemakkelijkt, verliest het sabelschermen zelf hiermee aan speelsheid en variatie van toegepaste technieken.

13. Behalve vertrouwdheid met de Europese geschiedenis en cultuur, verdient het aanbeveling om een gedegen kennis van de Franse taal en literatuur te hebben om de avonturen van Asterix volledig te kunnen appreciëren.

TR diss
2466

PROCESS-BASED MODELLING OF AEOLIAN BEDFORMS

PROCESS-BASED MODELLING OF AEOLIAN BEDFORMS

PROEFSCHRIFT

ter verkrijging van de graad van doctor
aan de Technische Universiteit Delft,
op gezag van de Rector Magnificus
Prof. ir K.F. Wakker,
in het openbaar te verdedigen ten overstaan van een commissie,
door het College van Dekanen aangewezen,
op donderdag 17 november 1994 te 16:00 uur

door

Johanna Maria Theresia STAM

civiel ingenieur
geboren te Madrid, Spanje

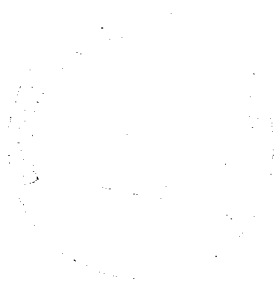

Dit proefschrift is goedgekeurd door de promotors
Prof. dr ir J.C. van Dam en Prof. drs F.R. van Veen

Samenstelling promotiecommissie:

Prof. dr R. Gaupp (Johannes Gutenberg Universität, Mainz)
Prof. dr J.W. Harbaugh (Stanford University, California)
Prof. dr J.H.J. Terwindt (Rijksuniversiteit Utrecht)
Prof. dr A.K. Turner (Colorado School of Mines, Colorado)
Prof. dr ir W. Zijl (TNO-GG en Vrije Universiteit Brussel)

Copyright © 1994, by J.M.T. Stam, Delft, The Netherlands.
All rights reserved. No part of this publication may be reproduced, stored in a retrieval system or transmitted in any form or by any means, electronic, mechanical, photocopying, recording or otherwise, without the prior agreement and written permission of the copy right owner.

CIP-DATA KONINKLIJKE BIBLIOTHEEK, DEN HAAG

Stam, Johanna Maria Theresia

Process-based modelling of aeolian bedforms /
Johanna Maria Theresia Stam. - [S.l. : s.n.]. - Ill.
Thesis Technische Universiteit Delft. - With ref. -
With summary in Dutch and Spanish.
ISBN 90-9007595-X
NUGI 816
Subject headings: aeolian dunes; geomorphology.

Cover: view of Kelso dunes, Mojave Desert, California, U.S.A. (photograph by the author)
Printed in The Netherlands by: Drukkerij Technische Universiteit Delft

To my parents

Acknowledgements

A thesis is the result of several years of effort, patience, dedication and, not least, of the help of a number of people to whom I wish to express my gratitude.

In the first place I thank my promotors: Prof. Dr ir J.C. van Dam for his support throughout my time at university; from the Italian study-tour through to assistantship, graduation and doctoral thesis, and Prof. drs F.R. van Veen, who, from the beginning, encouraged this adventure of allowing civil engineering to enter the geological world.

Thanks are due to Prof. Dr ir W. Zijl who, from the first experiences at TNO as my daily adviser, stimulated the development of interdisciplinary research and was always ready to help solve the mathematical and physical problems that appeared.

I am indebted to Prof. Dr J.W. Harbaugh who invited me to join the Geomathematics Group at Stanford University. A study period with a group such as this was an invaluable opportunity for learning how to do research. The members of this group are warmly thanked for their advice and assistance, especially Dr J. Wendebourg and Dr C.A. Ramshorn.

Prof. Dr A.K. Turner of the Colorado School of Mines is thanked for introducing me to the challenging problem of subsurface modelling. He provided the first contacts with Stanford University and arranged for my first encounter with modern and ancient aeolian deposits in the United States.

Constructive criticism, towards the end of the project, came from Dr K.W. Glennie and Dr R.A. Hunter in reviews of my drafts and articles. I am grateful for their experience and open minded approach, which proved invaluable to this novice researcher.

I would like to thank my colleagues at TNO for their companionship and help with bugs, computers and geological puzzles. For my fellow PhD students at the Faculty of Mining and Petroleum Engineering and TNO, my warmest appreciation of their friendship and interest. My thanks also go to the technical staff at TNO; the computer support group and the graphical design group for their help and assistance.

Special mention should also be made of the organisations that contributed financially to this study. In the first place, TNO-Institute of Applied Geoscience who sponsored the research and allowed me to use their facilities. For their financial support of the study periods at Stanford University I would like to acknowledge Koninklijke/Shell Exploratie en Productie Laboratorium, Stichting Moolengraaff Fonds, Nederlandse Organisatie voor Wetenschappelijk Onderzoek and the Universiteitsfonds Delft.

My deepest gratitude, however, is to my parents. They were my first inspiration, who best understood the stoss and lee sides of the research and who most enthusiastically supported and encouraged me through all my studies.

Jean-Marie Stam
Delft, November 1994

Contents

page

1. Introduction **1**
1.1 Modelling the subsurface 1
1.2 Applications of process-based models 2
1.3 Scales of processes 4
1.4 Scope of this thesis 6

2. The aeolian environment **9**
2.1 Introduction 9
2.2 General setting and characteristics of desert environments 9
2.3 Deposits in ancient aeolian environments 13
2.4 The recent aeolian environment 14
2.4.1 Bedform types and patterns 14
2.4.2 Dune growth and development 19
2.4.3 Wind regime and dune shape 20
2.4.4 Wind velocity over bedforms 24
2.4.5 Stratification types in aeolian deposits 25
2.5 Preservation of bedforms 27
2.6 Previously published mathematical models at bedform scale 29
2.7 Discussion 32
2.7.1 Concerning the results of field work 32
2.7.2 Concerning the modelling of the physical processes 32
2.7.3 Concerning models for ancient aeolian deposits 33

3. Basic equations and assumptions **35**
3.1 Introduction 35
3.2 Continuity equation 35
3.3 Flow characteristics 37
3.3.1 Laminar and turbulent flow 37
3.3.2 Ideal and real fluids and the boundary-layer approach 39
3.3.3 The logarithmic velocity profile 39
3.3.4 Qualitative analysis of airflow over a dune 40
3.4 Sediment transport 42
3.4.1 Sediment-transport mechanisms 42
3.4.2 Bagnold's sediment-transport formula 43
3.4.3 Other sediment-transport formulae 47
3.4.4 Discussion of sediment-transport formulae 47

4. Bedform migration **52**
4.1 Introduction 52
4.2 Simple wave approximation 53
4.3 Kinematic wave approximation 55
4.4 On the linearizations 57
4.4.1 The linear sediment-transport model 57
4.4.2 The linear shear-stress model 58
4.5 Numerical implementation 60
4.5.1 Choice of numerical method 60
4.5.2 Choice of boundary conditions 62
4.5.3 Testing the numerical method 63

5. Bedform migration and growth **65**
5.1 Introduction 65
5.2 Background of the flow model 65
5.3 Development of an analytical solution 67
5.4 Interpretation of the analytical model: an example 73
5.4.1 Analysis of the results 75
5.5 Effects of wind velocity, roughness length and wave number 77
5.5.1 Effect of the wind velocity on growth factor and migration rate 78
5.5.2 Effect of the roughness length on growth factor and migration rate 78
5.5.3 Influence of the wave number on growth factor and migration rate 79
5.5.4 An example of migration rates of dunes from Salton Sea (California) 80

6. Applying the theory to a computer model of non-sinusoidal bedforms **84**
6.1 Introduction 84
6.2 Problems with application to non-sinusoidal bedforms 84
6.2.1 Growth of artificial wave numbers 85
6.2.2 Numerical interaction of different wave numbers 86
6.2.3 Non-linearity 89
6.3 Application to non-sinusoidal bedforms; bedform stability 90
6.4 Avalanching 92
6.4.1 Avalanching routine 92
6.4.2 Application to a sine bedform 95
6.4.3 Application to a dune 98
6.4.4 Evaluation 99

7. Conclusions, discussion and recommendations **102**
7.1 Conclusions and discussion 102
7.1.1 On the modelling of bedform dynamics 102
7.1.2 On the sediment-transport equation 102
7.1.3 On the flow model 103
7.1.4 On the modelling results for bedform dynamics 103
7.1.5 On the equilibrium of bedforms 105
7.2 Applications and recommendations for further research 105

List of symbols **108**

Glossary of geological terms **112**

Appendix I **116**
Fourier series, Transforms and discreet Fourier Transforms

Appendix II **122**
Calculation of the flow field according to Jackson and Hunt

Appendix III **129**
EOLSIM, a two-dimensional programme for simulating the dynamics of aeolian dunes

Appendix IV **136**
Modelling permeability in imperfectly layered porous media II: a two-dimensional application of block-scale permeability

References **156**

Summary, Samenvatting, Resumen **164**

Curriculum Vitae **170**

Chapter 1

Introduction

1.1 Modelling the subsurface

One of the main problems regarding the exploitation and management of the earth's natural resources (groundwater, hydrocarbons and, to a minor degree, also coal, minerals etc.) is to know the distribution and properties of reservoirs, aquifers and rocks of economic value in the subsurface. The volumes of groundwater or hydrocarbons that can be abstracted, the transport of pollutants in groundwater, the extent of salt water intrusion in fresh groundwater, are all influenced by the variability of the properties of the ground. The use of fluid-flow simulators to study these problems requires quantitative information of the subsurface properties at each point. Such information can be obtained from four main sources: i) large-scale information obtained from measurements such as seismics; ii) local-scale information from pumping-tests (in hydrology) or production data (in petroleum engineering); iii) detailed information on selected points from samples, well-logs or cores; iv) information obtained by geologists from outcrops that have similar characteristics as the reservoir or aquifer under consideration (these are called geological analogues).

This information is integrated in a model of the subsurface, where the properties are defined at every point. Different disciplines work with different types of model. A general classification has been given in Fig. 1.1.1, although some denominations can have different meanings in different disciplines. A conceptual model (as used in a geological context) is a scheme of reality. Physical models are usually scale reproductions. Finally, mathematical models (used in an engineering context) schematize reality in formulae. The general advancement of computer methods and numerical techniques has led to the development of mathematical computer models to simulate the architecture of the subsurface. In this context, computer programmes that perform a simulation are called simulators.

By the nature of their approach, mathematical models for the subsurface can broadly be classified into stochastic and deterministic models. Stochastic models give a whole range of possible solutions for a set of input data, reconstructing spatial variability with the help of

frequency distributions. Stochastic models are subdivided into object-based models and sequence-based models (Dubrule, 1989). The former generate random geometries in space (e.g. Boolean models) while the latter generate the distribution of a property such as lithology or permeability (e.g. geostatistical techniques).

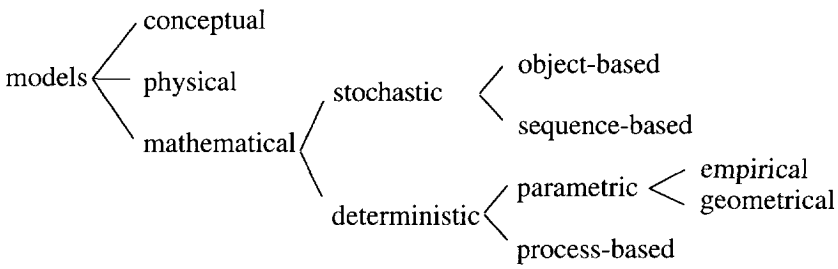

Fig. 1.1.1 Classification of models by their approach.

Deterministic models give one unique solution for a specific input, but can also be used in a stochastic framework by running the model with different sets of statistically generated input data. The stochastic character of the simulation is then given by the nature of the input data and not by the computer model itself. Though computer programmes increase the feasibility of this approach, this still depends on how much time is required for a run of the computer model. Deterministic models are parametric [1] when they are based on empirical or geometrical relationships, and process-based when they are based on the physical laws that govern the processes themselves. It should be noted that physical laws may have constants that can be calibrated experimentally, (e.g. Bagnold's sediment-transport formula, treated in section 3.4.2) but they still describe essentially a physical process. The object of this thesis is the development of a process-based model.Therefore the rest of this introduction will concern this type of model.

1.2 Applications of process-based models

Process-based models are mathematical models that simulate the physical processes. Such models have recently been developed in hydrology (Abbot et al., 1986a and b and Bathurst, 1986 a and b), as well as in geology (Tetzlaff and Harbaugh, 1989), but their application in geosciences is still in a pioneering stage. Their objectives can be summarized as follows:

[1] In an engineering context parametric models are generally referred to as conceptual models

i) As a predictive instrument to judge the effect of geological processes for engineering or environmental purposes. In this way it is generally applied in engineering practice for short-term effects of up to a maximum of about fifty years (e.g. river canalization), but it can also be applied for long-term predictions (e.g. desertification, safety of nuclear waste deposits).
ii) To test our assumptions about the real-world system. As process-based models give a continuous quantitative description of the subsurface, they can also be used to test the implication and sensitivity of modelling assumptions, for example the upscaling of permeabilities (Stam and Zijl, 1992).
iii) As a complement to models used in petroleum exploration. In future they could complement stochastic models by helping to determine realistic ranges for input parameters (e.g. characteristic lengths, widths and thicknesses of sand bodies, clay layers etc.) which at present are based on outcrop analogues. Process-based models could also serve on a more detailed scale than is possible with the actual resolution of seismic surveys. A difficulty in this use of process-based models is that they require a large number of input parameters of a climatic and hydrologic nature that is generally not obtainable from subsurface data. A contribution in this sense has been made by Koltermann and Gorelick (1992).

The general framework of this thesis is to develop and apply process-based simulators of sedimentation as an aid in modelling subsurface architecture and the resulting subsurface properties in terms of porosity and permeability (i.e. objectives ii and iii listed above). Simulating the succession and distribution of different genetic units is only the first step towards this ultimate goal. Further steps that need to be considered are:

i) Simulating diagenetic processes[2] (i.e. compaction, cementation and fracturing)
ii) Determination of the subsurface properties in terms of porosities, permeabilities and storage coefficients
ii) Quantification of the properties on the scale of grid-blocks as are used in fluid-flow simulators.

A first approach towards treating these aspects in a complete study was carried out by Stam et al. (1989) and a more detailed overview of the problems has been given in Stam et al. (1993)

The research has been focused on the aeolian environment. Aeolian sandstones are good hydrocarbon reservoirs because of their high primary porosity (e.g. the gas-rich North Sea Basin deposits of the Permian), and therefore are of interest to petroleum engineering. From

[2] Typical geological terms have been included in a glossary

a hydrological point of view, deposits of both coastal and desert dunes play an important role as fresh water reservoirs and in the natural purification of drinking-water (Stuyfzand, 1984). Dune morphology is of interest to other disciplines also; for example they form an ecologically important biotope, coastal dunes constitute an important protective barrier against the sea while desert dunes play a role in desertification and sand control in arid regions.

1.3 Scales of processes

The development of process-based models in geosciences would ideally comprehend all the processes that occur from the deposition of sediment by water or wind to burial, compaction, cementation, fracturing etc. so that values of subsurface properties (i.e. porosity, permeability and storage coefficient) can ultimately be obtained. This is difficult because of the large number of processes that occur and interact at different physical scales. In this context it is useful to distinguish four scales (see Fig. 1.3.1). This classification is based on a hierarchical sequence of heterogeneities developed by Weber (1986), which has been illustrated with examples from the aeolian environment.

i) The grain scale: the distribution of different grain sizes results in a determinate sorting and packing, which in turn affects anisotropy. Grains and pores determine the capillary forces in multi-phase flow, while cross-bedding results in anisotropy. Grain-scale distribution is essentially the result of autocyclic processes, for instance sediment which is transported by wind through saltation (autocyclic processes are those where the sedimentation of the depositing fluid itself is considered, without taking into account the effects of external factors that cause the flow).

ii) The genetic unit scale: a genetic unit (e.g. a dune) is deposited by a specific process. Genetic units display permeability zonations that either belong to the autocyclic process or are allocyclic effects (factors that affect the depositing agent, e.g. a change in wind direction or in the groundwater level). In the aeolian environment, dunes, draas and sand sheets are different genetic units, and permeability zonation is caused by different types of strata in a genetic unit (wind-ripple, grain-fall and grain-flow strata).

iii) The reservoir scale: the location, size and degree of connectedness of genetic units are of importance, permitting assessment of the reservoir volume and its exploitation. These properties are determined by allocyclic influences on the deposition process. Ergs (or sand seas, formed of draas and interdraa areas) are units at this scale in the aeolian environment.

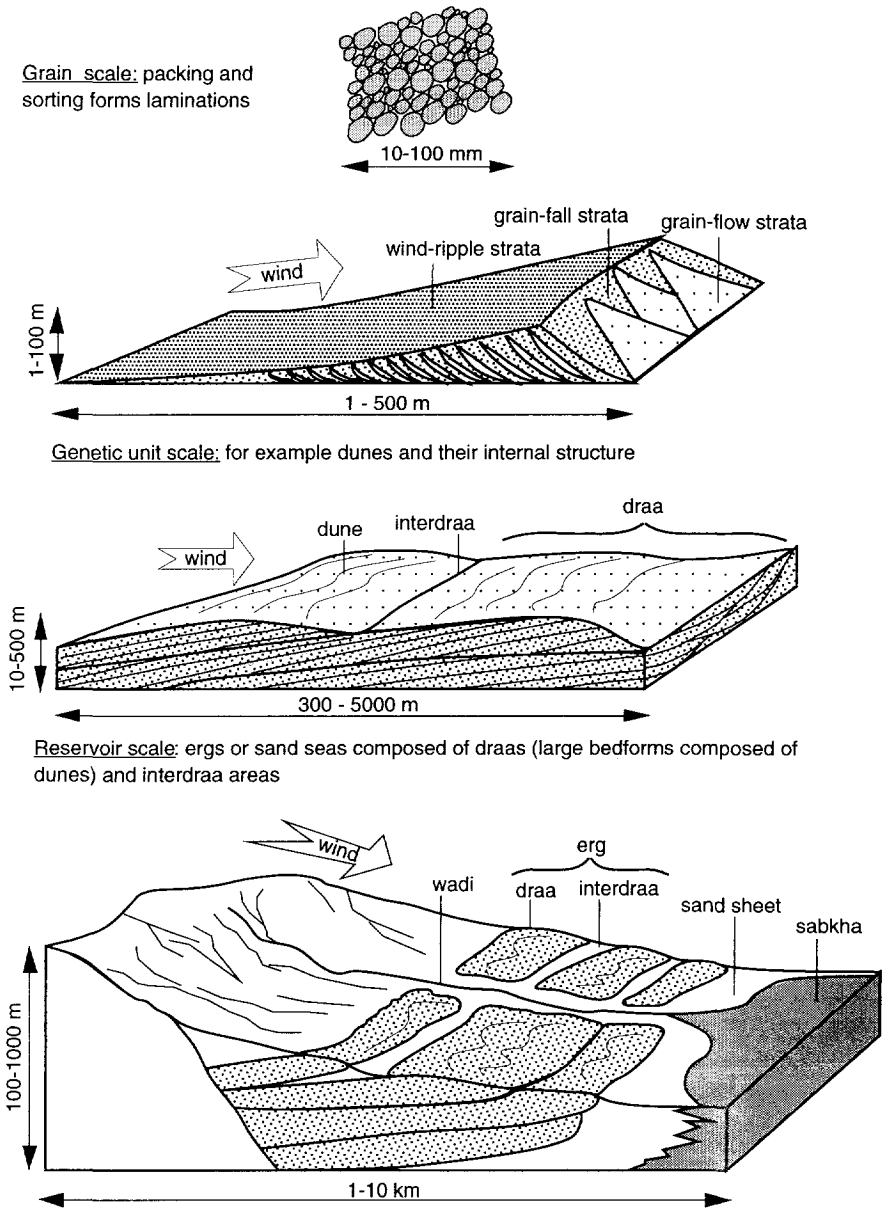

Fig. 1.3.1 *Scales of processes in the aeolian environment.*

iv) The basin scale: processes at this scale include tectonics and eustacy. Basins are essentially the largest units that include the heterogeneities at all the smaller scales. Deserts are often located in basins where the sand seas (ergs) are separated by ephemeral streams (wadi systems) and where desert lakes with marginal sabkhas form in the middle of the basin.

Purely process-based modelling implies simulating the physical processes of sedimentation on a grain scale. Simulating large depositional sequences on a grain-to-grain basis would create problems of computer time and memory. The genetic unit scale is the next smallest significant unit out of which, theoretically, a reservoir could be built. Processes at this scale (e.g. bedforms such as dunes and draas) result from the interaction between fluid flow and topography. The physics of fluid flow at this scale has been well developed, and many solution techniques exist. Sediment mechanics at grain scale is generalized by using transport equations with sometimes empirically calibrated parameters (e.g. Bagnold's sediment-transport equation). Reconstruction of sequences occurs by repeating calculations through successive time steps, or by extrapolating net accumulation rates over longer time periods (days, months or years). These results can be considered relevant at geological time scales, if it is considered that accumulations preserved, for instance, over a hundred thousand years result from processes of much shorter time lengths. These include deposition and erosion in successive cycles (similar to tidal deposits), and then preservation through larger-scale allocyclic effects (e.g. basin subsidence, marine transgressions or climate changes). This can also be taken into account for simulations at reservoir scale. At the reservoir scale the effect of allocyclic processes has to be modelled, which is done through initial or boundary conditions. Variation of these conditions through time is generally calculated in a parametric way. Finally, simulations at basin scale concentrate mainly on large-scale allocyclic processes such as tectonic subsidence, eustacy etc. which are often also modelled in a parametric way.

1.4 Scope of this thesis

This thesis will treat the modelling of the physics of aeolian sedimentation at the genetic unit scale of dunes. Henceforth this will be referred to as the dune scale. Many observational studies have been made in sedimentology, and recently some simulation models have also been developed (Wipperman and Gross, 1986; Rubin, 1987 and Weng et al., 1991). The present research focuses on the problem of the interaction of wind and topography and on the mechanisms for bedform growth and migration. The author considers that addressing this subject

from a physical basis will be a new contribution to the better understanding and quantification of aeolian sedimentation processes, and a step towards developing a process-based simulator for the aeolian environment. The combination of sedimentological studies with calculation methods from engineering applications is also a new approach. A clear example of this is that the analytical solution developed in this study is analogous to the analytical solutions used in the calculation of long tidal waves. It is important to note that all these calculations remain models (i.e. simplifications) of reality. The effects and interactions of processes described from field observations are much more complicated than the models. However, quantification of the essential processes can help one to understand the more complex reality, and this interdisciplinary relationship and would lead to an improved understanding of the physical processes in the aeolian environment.

The thesis is divided into the following chapters:

Chapter 2 comprises a literature review of the aeolian environment, concentrating mainly on bedform processes. This review shows that there are many questions that have come forward in field studies, which would be interesting to approach from a fundamental physical point of view. These questions form the context both for the present research and for future studies. A brief overview is also given of the mathematical models that have been published to date.

Chapter 3 treats the basic equations used in this study for modelling the genetic unit scale of dunes (sediment-continuity and sediment-transport equations) and discusses the assumptions for modelling dune morphodynamics. An analysis of the flow problem is made to understand the expected behaviour from a fluid-dynamic point of view, and to assess the possible limitations of the model developed in chapter 5.

Chapter 4 discusses models that result from simplifying the basic equations to linear relationships (the resulting models are known as the simple-wave equation and the kinematic-wave equation). This has three purposes: a) to illustrate the importance of the flow model compared to the sediment-transport equation; b) to evaluate the effects of linearizing the sediment-transport equation and c) as a basic solution to test the numerical scheme of the computer programme developed in chapter 6.

Chapter 5 develops a model based on a more detailed calculation of the wind velocity over a gentle topography. An analytical solution is developed for a sine-shaped dune. Analytical expressions are given for the shear stress, the sediment transport, the topography through time, the migration rate and the growth of sine-shaped dunes. These lead to a

good understanding of the migration and growth of dunes, and also serve to test the computer programme of chapter 6.

Chapter 6 generalizes the analytical solution for any gentle topography using Fourier Transforms. A computer programme called EOLSIM is developed for this, and solutions are devised for specific computational problems. Avalanching is considered as a process that counters dune growth and a simple avalanching routine is developed.

Chapter 7 summarizes the conclusions and discusses some of the possible implications and extensions of this research.

Finally, in one of the appendices, an article is included in which the author approaches the study of subsurface heterogeneities from the aspect of its properties. The specific subject treated here is the averaging of permeabilities in a layered subsurface. It was determined to which degree heterogeneities within the layers could be neglected and an arithmetic and harmonic average could be used. This work has been published as a journal article during this research period (Stam and Zijl, 1992). As topics such as this are a direct application of subsurface modelling, this article has been included within the thesis.

Chapter 2

The aeolian environment

2.1 Introduction

This chapter gives a review of published studies on the aeolian environment. First, an introduction is given of the general geographic and hydrologic characteristics of deserts. After that, a summary follows of the published studies on modern deserts, concentrated mainly on the dune scale. This review is grouped into subjects that have been highlighted during field studies and which have led to different hypotheses on dune dynamics. The compilation of the studies presented here is by no means complete, only the major studies having been selected. They are meant to indicate potential areas of interest to model from a mathematical-physical approach. The present study treats one of these aspects, the interaction of wind and topography. It is a basis that can be extended to treat further aspects of bedform dynamics. Finally, a review is also given of the mathematical models on the dune scale published so far.

2.2 General setting and characteristics of desert environments

Aeolian deposits are wind-laid sediments that occur either near sea shores, the shores of large lakes, or in arid deserts (in both hot and cold climates). Although the description of the general setting and much of the literature is focused on hot desert environments, the results of this study are applicable to aeolian deposits in general.

Modern deserts cover 20% to 30% of the world's landsurface, as shown in Fig. 2.2.2. They often occur in basins that have an internal drainage system, with bordering mountain ranges obstructing the passage of clouds so that these basins lie in a rain shadow (Glennie, 1970). Tectonics play an important role in the preservation of the desert sediments, and in the distribution of the facies of the desert environment. The basin topography determines the succession of facies (ergs, wadis and sabkhas), while the preservation of aeolian deposits is mainly due to basin subsidence.

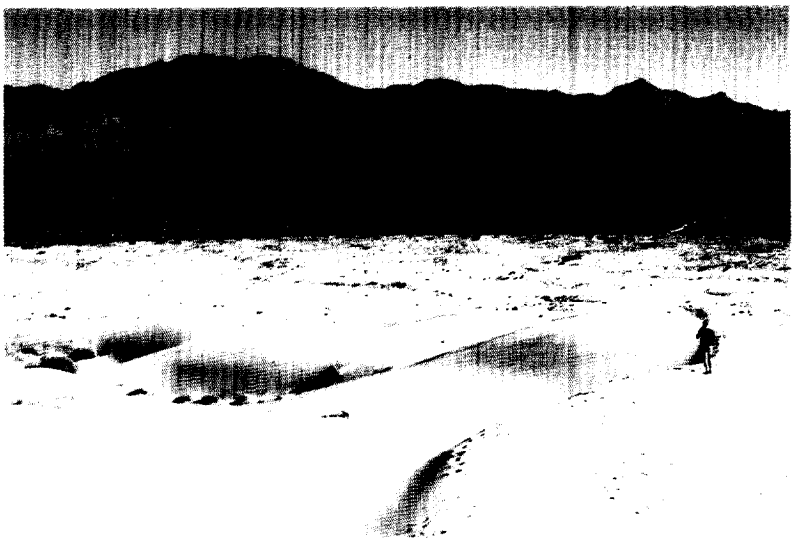

Fig. 2.2.1a *Overview of a valley in a modern desert (Kelso dunes, Mojave desert, California) showing different depositional environments: bordering mountain range in the back (Granite mountains), fan aprons formed by the streams coming from the mountains and dune field in the foreground.*

Fig. 2.2.1b *Dunes and interdune areas. The relatively flat areas between the dunes are interdunes.*

Fig. 2.2.1c *Dried bed of an arroyo, or ephemeral channel. Ephemeral channels form the drainage system of the desert valley.*

Fig. 2.2.1d *Dried-up playa lake or sabkha; the evaporite deposits of the desert lake. Note the typical dessication pattern formed by the saline crust.*

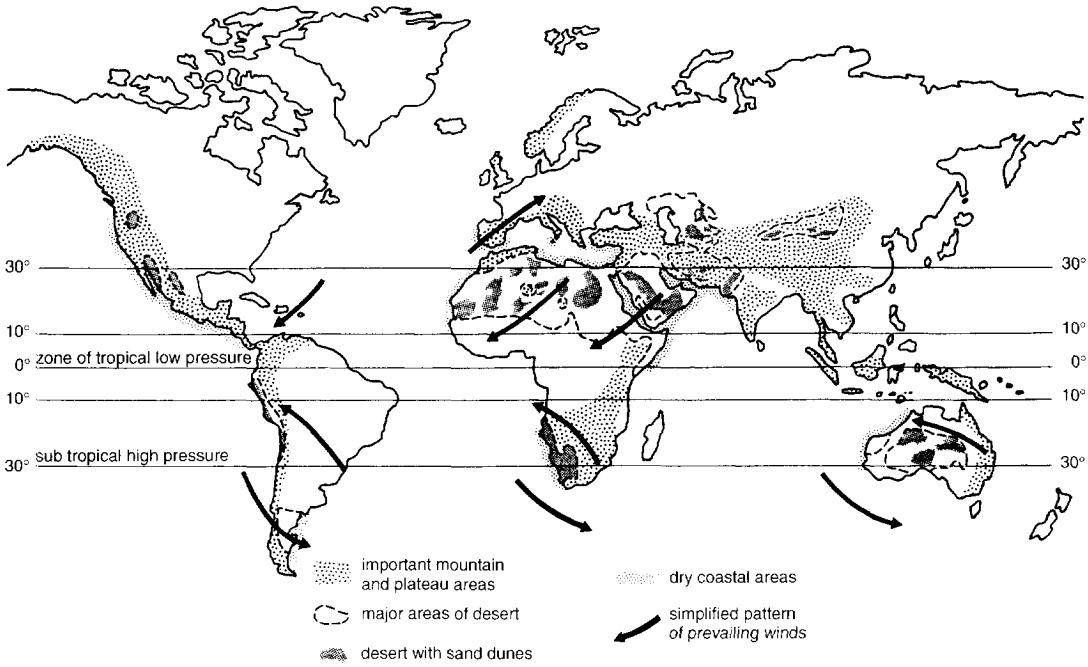

Fig. 2.2.2 *Distribution of the world's major deserts. The pattern of prevailing winds moves about 5° North of its mean position in July and 5° South in January. This simplified pattern is further modified by the large land masses wich heat up more rapidly in summer and cool more rapidly in winter than the adjacent oceans (after Glennie, 1970).*

Deserts are formed in arid climates, where potential evapotranspiration exceeds the precipitation, and the rainfall is insufficient to support more than very limited plant growth (the mean annual precipitation is usually less than 200 mm for semi-arid climates and less than 100 mm for hyperarid climates). Typical arid climates have a small amount of highly variable precipitation, both in space and in time. Sudden storms with high precipitation rates produce peak surface run-offs. Evapotranspiration rates are very high, so that ground-water recharge is very low. Drainage consists mainly of ephemeral streams (called wadis or arroyos) whose locations are sometimes inherited from the Pleistocene topography (Reading, 1986). During the late Pleistocene many of today's deserts also had a very arid climate, which became more humid during the early Holocene (Glennie, pers. comm.). The

upland drainage sections are formed by relatively well developed channels, the midland tracts show a more diffuse local drainage while the lowlands are practically riverless, and if there is sufficient rainfall, salt lakes (called salinas) may form at the lowest points in the basin (Slatyer and Mabbutt, 1964). Drainage is erosional in the uplands and aggradational in the lowlands. Fluvial processes are generally more evident in margins while aeolian sediments occur in the more central parts (Reading, 1986). Figure 1.3.1, which gives a scheme of scales in the aeolian environment, shows the distribution of depositional environments in a basin. An example of the different depositional sites in a modern desert (Kelso Dunes, California), with some characteristic desert features (interdune areas, desert lake and ephemeral streams), can be seen in Figs. 2.2.1a,b,c and d.

Normally, aeolian deposits are texturally characterised by clean, well sorted and rounded grains, generally between 0.1 and 1 mm in diameter. Coastal dunes are generally well sorted to very well sorted, while inland dunes are moderately to well sorted (Ahlbrandt, 1979). Sorting depends on the proximity to the source. A uniform sand will indicate a long distance from the source, so that both the coarsest and finest components will have been segregated. The source of the aeolian sediment can be: a) chemical and mechanical weathering products of the exposed rocks in the desert; b) unconsolidated sediments from alluvial fans c) coastal beaches bordering the deserts (Glennie, 1970). The original sources of the aeolian sediment can be located at great distance from the actual depositional setting (Ahlbrandt, 1974).

2.3 Deposits in ancient aeolian environments

The distribution of facies in a desert environment, as has been described above, is also recognizable in palaeoenvironments, such as the South Permian Basin, extending from the North Sea across to Poland. This basin is of importance for its hydrocarbon reservoirs in the Upper Rotliegendes formation. An interpretation of the distribution of the main facies in the South Permian Basin during the Early Permian is shown in Fig. 2.3.1 (after Glennie, 1984). These facies are: aeolian, wadi, sabkha and desert lake. Figures 2.3.2a,b,c,d and e show examples of the following characteristic features of some of these facies in cores:

i) Aeolian facies (Figs. 2.3.2a and b) form the main reservoir rock for the gas in the basin. They are characterized by clean sands where clay intercalations are nearly absent (Van Veen, 1975). Adjacent laminae of steeply dipping foresets show sharp grain size differences. Note their truncation by less steep laminae. In the aeolian facies interdune areas affected by groundwater can be recognized (Fig. 2.3.2c). These are damp sandflats showing

horizontal laminae, alternating light and dark streaks. Small-scale cross-bedding suggests local reworking by ephemeral streams.

ii) Sabkha deposits bordering the desert lake (Fig. 2.3.2d). These are mudflats consisting of argillaceous sandstones showing a somewhat chaotic structure, probably caused by adhesion of silts and clays to a slightly damp salt-covered sabkha surface.

iii) Desert-lake facies (Fig. 2.3.2e) consisting of red-brown mudstone formed by the clay deposits of the desert lake.

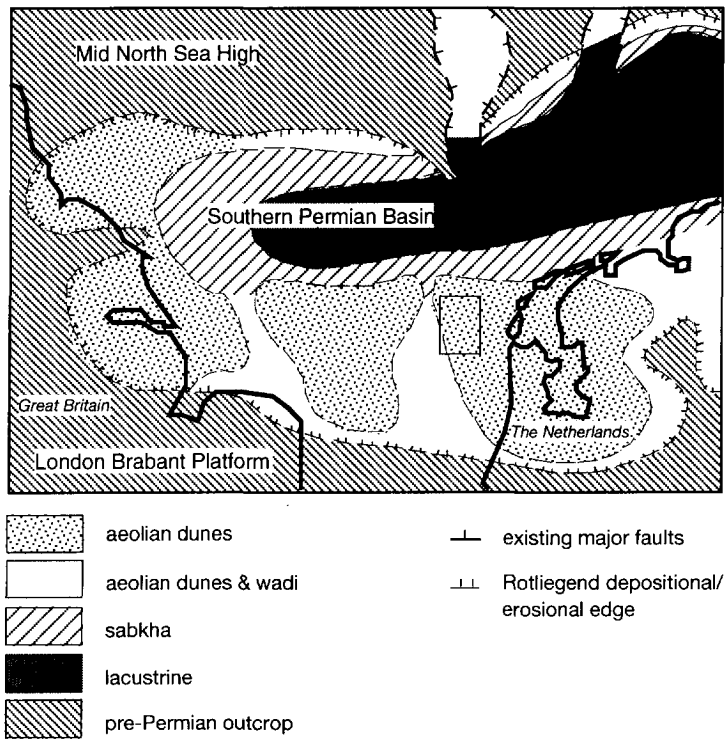

Fig. 2.3.1 Facies distribution and pattern of Early Permian (Rotliegend) in the North Sea area (after Glennie, 1984). The square marks the approximate position of block K, where the core of Fig. 2.3.2 is located.

2.4 The recent aeolian environment

2.4.1 Bedform types and patterns

Wind-blown sand accumulates into sand seas or ergs, where they assemble into a complex variety of bedforms. Wilson (1972) distinguishes three scales of aeolian bedforms: ripples, dunes and draas.

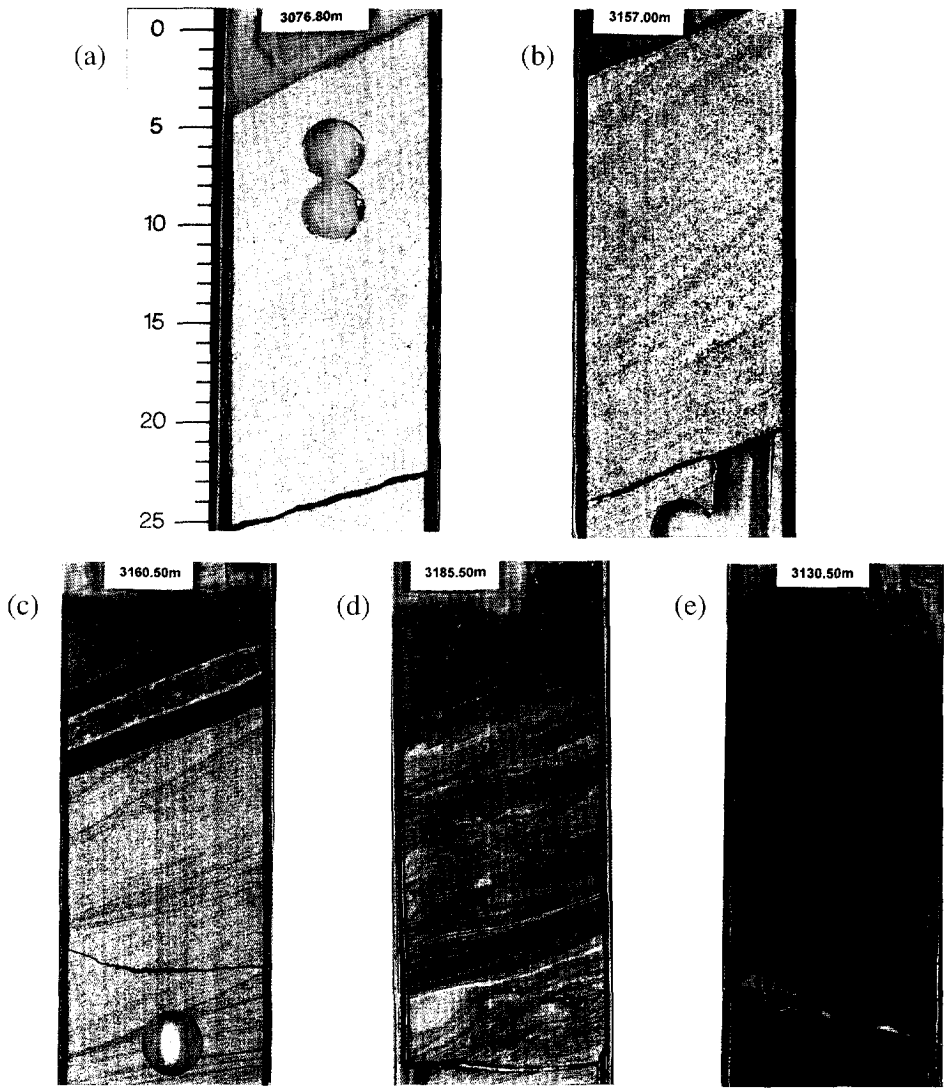

Fig. 2.3.2 *Examples of a core showing distinct facies of an ancient desert system (Southern Permian Basin). The core was taken with a deviation of approximately 20°. The approximate location of the core is indicated in Fig. 2.3.1. The scale is given in centimetres. Photograph published by courtesy of NAM (Nederlandse Aardolie Maatschappij);*
(a) aeolian facies forming the main reservoir. Note the angle discordancy between the sets of laminae; (b) aeolian facies; note how the laminae merge downward tangentially together, a characteristic feature at the base of grain-flow strata; (c) aeolian facies; damp sandflats (lower two-thirds); these are interdune areas affected by groundwater. Note the characteristic light and dark low-angle laminae; (d) sabkha deposits bordering the desert lake; These are mudflats consisting of argillaceous sandstones, showing a somewhat chaotic structure. (e) desert-lake facies; consisting of red-brown mudstone formed by the clay deposits of the desert lake.

Table 2.4.1 Dimensions and migration rates of aeolian bedforms (after Wilson, 1972)

	ripples	dunes	draas
wave-length [m]	0.15-2.50	3-600	300-5500
wave-height [m]	0.002-0.05	0.1-100	20-450
migration rate	1 $m \cdot h^{-1}$	0.1 $m \cdot d^{-1}$	0.01 $m \cdot a^{-1}$

Ripples and dunes can be considered as separate categories because no intermediate forms appear; i.e. the largest ripple is smaller than the smallest dune. Draas are a more complex bedform. They are the largest bedforms observed in aeolian accumulations. Though ripples and dunes are also subaqueous bedforms, draas are a typical aeolian bedform. According to Wilson (1972) they originated by merging together of juxtaposing dunes. They may have originated during earlier time periods (15 to 20 thousand years ago) as large dunes, under the influence of glacially-induced strong and persistent winds, and now have smaller dunes migrating over their surfaces (Pugh et al., 1993). Table 2.4.1. gives dimensions for the three types of bedforms according to Wilson (1972). An order of magnitude of their migration rates has also been added.

Ripples, dunes and draas display a regular spacing and pattern. This can be seen for dunes and draas on satellite images and aerial photographs (see Fig. 2.4.1), but also observed on the ground with small bedforms, such as smaller dunes and ripples. Wilson (1972) found that by plotting the areal frequency versus the wave-length of different bedforms the above three categories could be distinguished (Fig. 2.4.2a and b). By analysing sand samples from the Sahara desert, he found, moreover, that a plot of the bedform wave-lengths against grain-size diameter also showed the three bedform groups. This is an interesting result, although it should be taken into consideration that this relationship only applies to the location where the samples were taken, and is not necessarily a universally applicable relationship. Also, Wilson did not distinguish between dunes and draas of different shapes (i.e. longitudinal and tranversal), which have a notably different ratio between their wave-length and height.

Anderson (1990) analysed ripples as a self-organizing system that shows a spontaneous transition from a random distribution (where ripples originate) to a regularly spaced pattern. He concluded that this regularity results from the evolution of different sized ripples. Small fast-moving ripples catch up on larger slow-moving ripples, and are absorbed by them, resulting in the growth of the mean wave-length, and a decrease in the variability of the wave-lengths. It is also considered that migration rates of ripples are controlled by grain size; fast-moving ripples being finer grained and slow-moving ripples being coarser

Fig. 2.4.1 *Regularly spaced dunes in Shanxi-Shaanxi, Inner Mongolia. Note the dunes partly covering the Great Wall. Satellite image, published by courtesy of the International Institute for Aerospace Survey and Earth Sciences (ITC).*

grained (Glennie, pers. comm.). A similar self-organizing behaviour was described by Kocurek et al. (1992) for the behaviour of incipient dunes originating at random locations and migrating at different rates, so that cannibalization, overtaking and complete incorporation of one bedform in the other was observed, tending towards a state with fewer, larger and more regularly spaced dunes.

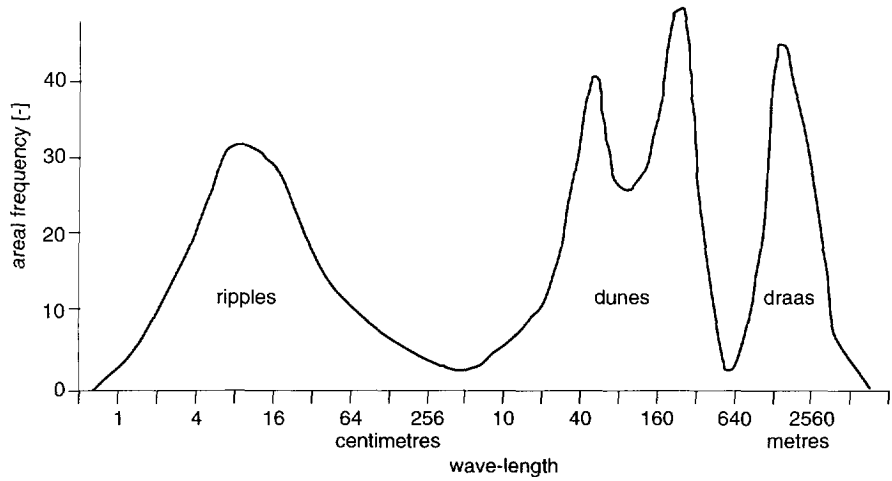

Fig. 2.4.2a *Areal frequency of different wave-lengths (after Wilson, 1972) Wilson calculates the areal frequency as* $dA_\lambda/d\log(\lambda)$. *Formally* $\log(\lambda)$ *is calculated as* $\log(\lambda/\lambda_0)$. *It is assumed that* $\lambda_0 = 1cm$ *in case of the ripples and* $\lambda_0 = 1\ m$ *in case of the dunes and draas.*

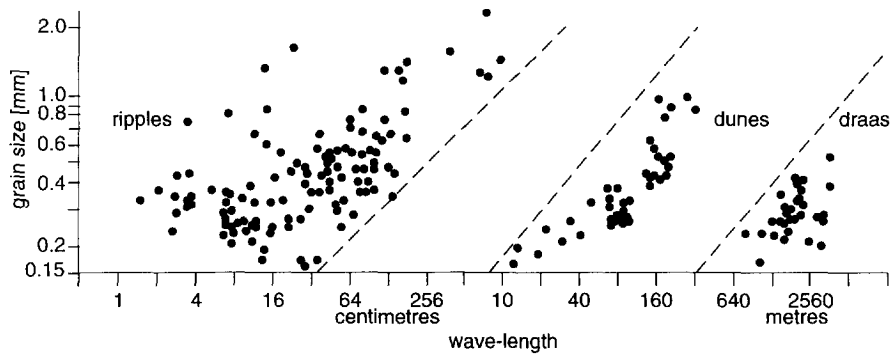

Fig. 2.4.2b *Bedform grain size plotted against wave-length (after Wilson, 1972). Three categories can be distinguished (ripples, dunes and draas). Sand samples and measurements were taken from one area (the Sahara). The lines dividing the clusters were placed more or less arbitrarily to indicate a maximum for the ripples and a minimum for the dunes and draas.*

2.4.2 Dune growth and development

Wilson (1972) describes the formation and development of aeolian dunes in detail. An initial irregularity acts as a nucleus that starts the development of a proto-bedform. Different sized nuclei lead to ripples, dunes or draas. He gives the following possible nuclei for dune formation:

i) A body or an obstacle standing out (e.g. a pebble)
ii) An inhomogeneity in the substratum leading to differential erosion
iii) The remnants of previous bedforms
iv) An irregularity produced by the flow (an eddy, a random feature in the turbulence).

These coincide to a certain degree with nucleation sites observed by Kocurek et al. (1992) associated with varying surface roughness, for example areas with grass, areas adjacent to vegetated mounts, areas within erosional depressions etc.

The further development of dunes has been observed in detail by Kocurek et al. (1992), and is illustrated in Fig. 2.4.3. They describe five stages:

i) Irregular patches of dry sand migrate from the original nucleation site (Fig. 2.4.3a). They are a few centimetres high, lacking a distinct crest and formed by wind-ripples. A slight acceleration and deceleration of the wind velocity is noted.
ii) These sand patches continue to migrate and develop into protodunes, of a height of 10-35 cm (Fig. 2.4.3b). They show a distinct crest line, but can have normal dune asymmetry, reversed asymmetry, or be of symmetrical shape. The transport mechanism is saltation, forming a deposit of wind-ripples.
iii) Protodunes continue to develop into a distinct asymmetrical shape. Their height ranges between 25-40 cm (Fig. 2.4.3c). A distinct lee face forms, where flow deceleration occurs, and sand grains entrained over the crest fall on the slip-face by effect of gravity, forming grain-fall strata.
iv) The dune develops into a definite barchan dune (Fig. 2.4.3d). Separation of the flow occurs and a wake zone forms. At the slip-face, the critical angle of repose (between 30° and 35°) can be reached. Then, the weight of the sand deposit exceeds the sheer stress and sand avalanches, forming grain-flow strata. Barchan dunes as small as 40 cm height have been observed (Kocurek et al., 1992), but their height can reach up to several tens of metres.
v) Barchan dunes merge laterally together, forming crescent-shaped ridges (Fig. 2.4.3e). If there is a sufficient availability of sand they will continue to develop into transverse dunes, the largest of which can be up to several kilometres long and up to 300 - 400 metres high.

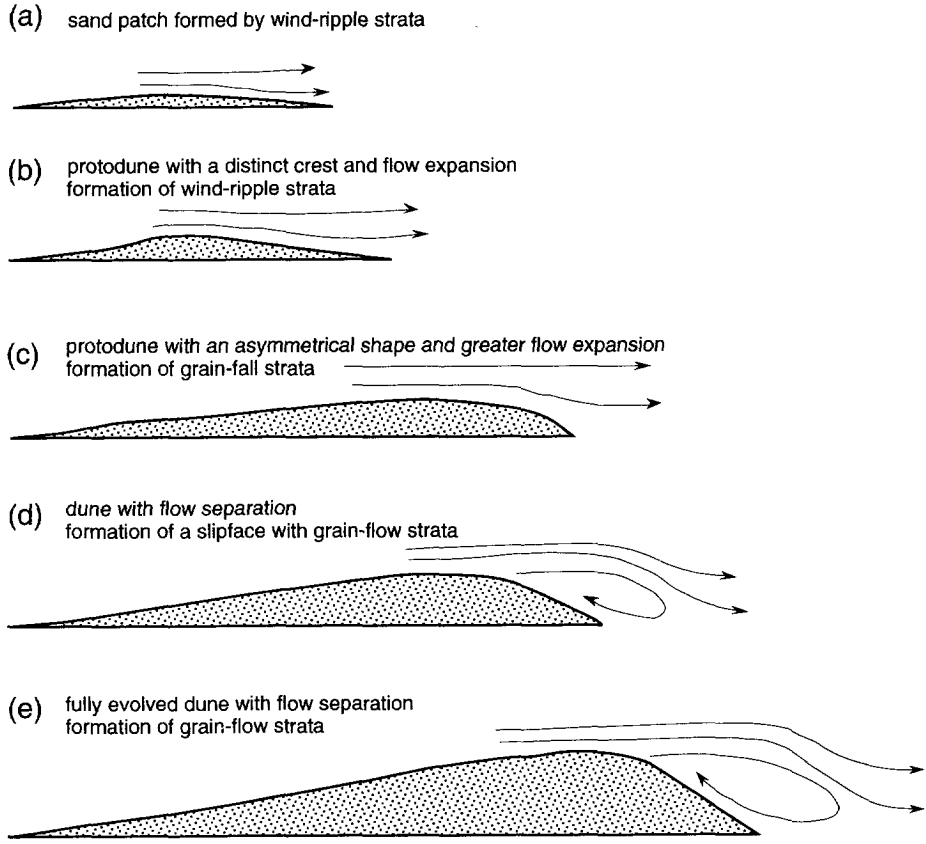

Fig. 2.4.3 Stages of dune evolution (after Kocurek et al., 1992).

2.4.3 Wind regime and dune shape

Wind regimes associated with dune types according to their shapes were analysed by Fryberger (1979), who made the first attempt at developing a standardized method to compare sediment transport in different areas by means of sand roses. Sand roses are circular histograms that represent the potential sediment transport, in different directions, computed over a certain time interval. He associated wind regimes with dune types: barchan and transverse dunes were associated with narrowly unimodal wind regimes; linear dunes with bimodal wind regimes and finally star dunes with winds of much wider directional variability. More detailed results were obtained experimentally by Rubin and Ikeda (1990). They reconstructed dunes of different shapes by subjecting subaqueous dunes in a flume to flows that alternated between two different directions. They found that transverse dunes were formed when the angle between two equally important transport

directions was less than 90°, when the angle was 180°, or at any angle when there was a dominant transport direction. Longitudinal dunes were formed when the angle between the flow directions was greater than 90° and transport was equally dominant in both directions. Further studies show us that the relationship between wind and dune shape is more complicated than we were first led to believe, especially when considering the three-dimensional character of the flow and bedforms. Cooke et al. (1993, p.368-396) extensively discuss dune morphodynamics and give an overview on the different theories of formations of linear dunes.

Sand roses as developed by Fryberger (1979), have subsequently often been used to characterize the sediment-transport regime of a particular area, in an analogous way to the use of wind roses (Fryberger et al., 1983 and 1984; Havholm and Kocurek, 1988 and Sweet et al., 1988). Sand roses give an idea of the potential yearly sediment-transport and can be used to compare different regimes or areas qualitatively. It should be noted, however, that the quantified information is unsuitable for further morphodynamical calculations. The main reason for this is that two factors, the wind strength and the length of time the wind blew, are merged together. Therefore it is impossible to distinguish if sediment transport is due to a strong wind having blown a short period, or a weaker wind having blown during a longer period. This type of data would be important for a morphodynamical study of dunes. For this type of study, wind roses divided into categories for different wind strengths, as used in Kolm (1982), are preferable.

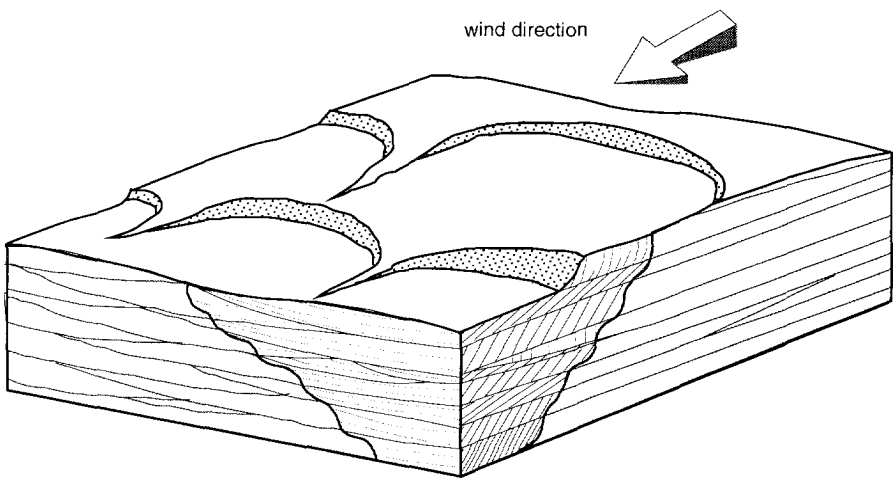

Fig. 2.4.4a *Scheme showing the cross-bedding formed by a transverse dune (after Weber, 1987). Note the low-angle cross-bedding perpendicular to the wind direction (called festoon cross-bedding) and the steeply dipping cross-bedding parallel to the wind direction.*

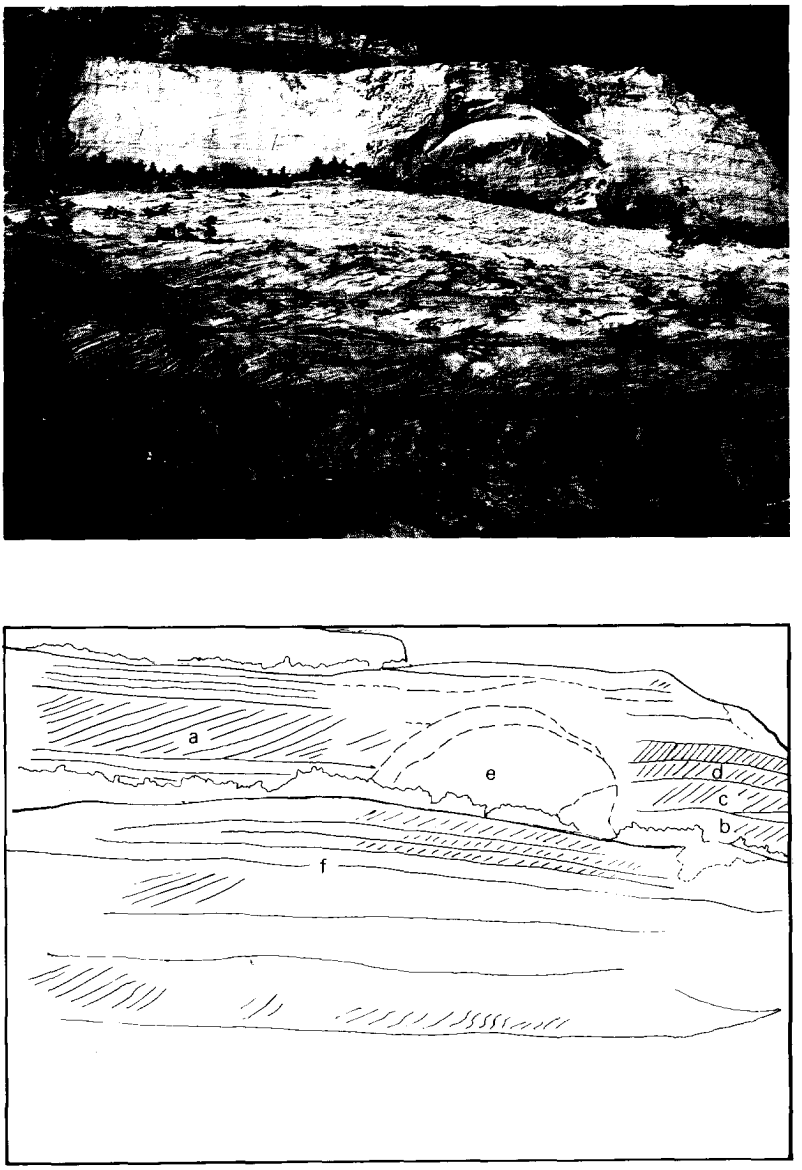

Fig. 2.4.4b *Example of an outcrop showing steeply dipping cross-bedding formed parallel to the wind direction in Zion National Park (Utah). Note the trees (approximately 2 m) for scale. The bedding formed by an individual dune can clearly be seen at (a) and of smaller dunes in (b) (c) and (d). A horizon indicating exposure at a different angle is marked by (f). A diagenetically altered zone is marked by (e).*

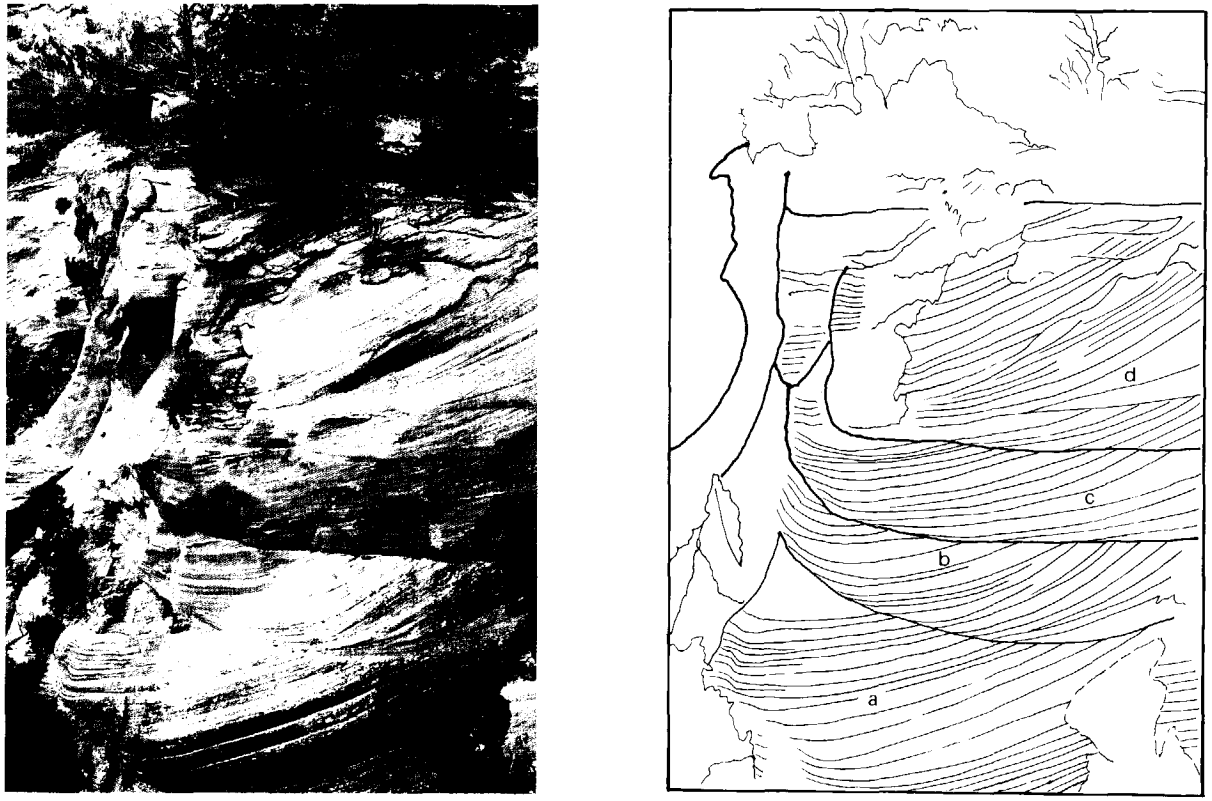

Fig. 2.4.4c *Example of festoon cross-bedding in an outcrop of a dune perpendicular to the wind direction, Zion National Park (Utah). Slight changes in the direction of the sediment flux (e.g. by changes in wind direction) can be seen by differences in the inclination angle of the laminae of the various beds: (a), (b), (c) and (d). Note the wedges of avalanche laminae, especially clear in (b) and (c). These indicate the bottom of the dune.*

Dune types (oblique, transverse or longitudinal) have been recognized in ancient aeolian sandstones (Kerr and Dott, 1988; Clemmensen and Blakey, 1989) by analysing palaeowind directions. One of the features that has always served to characterize aeolian sandstones is the superposition of giant cross-bed sets. These cross-bed sets show a characteristic geometry both perpendicular and parallel to the wind direction (see Fig 2.4.4a,b and c). This has been observed in the Jurassic Navajo Formation in Utah, U.S.A. (Doe and Dott, 1980; Weber, 1987). Data on lengths, thicknesses and widths of the cross-beds was gathered by Weber (1987) in the Canyon De Chelley (Arizona), and used as an analogue for the aeolian facies of the Permian Rotliegendes. These giant cross-beds may have been formed by much stronger winds than we observe today, if we accept the hypothesis that high-latitude glaciations during major glacial periods (Permo-Carboniferous and Pleistocene) might have caused a squeezing together of the air-pressure belts that control the wind pattern (Glennie, 1982 and 1984).

2.4.4 Wind velocity over bedforms

The velocity profile over a varying topography differs notably from the logarithmic velocity profile of turbulent flow over a flat surface (see section 3.3). Measurements of velocity profiles over dunes were made by Bradley (1980), Mulligan (1988), Sweet and Kocurek (1990) and by Arens (1994), while close-surface measurements of variations of wind speed and calculations of sediment transport were made for various flow models (Howard et al., 1978; Mikkelsen, 1989 and Weng et al., 1991). The acceleration that generally occurs at the stoss side is sometimes quantified in a speed-up factor, or the ratio between the wind velocity at the crest and that at the plinth of the dune (Lancaster, 1985). Flow decelerates at the lee side, and usually flow separation occurs and a wake zone forms with highly rotational flow (as was illustrated in Figs. 2.4.3d and e). This does not necessarily happen though, as indicated by Sweet and Kocurek (1990). They noted that the lee-face flow could be separated, but also attached without a wake, and deflected along the slipface. This depended on the dune shape, on the orientation of the dune brink in relation with the wind direction, and on the atmospheric thermal stability (which would affect the velocity profile). Sweet and Kocurek (1990) give empirically observed limits for these controlling factors.

Sediment transport over a bedform will vary according to the acceleration and deceleration of the flow velocity, causing the bedform to migrate. Field measurements have been made on the rates of erosion and deposition over a dune (Howard et al., 1978; Lancaster, 1985, 1988), but published data on migration rates is scarce and generally not uniform or complete (e.g. migration rates are given without

corresponding wind velocity or height of measurement). The most complete and extensive data on migration rates is given by Long and Sharp (1964), who published the migration rates of 47 barchan dunes in the Imperial Valley in California. Dune heights ranged approximately between 3 and 12 m. The migration rates were estimated from the difference in location of the individual dunes in the course of seven years. Estimated migration rates varied between 14 and 40 $m \cdot a^{-1}$ with an average of 25 $m \cdot a^{-1}$. Some orders of magnitude of bedform migration rates are given in Table 2.4.1. It can clearly be seen that there is a trend for small bedforms to migrate faster than large ones. Migration rates for ripples are in the order of 1 $m \cdot h^{-1}$, for dunes in the order of 0.1 $m \cdot d^{-1}$ and for draas in the order of 0.01 $m \cdot a^{-1}$.

2.4.5 Stratification types in aeolian deposits

The identification of the thinnest recognizable depositional strata in modern dunes results from the work of Hunter (1977). He described his observations of the dune field on Padre Island (Texas), and classified the strata into the following categories:

i) Planebed lamination forms by traction of sand grains. Wind velocities are high so that small pre-existing ripples are flattened out. However, after some time and under the same velocities, new ripples form that are more widely spaced than the previous ones. Hunter noted that the formation of planebed lamination was observed only once during his field study.

ii) Ripple strata form on the stoss side of dunes and on gently sloping lee sides (slopes smaller than the angle of repose; 34°). Ripples forming on lee slopes can be caused by shifts in wind direction, or by vortices in the wake zone. Ripples are formed by saltating grains, and they are oriented perpendicular to the local wind direction (Figs. 2.4.5 and 2.4.6 on page 34). They are therefore indicators of the local wind direction. Ripples migrating on the stoss surface of a dune generally cause erosion. Ripples can also migrate on a hard flat surface without net deposition and they can climb, which means they migrate while net deposition occurs. They can have any wind-induced orientation relative to the slope attitude.

iii) Grain-fall laminae form in the lee of a dune crest, in the zone of flow separation, where grains fall through the effect of gravity. The laminae are parallel with gradational contacts, so that individual laminae are difficult to identify. Therefore there is little grain-size segregation. Hunter (1977) observed rates of grain-fall deposition ranging from 1 to 5 $cm \cdot h^{-1}$ at wind speeds of about 9 $m \cdot s^{-1}$.

iv) Grain-flow cross-strata are caused by slump degeneration (through loss of cohesion between sand grains), and scarp recession (where a small sand flow occurs, which causes recession upslope and at the

sides). The occurrence of avalanching leading to grain-flow can also be seen in Fig. 2.4.5. Deposits formed by sand flow are shaped as a tongue or cone. They are graded, with the coarser grains concentrated near the base of the slipface as a result of shear sorting. The grain-flow strata are usually preserved, and can be identified in cores by its regular, steeply dipping cross-bed sets without any shale intercalations (see Fig. 2.3.2a and b).

Fryberger and Schenk (1981) reconstructed the formation of wind-ripple, grain-flow and grain-fall strata in a wind tunnel experiment, gathering information on their formation and migration rates. These experiments confirmed Hunter's (1977) observations. They concluded that the rate of deposition, wind velocity and wind duration control the specific sedimentary features of these strata. Wind velocities between 0.4 and 0.625 $m \cdot s^{-1}$ (recorded at heights ranging between 0.165 and 0.26 m) resulted in deposition rates of wind-ripple strata varying between 0.059 and 0.136 $cm \cdot min^{-1}$. The migration rates varied between 0.9 and 1.6 $cm \cdot min^{-1}$.

The aeolian structures identified by Hunter (1977), proved to be an additional means of distinguishing between subaqueous and aeolian sandstones (Kocurek and Dott, 1981; Clemmensen and Abrahamsen, 1983). Outcrop measurements of permeabilities in the different facies of the Page Sandstone (Northern Arizona) by Goggin et al. (1988) and Chandler et al. (1989) revealed that differences by orders of magnitude of permeability relate to the different stratification types. The lowest permeabilities correspond to the interdune strata and the strata outside the erg (averaging 665 mD)[1], followed by the wind-ripple strata (averaging 2289 mD). The highest permeabilities are found in the grain-flow strata (averaging 7820 mD). The interdune strata (occurring between dunes and also between ergs) are considered to be permeability barriers that would compartmentalize the reservoir. Van Veen (1975) described the permeability distribution of a core from the Rotliegendes aeolian cross-beds in the Leman Gas-Field. An alternation of high- and low-permeability streaks was observed. This was attributed to the regular avalanching at the lee side of the dunes. Some permeability measurements were taken of a small sample of the core. These varied between 12-36 mD for the highly permeable streaks, and between 0.5-2.5 mD for the poorly permeable streaks. These values are much lower than those given by Goggin et al. (1988) and Chandler et al. (1989). There may be many reasons for this difference, the main probably being diagenetic effects that occurred in the Rotliegendes.

[1] 1 mD = 10^{-15} m^2

2.5 Preservation of bedforms

A question that has frequently been raised relates to how aeolian deposits are preserved. Allen (1969) suggested that sets of cross-strata are formed by trains of climbing bedforms. Rubin and Hunter (1982) worked this out in a model. As a bedform migrates, it leaves a surface that is defined by the apparent advance of the trough. If the erosion at the stoss side equals deposition at the lee side, no net deposition occurs. If the lee side deposits are not eroded away by a following trough, then they are preserved, forming what is called a "climbing translatent stratum" (Hunter, 1977). This is usually called the "climbing bedform theory".

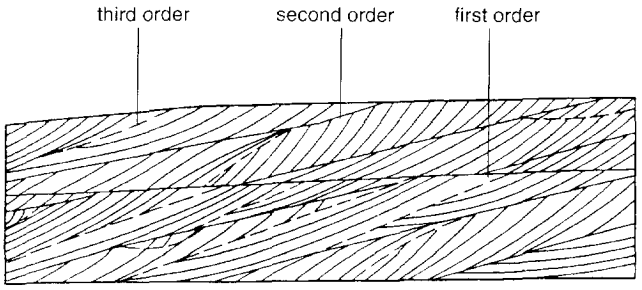

Fig. 2.5.1 *Hierarchy of bounding surfaces (after Reading, 1986).*

The trace that results from the migration of one bedform over another is a bounding surface. Brookfield (1977) identified a hierarchy of bounding surfaces, where a more important order of bounding surface truncates other less important surfaces (see Fig. 2.5.1). They mark a sequence where each process is overridden by another one acting on a larger spatial scale. There has been some discussion on the possible origins of these bounding surfaces, which is summarized by Kocurek (1988). The smallest bounding surface is the third-order bounding surface, caused by a reorientation of the lee face of a dune by a shift in wind direction. Second-order bounding surfaces result from dunes migrating over each other. First-order bounding surfaces can originate by different mechanisms; draas migrating over draas (Kocurek, 1981, 1988) or by a successive rise of the water table, where the aeolian sediments above the groundwater table are eroded away (Stokes, 1968). Figure 2.5.2 shows these two mechanisms. Finally super-bounding surfaces represent a hiatus in the whole period of aeolian deposition. They can be caused either by a climate change resulting in a protective mantle of vegetation that stabilizes the dune field (Talbot, 1985; Yang and Nio, 1993), or by a major marine transgression that reworks the surface sediment but preserves the deposits beneath (Glennie, 1970). First-order bounding surfaces and

super-bounding surfaces are important features for correlating aeolian units (Kocurek, 1988).

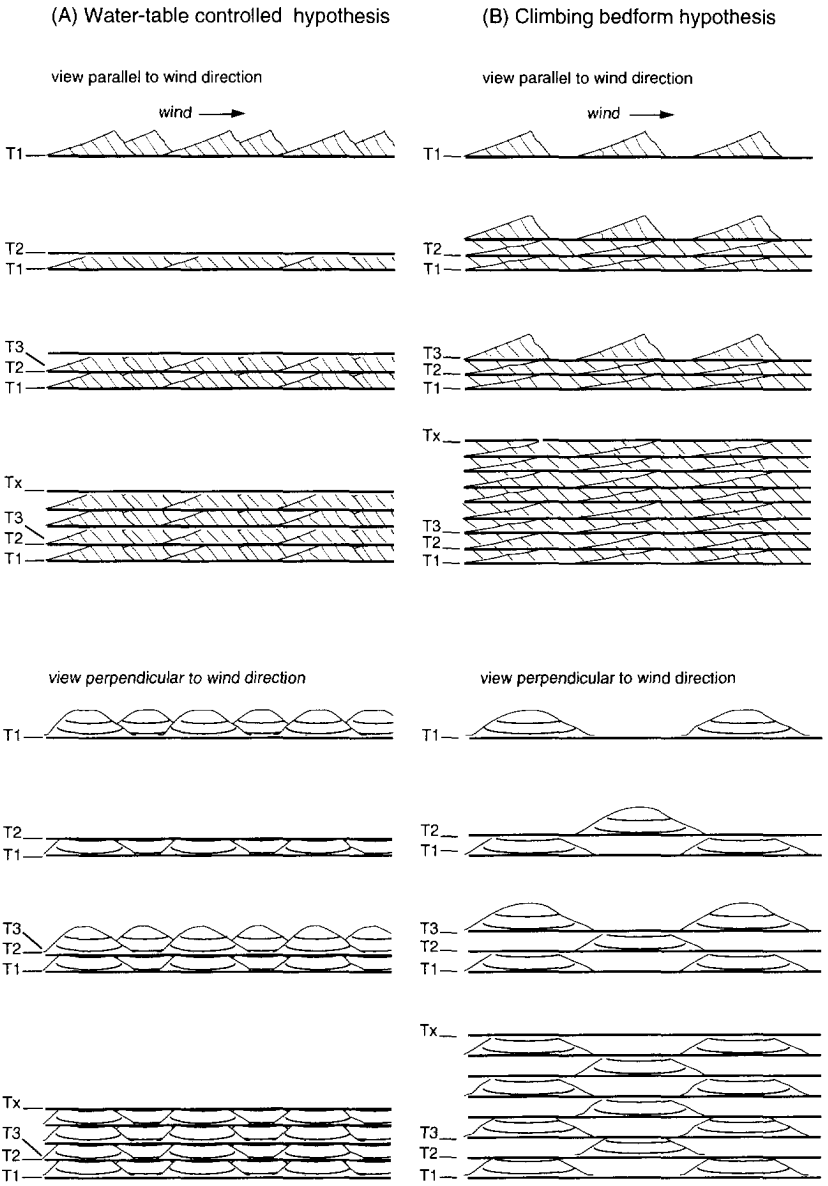

Fig. 2.5.2 *Scheme showing preservation of aeolian deposits by (a) rise of groundwater table and (b) by climbing bedforms, (after Kocurek, 1981). T1, T2 etc. indicate different time steps.*

On the whole it should be stressed that the most important process for preservation of aeolian deposits occurs at basin scale and is due to subsidence. Modern deserts that do not occur in subsiding basins have small preservation potential, while in the rapidly subsiding Rotliegendes Basin preservation potential was very high.

2.6 Previously published mathematical models at bedform scale

Much research has been undertaken at the grain scale, on the physics of saltation (Bagnold, 1941; Anderson, 1987, 1988; Anderson and Haff, 1991; McEwan and Willets, 1991). Anderson (1988) developed his work on saltation to simulate the formation of grain-fall strata at the lee side of a dune. The deposition rate showed a maximum some decimetres from the brink, after which it decreased roughly exponentially (Fig. 2.6.1). The characteristic decay length that results from this exponential formula, was calculated to be of the order of one metre for a typical shear velocity of 0.5 $m \cdot s^{-1}$. This, being less than the slip-face length, leads to oversteepening and avalanching, so that the point where avalanching started could be predicted.

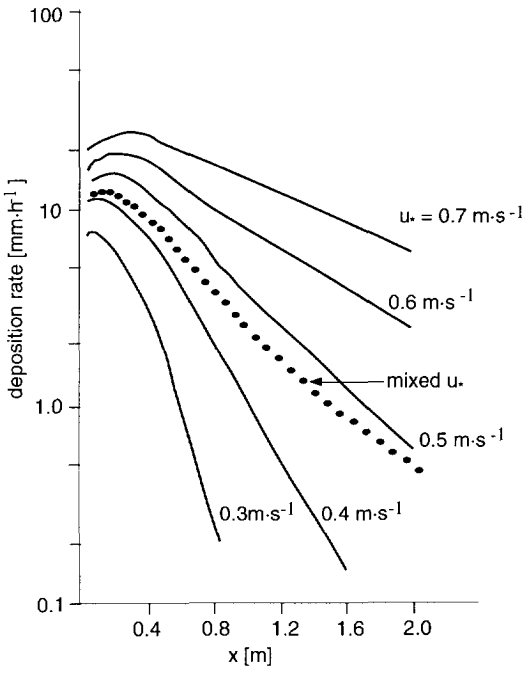

Fig. 2.6.1 *Deposition rates as a function of distance down the lee face, for different shear velocities u∗. Note that the maximum deposition rate occurs some distance after the apex (after Anderson, 1988).*

Hunter (1985) developed a kinematic model for calculating the succession of grain-fall and avalanching occurring at the lee face of a dune. It is a two-dimensional parametric model, where the rate of formation of grain-fall strata is a negative power function of the distance. Assumptions need to be made for the decline rate of this negative power, and also for bedform migration rate, bedform height, avalanching speed and angles. The model gives estimates for proportions of bottomset and foreset deposits, and the ratio of grain-fall and grain-flow strata in the foreset deposits. Structural differences between subaqueous and aeolian lee-side deposits could be reconstructed.

One of the first models to simulate the migration of a dune was developed by Howard et al. (1978). They made a three-dimensional simulation of a barchan dune migrating in equilibrium. A prototype dune was chosen in Salton Sea (California). The velocity field over the topography was obtained from measurements. With this velocity field the sediment transport over the dune was determined using Bagnold's sediment-transport equation (this will be treated in chapter 3) adapted for slopes. The erosion and deposition were calculated and compared to measurements on the real dune. Corrections for surface slope and for the lag between the transport rate and the change in wind velocity were included in the sediment-transport formula, but neither of these two corrections was found to be an improvement. The model by Howard et al. (1978) was the first attempt at quantifying dune morphodynamics. It did not include any fluid-dynamic calculation of the flow field. The flow field was taken from measurements and considered unchanged throughout the simulation. As the dune was assumed to be in equilibrium this approximation is correct. Due to this static flow model, Howard et al. (1978) had to make a somewhat artificial distinction between the influence of the convergence and divergence of the streamlines and of the variations of the shear stress over the dune, which are two related aspects. This means, however, that it is difficult to model the dynamic relationship between flow field and sediment transport, (i.e. changes in dune morphology caused by changes in wind velocity and vice versa). A later model was developed in Howard and Walmsley (1985), using a flow model developed by Jackson and Hunt (1975). Though the results were found encouraging it did not lead to a stable simulation of a dune migrating in equilibrium.

Fisher and Galdies (1988) published the code of a three-dimensional geometrical model for simulating dune migration. The geometry of the plan view of the dune was described with ellipses and parabolae. In the vertical plane the dune was divided into triangular cross-sections. The wind drag was calculated from the wind velocity with the Prandtl-Von Kármán logarithmic profile (see section 3.3). The

sediment transport was determined with a variation of Bagnold's (1941) formula. It is unclear how the rate of advance of the dune was calculated in this model, but it depended on proportionality factors determined by the dune geometry.

The first model to combine actual three-dimensional flow calculations with a sediment-transport formula, was developed by Wipperman and Gross (1986). Flow velocities were calculated for a given topography with a numerical flow model. Erosion and deposition were determined as well as the redistribution of sand at the slipface. Their simulations showed how a conical heap of sand evolved to a barchan dune in equilibrium with the wind regime. Different shapes resulted from high and low wind velocities, the wings of the barchan being much more developed under a high wind velocity. Wind velocity and speed-up factors were compared with the measurements published by Howard et al. (1978) and found to be in good agreement.

Another three-dimensional model was developed by Weng et al. (1991). An important part of their research was concentrated on revising and improving the flow model for the wind velocity over a dune. It was a three-dimensional boundary-layer flow model, based on the theory originally developed by Jackson and Hunt (1975). The flow model simulates flow without boundary-layer separation. Wind velocity and sediment-transport calculations were compared with their measurements over a barchan dune in Oman and also with the measurements by Howard et al. (1978). Their results were considered encouraging.

There are few models that focus on ancient aeolian sandstones. Rubin and Hunter (1982) developed a model for simulating bedclimbing (referred to in section 2.5), from which the strata thickness left by a migrating dune could be determined. Rubin (1987) developed a geometric model to reconstruct ancient bedforms and cross-bedding. Based on input parameters such as bedform spacing, steepness, asymmetry, migration rate and direction, the bedforms were reconstructed from two sets of sinusoidal curves at a different angle, which represented the angle between the migration direction of two sets of bedforms. This model serves as a very helpful tool for understanding the complex three-dimensional geometry of bedforms and cross-bedding that must sometimes be deduced from few sections and limited information in the field.

2.7 Discussion

2.7.1 Concerning the results of field work

From the above summation it can be seen that a huge amount of descriptive field work and measurements has been carried out. This has led to a series of interesting questions and hypotheses that can be tested by fluid-dynamic simulations. The present study focuses on one such an aspect (the interaction of wind flow with topography). On the basis of the results of this study some answers can be given to questions such as: how does a dune evolve from a protodune to an equilibrium state where it advances without changing shape? What are the controls on the growth and migration rates of bedforms? There are still a number of topics of considerable interest that remain to be explained; such as the reason for the regular spacing of bedforms, and why smaller bedforms are incorporated into larger ones. Also, the theory of climbing bedforms (Rubin and Hunter, 1982) is not yet properly understood from a fluid dynamic point of view. An apparent contradiction exists between the assumption of equilibrium bedforms that migrate without significant change of shape so that erosion on the stoss side equals deposition on the lee side, and of bedforms that deposit sediment while climbing.

2.7.2 Concerning the modelling of the physical processes

Most of the work on the physics of aeolian processes has been undertaken at the grain scale (Werner and Haff, 1988; Andersen, 1987, 1990; McEwan and Willets, 1991). This has not been reviewed here because it is not the theme of the present study.

The first models for simulating dune dynamics did not actually calculate the velocity field over the topography and either assumed that the dune is in equilibrium and migrates without changing its shape (Howard et al., 1978) or formulated a geometrical relationship for the sediment deposition (Fischer and Galdies, 1988). Neglecting to account for the influence of topography on flow velocity is a serious limitation when trying to understand the interaction of flow and dune morphology (as would be necessary for some of the questions raised in the previous section). These can be described as simulation models with a static flow field.

A considerable advance was made with the models that included three-dimensional flow calculations dynamically (Wipperman and Gross, 1986; Howard and Walmsley, 1985 and Weng et al., 1991). Of this group, two are based on Jackson and Hunt's (1975) flow model

(Howard and Walmsley, 1985 and Weng et al., 1991). Both presented a short simulation of a dune, giving the flow fields, sediment-transport and migration rates. Howard and Walmsley (1985) had stability problems after about 20 to 30 iterations in a simulation, therefore they were unable to simulate longer time periods. Weng et al. (1991) concentrated mainly on improving the flow model and less on making morphodynamic predictions. In both cases simulations are a "snap shot" of dune dynamics at a given instant. Wipperman and Gross's (1986) model shows a morphodynamic simulation of a conical pile of sand developing to a barchan dune. They used a numerical flow model for their simulations.

It is the purpose of the present study to contribute to the understanding of the physics of flow and bedform evolution in terms of the fluid-dynamic controls of bedform growth and migration. Rather than a detailed calculation of a flow field at a time step (as in Howard and Walmsley, 1985 and Weng et al., 1991), long-term dune behaviour and evolution is modelled. Simulations will be based on analytical rather than on numerical methods (as in the model of Wipperman and Gross, 1986). A complete analytical solution is developed, which makes it more appropriate for understanding the relationships between flow parameters (e.g. wind velocity) and bedform response (migration and growth rates). The generalization of this analytical solution resulted in a simulation model. By including avalanching, the instability encountered by Howard and Walmsley (1985) is partly avoided. The results of the present work should help to test the concepts developed in field observations and also serve as a guideline for improved field measurement campaigns.

2.7.3 Concerning models for ancient aeolian deposits

Finally, the current models that relate modern processes to structures recognizable in ancient sandstones are still based on parametric assumptions (Rubin and Hunter, 1982; Hunter, 1985 and Rubin, 1987), rather than on physical theory. These parametric models improve our insight of the distribution of stratification and bedform shapes, but in this area there is still a great deal of further research to be carried out. It is considered that the model to simulate dune dynamics presented in this study could be developed further to simulate aeolian structures (e.g. grain-size distributions). Specific recommendations for further research by which to achieve this are given in chapter 7. From this it can become a tool for reconstructing ancient formations, though in this respect there is still much work to be done.

Fig. 2.4.5 *Merging barchanoid dunes. Note the formation of ripples parallel to the crest on the stoss side. The lee side shows the grain-flow tongues caused by avalanching. At the toe of the dune wind ripples can be observed again. They were formed prior to the avalanching strata. These ripples are oriented perpendicular to the dune crest, which indicates that the wind direction at that moment differed from the general wind direction responsible for the formation of the dune (photograph taken at the Kelso Dunes, Mojave Desert, California).*

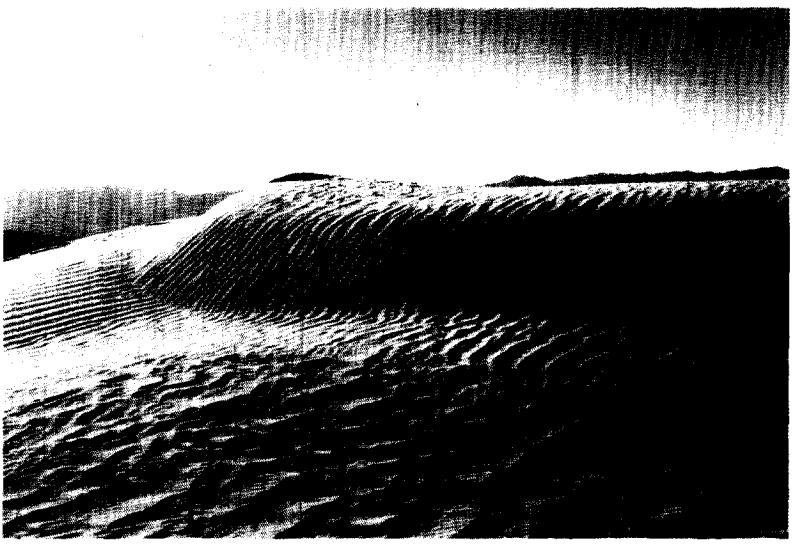

Fig. 2.4.6 *Formation of ripples on a transverse dune. Note that in this case the ripples are oriented perpendicularly to the dune crest and migrate over the lee side of the dune. This indicates that the actual wind direction differed from the general wind direction responsible for the formation of the dune (photograph taken at the Kelso Dunes, Mojave Desert, California).*

Chapter 3

Basic equations and assumptions

3.1 Introduction

In this chapter the basic physical equations needed to describe the dynamics of bedforms will be explained. The main equation to describe bedform dynamics is the sediment-continuity equation, which will be treated in section 3.2. An important part of the sediment-continuity equation is determined by the sediment transport (the sediment in this case being sand). This is generally calculated from a sediment-transport equation, which depends mainly on the flow velocity. Therefore, section 3.3 will treat the fluid-mechanical aspects of flow over a dune. In section 3.4 the sediment-transport aspects are discussed. As an introduction to the sediment-transport processes at the dune scale, a summary of the mechanisms of sediment transport at the grain scale will be given. After this the sediment-transport formulae themselves, used for modelling transport at the dune scale, will be discussed.

3.2 Continuity equation

The basic equation that describes the dynamics of sedimentation is the sediment-continuity equation.

The sediment-continuity equation shows that a change in the rate of sediment transport ∂q_x and ∂q_y during a time lapse ∂t results in a change in topographic height ∂h over an area ∂x ∂y. This is schematized in Fig. 3.2.1. The sediment-continuity equation is expressed as:

$$\frac{\partial h}{\partial t} = -\frac{1}{\sigma}\left(\frac{\partial q_x}{\partial x} + \frac{\partial q_y}{\partial y}\right) \qquad (3.2.1.)$$

Where:

h = topographic height [m]
t = time [s]
σ = sediment density [kg·m^{-3}]
q_x = sediment-transport capacity in the x-direction per unit length in the y-direction [kg·m^{-1}·s^{-1}]

q_y = sediment-transport capacity in the y-direction per unit length in the x-direction [kg·m^{-1}·s^{-1}]

x,y = Cartesian coordinates in the horizontal plane [m]

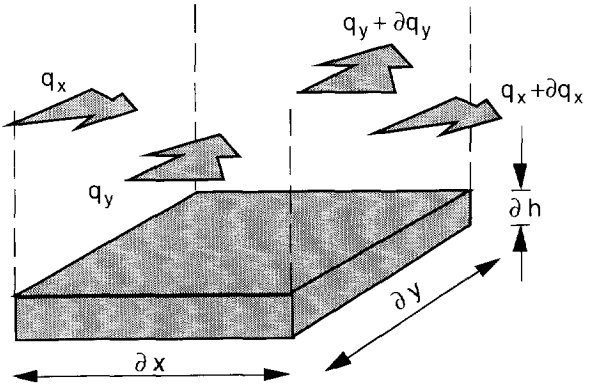

rise of topography = sediment in - sediment out

$$\partial h\, \partial x\, \partial y\, \sigma = -\partial q_x\, \partial y\, \partial t - \partial q_y\, \partial x\, \partial t$$

$$\frac{\partial h}{\partial t}\sigma = -\frac{\partial q_x}{\partial x} - \frac{\partial q_y}{\partial y}$$

Fig. 3.2.1 *Schematization of the sediment-continuity equation.*

If erosion occurs, the change in topography in that time interval $\partial h / \partial t$ will be negative. This means that more sediment leaves the area than enters it, and sediment transport will increase over an interval of space, then the sum of $\partial q_x / \partial x$ and $\partial q_y / \partial y$ will be positive. In the same way, if deposition occurs $\partial h / \partial t$ will be positive so that sediment transport decreases over an interval of space and the sum of $\partial q_x / \partial x$ and $\partial q_y / \partial y$ will be negative. It must be noted that the sediment-transport rates q_x and q_y are height-integrated values, which means the total sediment transport along the vertical height in a specific direction. In this study, the modelling has been simplified to a two-dimensional cross-section with a length in the x-direction and a vertical height in the z-direction, and a one-dimensional sediment-transport rate, which will be designed as $q = q_x$ and $q_y = 0$.

The physical process of sediment transport forms an important part in the sediment-continuity equation. Wind can transport a certain amount of sediment, depending on its flow characteristics (velocity, humidity etc.) and on the sediment parameters (grain size, density etc). The sediment-transport capacity can be considered an equilibrium value, and the air will erode or deposit sediment to maintain this equilibrium

value. If it is assumed that there is always enough sediment available, the real sediment transport can be taken equal to the sediment-transport capacity. This implies that the air is always transporting the maximum amount of sediment that is possible, and thus can be considered saturated. Moreover, it will be assumed that this transport capacity changes immediately when wind velocity changes, so that there is no lag between sediment transport and wind velocity.

3.3 Flow characteristics

In this section the assumptions for fluid-flow modelling will be discussed. This will help to understand the simplifications of the flow models used in chapters 4 and 5. For this purpose, it is also useful to explain several basic concepts in fluid mechanics which are sometimes confused. They refer to laminar and turbulent flow, ideal and real fluids and to the boundary-layer approach.

3.3.1 Laminar and turbulent flow

Flow can be laminar or turbulent. Laminar flow moves in parallel layers, without any macroscopic mixing between them. Turbulent flow is much more chaotic, and the fluid mixes perpendicularly to the mean flow direction. The transition from laminar to turbulent flow depends on the flow velocity and on the shape of the object in or around which the fluid flows. The transition is characterized by the Reynolds number:

$$Re = \frac{u\,L}{\nu} \tag{3.3.1}$$

where:

Re = Reynolds number [dimensionless]
u = flow velocity [$m \cdot s^{-1}$]
L = characteristic length [m]
ν = kinematic viscosity [$m^2 \cdot s^{-1}$]

Below a critical Reynolds number flow is laminar, while above it becomes turbulent. The value of the critical Reynolds number depends on the flow situation (flow through a pipe, around a sphere etc). For flow over a flat plate of length L, the critical Reynolds number is $5 \cdot 10^5$. Most flow occurring in nature is turbulent; this definitely applies to fluids such as water and air. From Eq. (3.3.1) it can be seen that laminar flow would occur only at an extremely low velocity or a high viscosity (e.g. the kinematic viscosity of air at 20°C is $1.5 \cdot 10^{-5}$ $m^2 \cdot s^{-1}$ and that of water is $1.0 \cdot 10^{-6}$ $m^2 \cdot s^{-1}$).

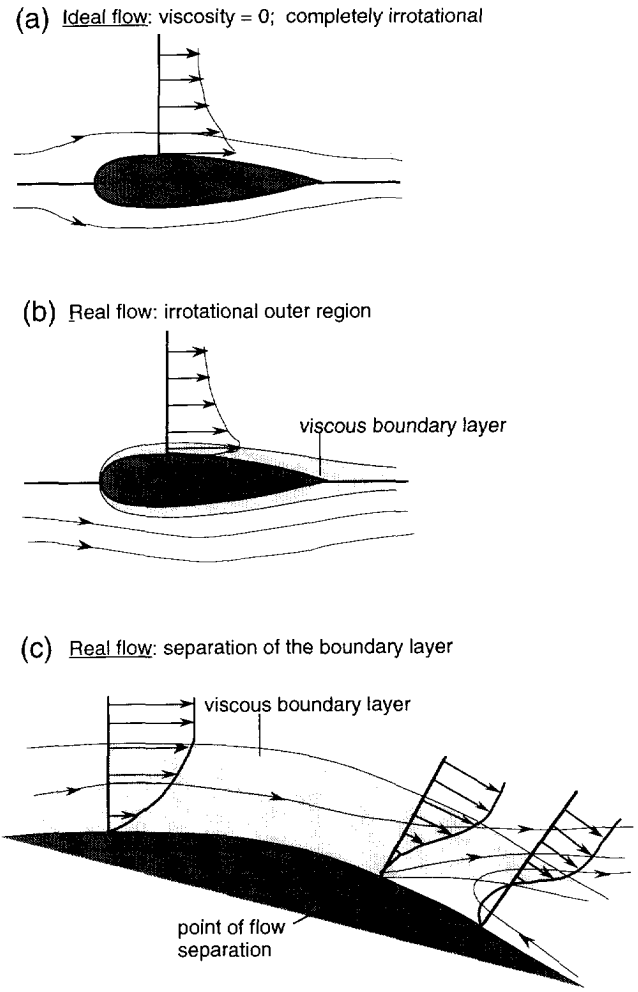

Fig 3.3.1 *Velocity profiles of (a) idealized flow past a solid object; (b) real flow past a solid object; (c) schematization of the separation of the boundary layer.*

By its chaotic nature, turbulent flow is not constant in time, and if the flow velocity were to be measured at a certain point, it would show random variations. In a statistical sense, however, it can be taken as being steady with time (i.e. stationary), so that an average velocity can be considered. In this way, an average velocity profile relative to the height can be considered. The following two sections will treat the average velocity profile in turbulent flow, which does not necessarily show rotation or vorticity.

3.3.2 Ideal and real fluids and the boundary-layer approach

Ideal fluids are those that have no viscosity. They slip past a solid surface, with a non-zero velocity (Fig. 3.3.1a). The theoretical flow behaviour of ideal fluids has been extensively studied and many solution techniques have been developed in the past. Streamlines roughly follow the solid object, and flow is irrotational (it is irrelevant whether flow is laminar or turbulent). Irrotational flows can be solved using the Laplace equation for the velocity potential (they are therefore sometimes called potential flows). The pressure then follows from Bernoulli's equation (this will be treated further in this section). Real fluids, however, have a certain viscosity, due to which they will adhere to the surface of a solid boundary, so that no slip occurs and the velocity at the solid surface is zero (Fig. 3.3.1b). If the viscosity is small, its effect can be confined to a thin layer around the boundary, called the boundary layer. With boundary-layer models, it is assumed that viscosity effects are important in the boundary layer and negligible outside the boundary layer. Outside the boundary layer, therefore, the flow acts as that of an ideal irrotational fluid, and can be solved using potential-flow theory. This irrotational flow solution imposes pressure and velocity on the boundary layer.

With certain shapes of the boundary (e.g. with blunt bodies), or when flow velocities are high enough, the boundary layer separates from the solid body and eddies are formed in the wake (Fig. 3.3.1c). In this case, rotational effects become important throughout the wake zone, and boundary-layer assumptions are not valid any more. Upstream of the point of flow separation, however, boundary-layer theories are still a good approximation of the flow behaviour.

3.3.3 The logarithmic velocity profile

A fully developed boundary layer of turbulent flow over a solid surface parallel to the flow has a logarithmic velocity profile (as was deduced by Prandtl and his pupil Von Kármán):

$$u(\Delta z) = \frac{u_*}{\kappa} ln \frac{\Delta z}{z_r} \qquad (3.3.2)$$

where:

$u(\Delta z)$	=	flow velocity [m·s^{-1}] at Δz [m]
u_*	=	shear velocity [m·s^{-1}]. Bagnold (1941) called this the friction velocity or drag velocity
κ	=	Von Kármán constant (=0.4)

z_r = roughness length [m], determined by the roughness of the surface. For a horizontal surface, $z_r = d/30$ is usually taken (Bagnold, 1941 p.50), where d [m] is the average grain diameter

Δz = height above the topography [m]

The shear velocity of the flow is defined as:

$$u_* = \sqrt{\frac{\tau}{\rho}} \tag{3.3.3}$$

where

τ = shear stress [Pa]

ρ = fluid density [kg·m^{-3}]

The shear velocity is a very important parameter. It has the same dimension as the velocity, but it does not have a physical meaning. Its importance comes from the fact that it characterizes the fluid velocity independently of its height of measurement. The velocity profile (Eq. (3.3.2)) for the wind is therefore completely defined by a wind characteristic (u_*) and a characteristic of the surface over which it blows (the surface roughness, z_r).

3.3.4 Qualitative analysis of airflow over a dune

In the preceding two sections it has been explained that a fully developed boundary layer in a turbulent flow over a flat solid surface has a logarithmic velocity profile, and that above this boundary layer the flow velocity can be calculated from irrotational flow theory. In this section the effect that a dune topography has on the boundary layer will be discussed. This gives a first qualitative analysis of the behaviour of the wind velocity and pressure over a dune topography.

To determine irrotational steady flow, the Euler equation for inviscid steady flow can be used. The Euler equation is obtained from the Navier-Stokes equation of motion, by assuming that the fluid is incompressible and its viscosity negligible.

$$-\frac{1}{\rho}\frac{dp}{dx} = U\frac{dU}{dx} \tag{3.3.4}$$

where:

ρ = fluid density [kg·m^{-3}]

p = fluid pressure [Pa]

U = flow velocity at the upper edge of the boundary layer [m·s^{-1}]

or from its integral form which is Bernoulli's law:

$$p + \frac{1}{2}\rho U^2 = \text{constant} \tag{3.3.5}$$

Figure 3.3.2a illustrates the flow over a dune. On the stoss side of the dune, before the apex, the streamlines converge and acceleration occurs. According to Eq. (3.3.4) or (3.3.5) pressure will decrease, so that $dp/dx < 0$. This is called a favourable pressure gradient because the pressure gradient aids the flow in its motion. On the lee side the stream lines diverge again, flow decelerates so that pressure increases, and $dp/dx > 0$. This is called an adverse pressure gradient because the pressure gradient opposes the flow. Figure 3.3.2.b illustrates the velocity profiles that correspond to this flow. If the adverse pressure gradient is large enough the flow reverses direction, and separation of the boundary layer occurs (as in Fig. 3.3.1c).

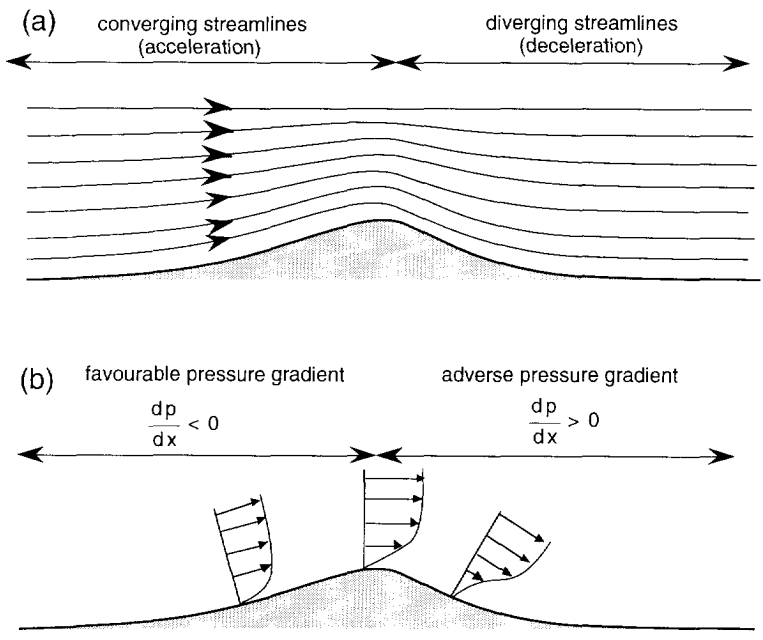

Fig. 3.3.2 *Scheme showing (a) air flow over a dune; (b) velocity profiles of the boundary layer with favourable and adverse pressure gradients.*

3.4 Sediment transport

Sediment grains are transported by wind. As an introduction to the sediment-transport equation, this section will start by giving a review of the sediment-transport mechanisms at the grain scale. The total mass flux of all the sediment grains is expressed in a sediment-transport equation. A great amount of research has been directed to developing expressions for the calculation of sediment transport as a function of wind velocity. One of the first transport equations was Bagnold's (1941 p.67). Most other formulae were later developed from the same basic ideas. Bagnold's formula is still the one which is most frequently used, and it has also been applied in this research. Therefore, this will be treated more extensively. A short discussion of other transport formulae will be given later in this section.

3.4.1 Sediment-transport mechanisms

Sediment is transported by fluids (air or water) through three mechanisms: suspension, saltation and surface creep (Bagnold, 1941, p.37). Sediment transported by suspension forms the suspended load, while sediment transported by saltation and surface creep forms the bed-load. Bagnold (1941), through his experimental work, made a significant contribution to the understanding of grain mechanics. Recently however, there has been considerable progress in this field (for an overview see Anderson et al., 1991).

Suspension occurs when a sediment particle is completely surrounded and carried by a fluid (air or water). This mode of transport is more important in water than in air. The reason for this being the difference in density between the two fluids, due to which the drag force exerted on a sediment grain by water will be much higher than by air. The particle in air will have a smaller buoyancy than in water, so that only the smallest particles will be transported by air. Transport through suspension is of lesser importance in beach and desert environments (Bagnold, 1941; Illenberger and Rust, 1988) although it plays a dominant role in loess deposits (Reading, 1986).

Saltation is generally better developed in air than in water. It is the most important transport mechanism for sediment by wind. Saltation is a bouncing motion (Fig. 3.4.1), where a sediment particle is projected into the air by the momentum transmitted to it by another particle. After receiving this momentum, the sediment particle rises in the air, once free of the bed it is accelerated more easily by the wind and carried for a small distance after which it strikes the ground again. On striking the ground, part of the energy it has received by the air is spent in ejecting other particles in the same type of movement. There has been

some controversy whether the initial impulse that makes a grain rise in saltation is air lift (Williams et al., 1990) or the impulse from other saltating grains (Rumpel, 1985; Anderson, 1987 and Werner and Haff, 1988). Recent research indicates that it seems probable that, in the absence of any other disturbance, particles are set in motion by the wind, presumably some are lifted aerodynamically and others are pushed forward by the wind before they take off (Nickling, 1988; Anderson et al., 1991 and Willetts et al. 1991). Within seconds a steady state is reached and air lift is rare (Anderson and Haff, 1988).

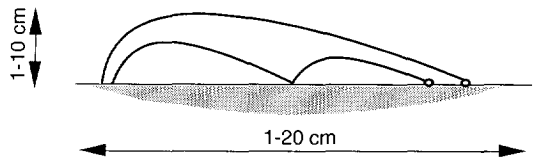

Fig. 3.4.1 *Typical saltation trajectories of sand grains in air (after Bagnold, 1941).*

Sand grains can move forward under the force of impact of the bombarding grains, without being affected by the wind. Bagnold (1941) calls this surface creep, judging it to be a quarter of the sediment load. Anderson et al. (1991) sharpen this definition and distinguish between reptation and surface creep. Reptating grains are those that do not have enough energy to eject other grains. They form an important part of the cloud of sand in transport but contribute little to the actual transport rate itself due to their short jump lengths (Anderson et al., 1991). Surface creep is the transport mode where gravity forces and forces from the contacts between grains dominate over forces from the fluid (e.g. due to the rearrangement of the sand-bed caused by the saltation and the grains rolling off the lee side of ripples).

3.4.2 Bagnold's sediment-transport formula

Effect of saltating sand on the wind velocity

According to Prandtl's logarithmic profile, the velocity of wind over a flat surface varies logarithmically with the height. Bagnold noted that the logarithmic velocity profile was affected by the saltating sand, and he quantified this effect by including the threshold velocity of the sand grains as follows:

$$u(\Delta z) = \frac{u'_*}{\kappa} ln \frac{\Delta z}{z'_r} + u_{thr} \qquad (3.4.1)$$

where:

u'_* = saltation shear velocity [m·s^{-1}]

z'_r = roughness length during saltation, which is greater than the roughness length (z_r) of a fixed surface (i.e. a surface without saltation). It is understood that Bagnold used the ripple height [m]

u_{thr} = threshold velocity [m·s^{-1}]

The shear velocity during saltation was defined as:

$$u'_* = \sqrt{\frac{\tau'}{\rho}} \tag{3.4.2}$$

Where

τ' = shear stress due to saltation [Pa]

The threshold velocity of a sand grain at a height Δz can be obtained from its threshold shear velocity by applying Eq. (3.3.2). The threshold shear velocity, for $d > 0.1$ mm, is given by (Bagnold, 1941):

$$u_{*thr} = A_t \sqrt{\frac{\rho_s - \rho}{\rho} g\, d} \tag{3.4.3}$$

where:

u_{*thr} = threshold shear velocity of a given grain size [m·s^1]

A_t = constant [dimensionless].
= 0.1 to initiate saltation (called the fluid threshold)
= 0.08 to maintain saltation (called the impact threshold)

ρ_s = grain density [kg·m^{-3}]

g = gravitational acceleration = 9.81 m·s^{-2}

d = grain diameter [m]

The effects of the velocity profile for saltating sand in comparison to the normal logarithmic velocity profile, are illustrated in Fig. 3.4.2. The effect of the saltation is an increased roughness. The impact threshold shear velocity is the minimum velocity necessary to keep saltation going. At this velocity both profiles (with and without saltation) coincide. The fluid threshold velocity is the minimum necessary to dislodge a grain from its position (and so to initiate saltation). This must necessarily be higher than the impact threshold velocity. The distinction between the two threshold velocities is due to Bagnold (1941), and is important when considering the initiation of saltation. The fluid threshold velocity, however, does not have any further consequences for this study on modelling bedforms, as saltation in this case is considered as a continuous process.

The sediment-transport equation

The basic form of Bagnold's transport equation is:

$$q = C_1 \sqrt{\frac{d}{D}} \frac{\rho}{g} u'^3_* \tag{3.4.4}$$

Where:

q	=	sediment-transport capacity [kg·m^{-1}·s^{-1}]
C_1	=	an empirical dimensionless constant which is equal to: 1.5 for nearly uniform sands 1.8 for naturally graded sands as found in dunes 2.8 for sands with a very wide range of grain sizes
D	=	grain diameter of a standard 0.25 mm sand [m]

This equation was derived by considering the kinematics of saltation, and by including the surface creep as a fraction of the saltation load. The dependency on the square root of the grain diameter was derived empirically.

By including the modified velocity profile Eq. (3.4.1), Bagnold included the effect of the threshold velocity:

$$q = C_2 \sqrt{\frac{d}{D}} \frac{\rho}{g} \left(u(\Delta z) - u_{thr}\right)^3 \tag{3.4.5}$$

where

$$C_2 = C_1 \left(\frac{\kappa}{ln\left(\frac{\Delta z}{z'_r}\right)} \right)^3 \tag{3.4.5a}$$

This form of the transport equation permits us to quantify the effects of different grain sizes. Larger grains have higher threshold velocities, so the transport capacity for that diameter will be lower. As an example, we can consider a case where wind of a constant velocity passes from a surface covered with fine sand to a surface covered with coarser sand. In the first place there will be a change in surface roughness, which will affect the velocity profile Eq. (3.3.2) where z_r will increase so that the logarithm will decrease. This effect is only noted some distance downstream of the change. The major effect is that the coarser grains have a higher threshold velocity, so that the transport capacity will decrease. The excess of sand will be deposited. It is important to note that when using the transport equation as in Eq. (3.4.5), it is only valid for horizontal surfaces, where the logarithmic velocity profile as in

Eq. (3.3.2), or its modified form Eq. (3.4.1), applies. The transport equation in the form of Eq. (3.4.4) using the shear velocity is independent of any determinate velocity profile. It is therefore much more generally applicable.

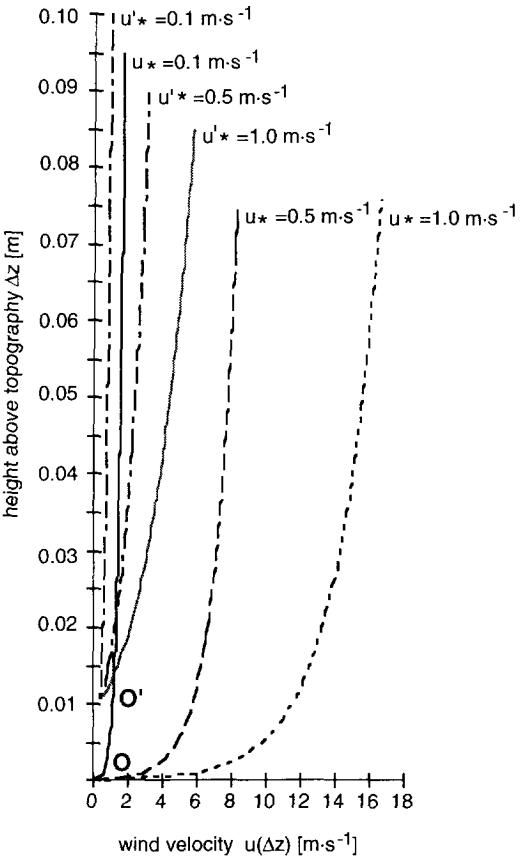

Fig. 3.4.2 *Logarithmic velocity profiles for different shear velocities, with and without the effect of saltation. The variation of wind velocity with height according to the logarithmic velocity profile has been indicated with u*. These profiles have been calculated with Eq. (3.3.2), assuming a surface roughness of 0.1 mm (an order of magnitude corresponding to sand grains). Velocities converge at this focal point (O). The velocity profile modified by Bagnold (1941) to account for saltation, is also shown for the same shear velocities, and indicated with u'* . These profiles have been calculated with Eq. (3.4.1), assuming a surface roughness of 10 mm (an order of magnitude corresponding to the ripple height) and a threshold velocity of 0.4 m·s^{-1} . These profiles converge at a higher focal point (O'), which is the effect of the increased surface roughness. The slight shifting to the right of the focal point is the effect of the threshold velocity.*

3.4.3 Other sediment-transport formulae

Many other sediment-transport formulae were later developed. An overview has been given in Table 3.4.1. Horikawa et al. (1983) and also Sarre (1988) divide the sediment-transport formulae into three categories: a) those where sediment transport is calculated as a simple function of wind velocity, b) those where sediment transport is a function of shear velocity and c) those that include the effect of a minimum threshold shear velocity.

Sediment transport as a function of wind velocity:
These are the most simple expressions, empirical formulae that are straightforward correlations between wind velocity occurring at a datum height and the resulting sediment transport (O'Brien and Rindlaub, 1936 and Borówka, 1980).

Sediment transport as a function of shear velocity:
This category concerns expressions that, like Bagnold's, are based on the shear velocity $u'*$ (Zingg[1], 1953; Williams, 1964 and Hsu, 1971, 1973). Their major disadvantage is that they always result in a positive sediment transport, even for velocities under the threshold velocity.

Sediment transport including the effects of a threshold shear velocity:
The third category of sediment-transport formulae (Kawamura[2], 1951; Lettau and Lettau, 1977 and White, 1979) concern those expressions that include the threshold velocity. Shear velocities below a threshold shear velocity result in negative sediment transports. An extra condition is usually included so that the sediment transport is zero for shear velocities below threshold shear velocity.

3.4.4 Discussion of sediment-transport formulae

When applying empirical or semi-empirical formulae, it is important to distinguish under what conditions they have been derived and calibrated. These formulae can be divided into those derived from wind-tunnel studies (Bagnold, Zingg, Williams and White) and those derived from measurements of sediment transport on beaches (O'Brien and Rindlaub, Borówka, Lettau and Lettau, and Hsu). Formulae derived from wind-tunnel studies must necessarily have scale inaccuracies because it is virtually impossible to incorporate the effect of large-scale turbulence in a wind-tunnel simulation. They have, however, the advantage of isolating the phenomenon of sediment transport through wind without including influences of changing atmospheric conditions

[1] from Sarre (1988)
[2] from Horikawa et al. (1983)

(air humidity, temperature etc.). In formulae derived from beach studies, sediment-transport capacity is influenced by the capillary forces on the moist surface layers of a wet beach (Svasek and Terwindt, 1974). Sarre (1988) also observes this to happen when the moisture level is above 14% in the top 2 mm .

The transport capacity has been calculated with the formulae of Table 3.4.1, and is shown in Figs. 3.4.3a and 3.4.3b. Borówka's (1980) formula has not been included because it was expressed as sediment transport per unit surface-area instead of per unit width ($kg \cdot m^{-2} \cdot s^{-1}$ instead of $kg \cdot m^{-1} \cdot s^{-1}$) and it was derived as a linear regression from measurements over a small surface (only 20 cm^2). Therefore it was considered that by adapting the formula and including it in Figs. 3.4.3a,b it would not be compared objectively with the other formulae. The transport capacity according to O'Brien and Rindlaub's (1936) formula has been computed using the velocity according to Eq. (3.3.2). The threshold shear velocities come from Eq. (3.4.3). Calculations have been made for one grain diameter (0.25 mm). It can be seen that the highest values are obtained with Lettau and Lettau's formula, and the lowest with William's formula. Figure 3.4.3b shows the transport capacity for a wide range of shear velocities (up to 1 $m \cdot s^{-1}$ which is equal to a wind velocity of about 16 $m \cdot s^{-1}$ measured at 1 m height). It can be seen that there are three groups of formulae, giving a high, a middle and a low estimate of sediment transport. The high estimates are given by Lettau and Lettau, Kawamura and White. Middle values are given by the formulae of Bagnold and Zingg. Finally the low estimates are given by O'Brien and Rindlaub, Williams and Hsu.

Sarre (1988) evaluates all the cited formulae with measurements on Saunton Sands beach (South West England). He concludes that Bagnold's, Zingg's and Hsu's formulae all underestimate sediment-transport capacity. These are all formulae depending on shear velocity only. Kawamura, Lettau and Lettau and specially White (whose expressions include a threshold-velocity term) give the most accurate estimates. Howard et al. (1978) also state that the largest inaccuracy occurs at wind velocities near the threshold velocity. At those velocities, sediment transport is underestimated by the formulae derived by Bagnold, Zingg and Williams (all wind-tunnel derived formulae as a function of shear velocity) and is better predicted by Lettau and Lettau (who include a threshold velocity term). Horikawa et al. (1983) compare Bagnold's and Kawamura's formulae up to very high shear velocities (ranging from 0.6 to 3 $m \cdot s^{-1}$). They conclude that the predictions of both formulae are accurate for well sorted sands, but underestimate the transport for widely distributed grain diameters under high velocities. Svasek and Terwindt (1974) compare Bagnold's and Kawamura's formulae with measurements on a Dutch beach,

deriving the best fit by changing their coefficients. They state that close to threshold velocities of $u*_{thr} = 0.4$ m·s^{-1} both formulae give great discrepancies with their measurements. They attribute this to the capillary forces of moist beaches.

Table 3.4.1 *Overview of sediment-transport formulae*

author	sediment-transport formula	comments
O'Brien and Rindlaub (1936)	$q = C\,u^3$ $C = 2.1873 \cdot 10^{-5} kg \cdot s^{-2} \cdot m^{-4}$ u measured at 1.524m	beach measurements dependent on u
Bagnold (1941)	$q = C \sqrt{\frac{d}{D}} \frac{\rho}{g} u'^3_*$ generally $C = 1.8$ [-]	wind-tunnel derived dependent on $u'*$
Kawamura (1951) ([1])	$q = C \frac{\rho}{g} (u'_* + u_{*thr})^2 (u'_* - u_{*thr})$ $C = 2.78$ [-]	wind tunnel derived includes $u*_{thr}$ term
Zingg (1953) ([2])	$q = C \left(\frac{d}{D}\right)^{0.75} \frac{\rho}{g} u'^3_*$ $C = 0.83$ [-]	wind-tunnel derived dependent on $u'*$
Williams (1964)	$q = A \frac{\rho}{g} u'^B_*$ $A = 0.1702$ [-] $B = 3.4222$ [-]	wind-tunnel derived dependent on $u'*$
Hsu (1971)	$q = C\ Fr^3 = C \left(\frac{u'_*}{(\rho g)^{0.5}}\right)^3$ $C = exp\left(-0.47 + 4.97 \cdot 10^{-3} d\right) 10^{-1} kg \cdot m^{-1} \cdot s^{-1}$	Ecuadorian beach dependent on $u'*$
Lettau and Lettau (1977)	$q = C \sqrt{\frac{d}{D}} \frac{\rho}{g} (u'_* - u_{*thr}) u'^2_*$ $C = 4.2$ [-]	includes $u*_{thr}$ term
White (1979)	$q = C \frac{\rho}{g} u'^3_* \left(1 - \frac{u_{*thr}}{u'_*}\right) \left(1 + \frac{u^2_{*thr}}{u'^2_*}\right)$ $C = 2.61$ [-]	wind tunnel derived includes $u*_{thr}$ term
Borówka (1980)	$Q = C\,u^{4.68}$ $[kg \cdot m^{-2} \cdot s^{-1}]$ $C = 2.5 \cdot 10^{-6}$ u measured at 1m	calculates the sediment transport per m^2 (Q) Baltic beaches dependent on u

([1]) from Horikawa et al. (1983). ([2]) from Sarre (1988).

q = sediment-transport capacity [kg·m^{-1}·s^{-1}];
Q = sediment-transport capacity per surface unit [kg·m^{-2}·s^{-1}]; C = general constant in sediment transport formulae [variable]; Fr = Froude number; ρ = air density [kg·m^{-3}]; g = gravitational acceleration = 9,81 [m·s^{-2}]; d = grain diameter [m]; D = diameter of standard 0.25 mm sand [m]; $u*_{thr}$ = threshold shear-velocity [m·s^{-1}]; $u'*$ = saltation shear velocity [m·s^{-1}]; u = wind velocity [m·s^{-1}].

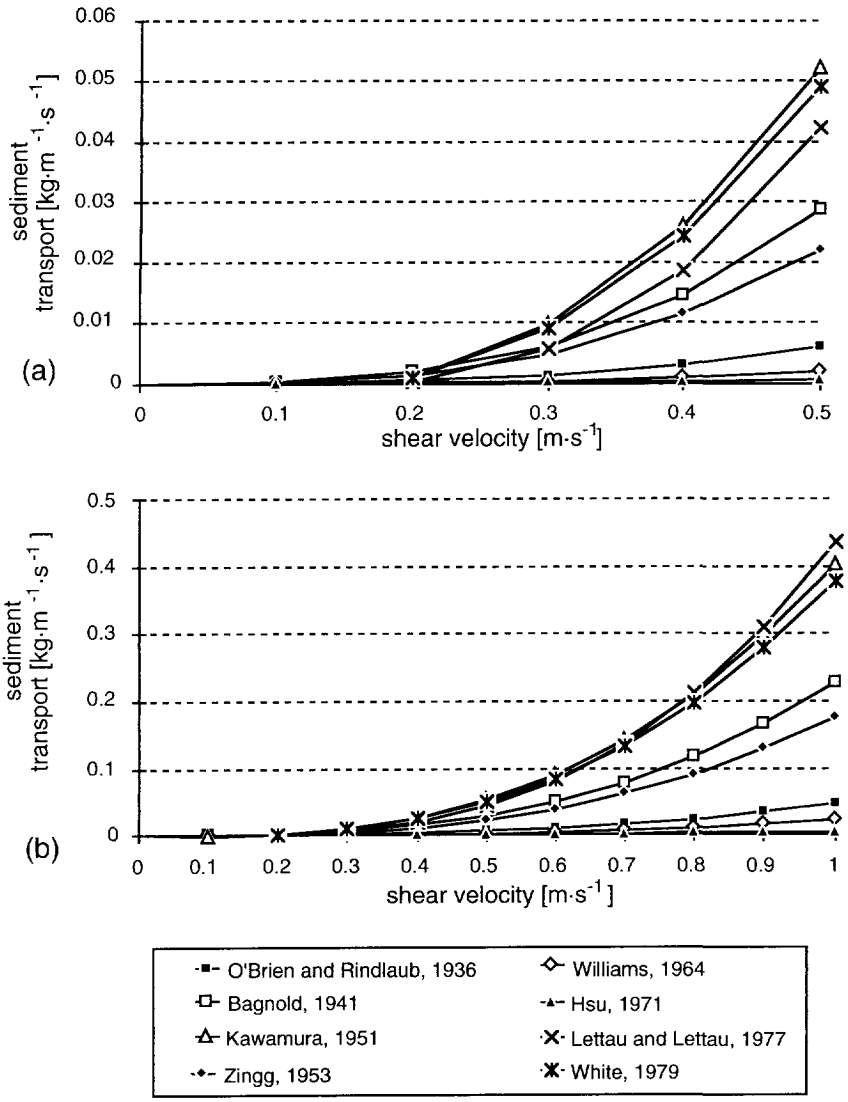

Fig. 3.4.3 *Sediment-transport capacity according to different sediment-transport formulae for (a) moderate shear velocities; (b) high shear velocities.*

In the present study Bagnold's transport formula has been used because it is the most popular one. Although it may underestimate the sediment-transport capacity, there are no clear arguments favouring one of the other specific formulae. Furthermore, considering the recent development of research on the physics at the grain scale (Anderson and Haff, 1991), it can be expected that more accurate expressions for the

sediment transport capacity will be developed in the near future. It should also be considered that the important parameter for erosion and deposition is the spatial derivative of the sediment-transport capacity (Eq. (3.2.1)). This means that the difference of sediment transport from one point to another (which is mainly determined by the wind velocity) is more important than the concrete value itself. It is also important to use a formula that depends on the shear velocity and not on the velocity measured at a specific height, because the shear velocity is a characteristic parameter of the velocity profile, and independent of the height of measurement. This is why Bagnold's original version of the transport formula given in Eq. (3.4.4) has been preferred to Eq. (3.4.5), even though it does not contain an explicit threshold velocity term. It can be considered that this equation is applicable when saltation occurs which is above the threshold shear velocity (Eq. (3.4.3.)). Below the threshold shear velocity the sediment transport capacity would be zero.

Chapter 4

Bedform migration

4.1 Introduction

In the previous chapter it has been explained that the basic equations describing the system of moving bedforms in a flow field are the sediment-continuity equation and the sediment-transport equation, which, for the one-dimensional case, can be written as:

$$\frac{\partial h(x,t)}{\partial t} = -\frac{1}{\sigma}\frac{\partial q(x,t)}{\partial x} \tag{4.1.1}$$

and

$$q(x,t) = f(\tau(x,t)) \tag{4.1.2}$$

This system of equations forms a model for describing the evolution of the topography through time. Though sediment transport depends on many factors (e.g. humidity, grain diameter) it is mainly determined by the wind velocity (or a related parameter such as the shear stress). If we consider the wind velocity as a steady flow (i.e. that the wind blows at a constant rate through time), the local variations of the wind velocity (i.e. the convective acceleration) will depend only on the topography. In that case the sediment-transport capacity could directly be written as a function of the topography (i.e. $q(x,t)$ would be a unique function of $h(x,t)$). In that case Eq. (4.1.2) can be substituted in (4.1.1) giving one partial differential equation (PDE) for $h(x,t)$. In physics, this type of PDE describes vibrating systems and wave motions (hyperbolic PDEs). A PDE contains partial derivatives of a function depending on more than one variable, such as the topographic height $h(x,t)$, which depends on time t and space x. Many laws of physics are expressed in PDEs, and mostly these laws describe physical phenomena by relating time-and-space derivatives. The objective of this chapter is to show that by making simple assumptions for the shear stress and for the sediment-transport capacity, simple models can be obtained that explain a number of characteristics of migrating bedforms. This also helps to distinguish between the effects of the non-linear sediment-transport formula and the effects of the flow model. Furthermore, these simple models are useful to test the numerical programme for dune simulations (used later in chapters 5 and 6).

4.2 Simple wave approximation

The simplest mathematical assumption that can be made for Eq. (4.1.2) is that the sediment transport varies linearly with the shear stress:

$$q(x,t) = q_0 + A_1 \tau(x,t) \tag{4.2.1}$$

where q_0 is a constant basic sediment-transport and A_1 the linearity constant. If topographic variations are relatively small, we can generally state that the shear stress is formed of a constant basic term (τ_0), and a correction term (τ_1) that varies with space and time:

$$\tau(x,t) = \tau_0 + \tau_1(x,t) \tag{4.2.2}$$

If, in a first approximation, this correction is assumed to be linear with the topographic height:

$$\tau_1(x,t) = A_2 h(x,t) \tag{4.2.3}$$

the sediment-transport equation becomes:

$$q(x,t) = q_0 + A_1 \tau_0 + A_3 h(x,t) \tag{4.2.4}$$

where:
$A_3 = A_1 A_2$

Taking the derivative of Eq. (4.2.4) we obtain:

$$\frac{\partial q(x,t)}{\partial x} = A_3 \frac{\partial h(x,t)}{\partial x} \tag{4.2.5}$$

which, substituted in the continuity equation becomes:

$$\frac{\partial h(x,t)}{\partial t} + \frac{A_3}{\sigma} \frac{\partial h(x,t)}{\partial x} = 0 \tag{4.2.6}$$

This is called the simple wave equation, and it describes the propagation of a wave at constant velocity. The ratio

$$c = \frac{A_3}{\sigma} \tag{4.2.6a}$$

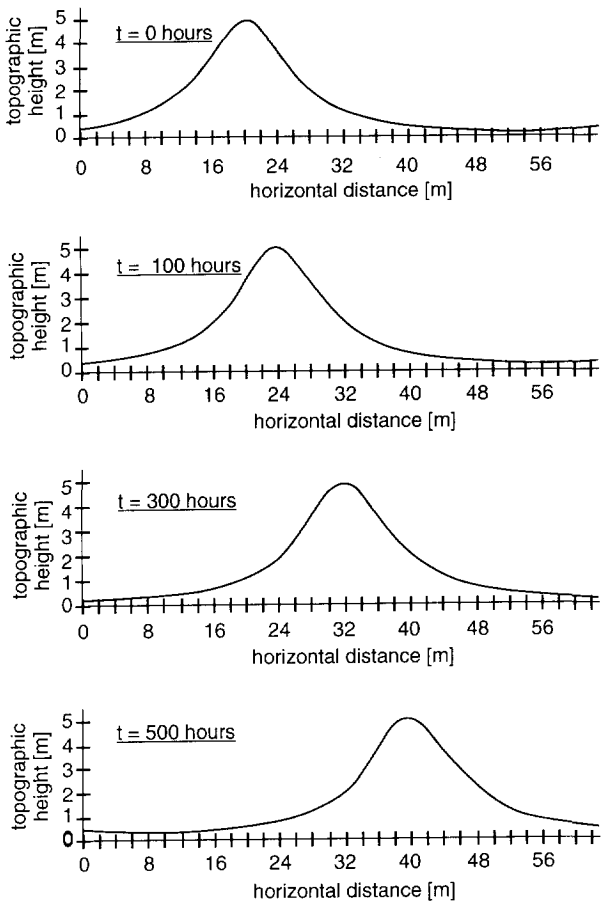

Fig. 4.2.1 *Migration of a simple wave. The simple-wave equation, in this case, results from combining a linear shear stress and a linear sediment-transport formula. The specific values used in this example are given in Table 4.4.1.*

is generally called the wave velocity or celerity. In this case, which concerns the morphodynamics of dunes, this is equal to the migration rate (a term that will be used from here on). The wave will advance at a constant rate c without changing its shape. Formally the solution of Eq. (4.2.6) is given by:

$$h(x,t) = f(x - ct) \tag{4.2.7}$$

Equation (4.2.7) expresses that at a certain point x at a certain time t the topography will have the same height as it had at the start (at t=0) at a point $(x\text{-}ct)$. The topography can be any function of $(x\text{-}ct)$. An example is shown in Fig. 4.2.1. It is important to note that this is a

simplified two-dimensional model, which is acceptable when the reality can be schematized to two dimensions. This is essentially the case in transverse dunes. Other type of dunes (barchans, longitudinal dunes) result from a three-dimensional interaction beteen wind and topography, and cannot be schematized in a two-dimensional model.

4.3 Kinematic wave approximation

A second approximation can be made by using a sediment-transport formula instead of a linear relationship with the shear stress. Bagnold's formula can be taken:

$$q(x,t) = C_B \ \tau(x,t)^{3/2} \tag{4.3.1}$$

The constant C_B [$s^2 \cdot m^{1/2} \cdot kg^{-1/2}$] groups Bagnold's constants and grain parameters.

If the linear shear stress Eqs. (4.2.2) and (4.2.3) are still assumed, we obtain:

$$q(x,t) = C_B\left(\tau_0 + A_2 h(x,t)\right)^{3/2} \tag{4.3.2}$$

and

$$\frac{\partial q(x,t)}{\partial x} = \frac{3}{2} C_B\left(\tau_0 + A_2 h(x,t)\right)^{1/2} A_2 \frac{\partial h(x,t)}{\partial x} \tag{4.3.3}$$

so that:

$$\frac{\partial h(x,t)}{\partial t} = -\frac{3}{2}\frac{C_B}{\sigma} A_2\left(\tau_0 + A_2 h(x,t)\right)^{1/2} \frac{\partial h(x,t)}{\partial x} \tag{4.3.4}$$

If this expression is compared with the simple wave equation Eq. (4.2.6) it can be seen that the migration rate is not a constant but a more complicated expression that varies with the topographic height:

$$c = \frac{3}{2}\frac{C_B}{\sigma} A_2\left(\tau_0 + A_2 h(x,t)\right)^{1/2} \tag{4.3.5}$$

This means that the dune advances while changing shape. From the form of Eq. (4.3.5) we see that the migration rate increases with height, which means that the top of the dune will advance more rapidly than the base. The lee side of the dune will tend to become steeper and the peak

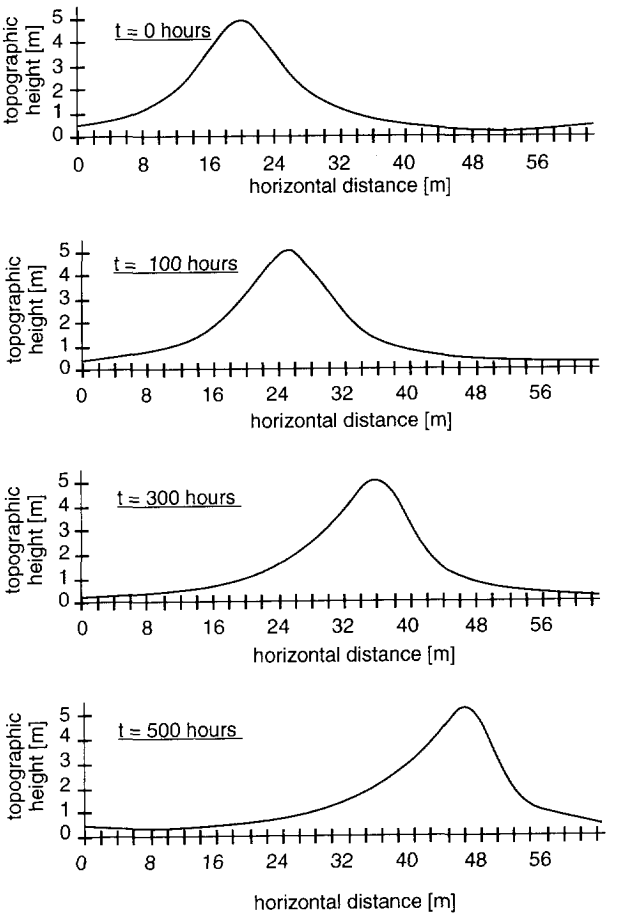

Fig. 4.3.1 *Migration and deformation of a kinematic wave. The kinematic-wave equation, in this case, results from combining a linear shear-stress model and Bagnold's sediment-transport formula. The specific values used in this example are given in Table 4.4.1.*

will eventually overtake the slipface (Fig. 4.3.1). According to this mathematical solution, after a certain time, the peak will completely hang over the base. In reality, however, the maximum angle of repose for sediment will be surpassed and avalanching will occur at the slipface, limiting this asymmetrical shape. This is a well known type of equation called a breaking-wave equation (because of this behaviour of the solution). The behaviour of the solution will be similar for any non-linear sediment-transport equation (as given in section 3.3), as long as $\partial c(h)/\partial h > 0$ (or as long as the peak has a higher velocity than the base). This example illustrates that the deformation of a bedform in a

"dune-like shape" is partly due to the non-linear relationship between sediment transport and shear stress.

4.4 On the linearizations

The two models presented in the previous sections have been made under the assumption that the sediment transport and/or the shear stress only varies slightly. Such cases can be simplified to a linear expression by linearizing them. Any function $f(y)$ can be linearized by using a Taylor expansion according to:

$$f_l(y) = f(a) + \left(\frac{df(y)}{dy}\right)_a (y-a) + E \qquad (4.4.1)$$

where $f_l(y)$ is the linearization of the function $f(y)$ in point a . The error E is of the order:

$$E = \frac{1}{2}\left(\frac{d^2 f(y)}{dy^2}\right)_\xi (y-a)^2 \qquad \xi = a+\gamma(y-a) \quad 0<\gamma<1 \qquad (4.4.2)$$

4.4.1 The linear sediment-transport model

Sediment-transport equations are generally nonlinear in velocity or shear stress, as has been presented in section 3.4. Bagnold's formula contains the shear stress to the power 3/2 or the shear velocity to the third power. The linearization can be applied to Bagnold's sediment-transport formula to express it as a linear function of the shear stress. The formula expressed in terms of the shear stress is:

$$q = C_B\, \tau(x,t)^{3/2} \qquad (4.4.3)$$

where C_B [$s^2 \cdot m^{1/2} \cdot kg^{-1/2}$] groups the constants and grain parameters according to:

$$C_B = C_1 \frac{1}{g\sqrt{\rho}} \sqrt{\frac{d}{D}} \qquad (4.4.3a)$$

With $\tau(x,t) = \tau_0 + \tau_1(x,t)$ this can be linearized to:

$$q_l(\tau) = C_B\, \tau_0^{3/2} + \frac{3}{2} C_B\, \tau_0^{1/2} \tau_1(x,t) \qquad (4.4.4)$$

This equation is similar to Eq. (4.2.1) in that it is linear. The error would be of the order

$$E = \frac{1}{2}\left(\frac{3}{2}C_B\,\xi^{-1/2}\right)\tau_1^2(x,t) \qquad \xi = \tau_0 + \gamma\left(\tau_1(x,t)\right) \quad 0 < \gamma < 1 \qquad (4.4.5)$$

Table 4.4.1 *Numerical example of Bagnold's linearized transport formula*

physical constants	assumed values	equation number	calculated value
$g = 9.81\,m{\cdot}s^{-2}$	$d/D = 1$	4.4.3a	$C_B = 0.167\ kg{\cdot}m^{-1/2}{\cdot}s^{-1/2}$
$\rho = 1.2\ kg{\cdot}m^{-3}$	$u* = 0.686\ m{\cdot}s^{-1}$	3.3.3	$\tau_0 = 0.565\ Pa$
$C_l = 1.8$	$\tau_1 = 0.1\ h(x,t)$	4.4.3	$q = 0.09056\ kg{\cdot}m^{-1}{\cdot}s^{-1}$
σ [1] = $1675\ kg{\cdot}m^{-3}$	calculate sediment transport at x_i,t_i	4.4.4	$q_l = 0.0709 + 0.0188\ h(x_i,t_i)$ $= 0.0897\ kg{\cdot}m^{-1}{\cdot}s^{-1}$
	where $h(x_i,t_i) = 1$ m	Error: $q - q_l$	$0.000808\ kg{\cdot}m^{-1}{\cdot}s^{-1}$
	so that $\tau(x_i,t_i) = 0.565 + 0.1{\cdot}1.0 = 0.665$ Pa	4.4.5 (max. error)	$E = 0.0015\ kg{\cdot}m^{-1}{\cdot}s^{-1}$ $\approx 1.7\%$

The approximation by the linearization can be illustrated with the numerical example given in Table 4.4.1. In this case the linearized formula gives an error of $0.0015\ kg{\cdot}m^{-1}{\cdot}s^{-1}$ which is approximately 1.7% of the non-linearized formula. This example shows that only a very small error is made by using a linearized formula. The advantage of using a linearized formula as (4.4.4) is that there are only linear variable terms (in this case $\tau_l(x,t)$), which simplifies computations and permits an analytical solution to be found more easily (as will be developed in chapter 5).

4.4.2 The linear shear-stress model

It has been assumed that if the variations of the topography are very gradual the effect on the shear stress would be small, and the shear stress could be considered a linear function of the topographic height. However, in reality, shear stress does not vary linearly with topography. This has been illustrated in Fig. 4.4.1, where the variation of shear stress with the topographic height has been calculated with a more accurate model (developed by Jackson and Hunt, 1975, Appendix II) for two example topographies. Besides the fact that the shear stress is not a linear function, it can also be seen that it has a hysteresis effect. This is caused by the loss of momentum because of the additional surface shear stress that accompanies the increase of wind velocity over

[1] including porosity

the surface of the hill. This momentum loss is accounted for in the Navier-Stokes equations from which the model that calculates the shear stress in Fig. 4.4.1 is derived. Therefore the shear stress (and the wind velocity) at a particular topographic height at the lee side of the bedform will be smaller than the shear stress at the same height at the stoss side.

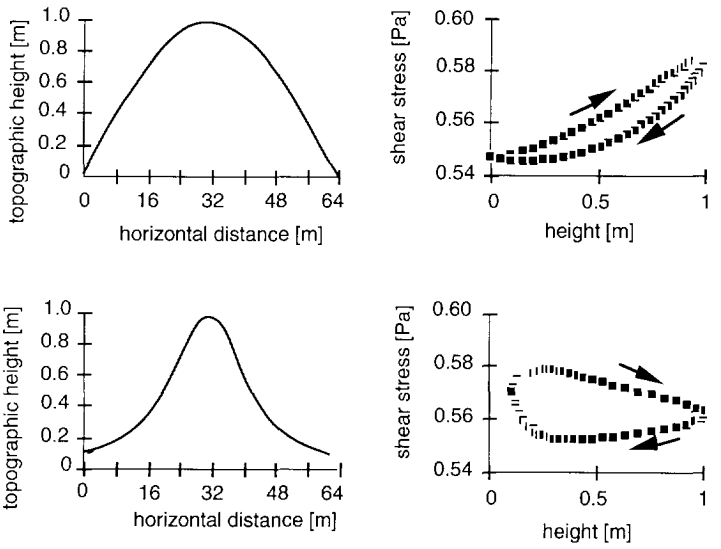

Fig. 4.4.1 *Two examples of different topographies with their corresponding relationship between topographic height and shear stress. Shear stresses have been calculated using Jackson and Hunt's model (1975).*

The topographies in Fig. 4.4.1 have the same height, but different shapes: half a sine and a Gaussian profile. In both cases it can be seen that the influence of the topography on the shear stress is relatively small (e.g. at most 0.05 Pa in the case of the half-sine, which is approximately 10% of the lowest shear stress), though it is not linear. It should be noted that the error introduced by a linear shear stress is much larger than the error made by linearizing the sediment-transport formula.

Because of the small variations in shear stress it seems acceptable, as a first approach, to model the shear stress as a linear function of the topographic height. This in combination with a linear transport equation leads to the simple wave model for a wave migrating at a constant velocity. Though this model parts from simplifying assumptions, it describes the behaviour of fully developed dunes migrating while maintaining their shape. Therefore, also from a practical point of view, it is of interest to take this model into consideration.

4.5 Numerical implementation

The solution developed in the previous section is very suitable for checking and evaluating the numerical implementation of the system formed by Eqs. (4.1.1) and (4.1.2). By assuming linear relationships for the transport and for the shear stress we obtain Eq. (4.2.6) which is one of the most simple mathematical equations, of which the behaviour of its solution (Eq. (4.2.7)) is known. For the numerical implementation of the system several things need to be considered. A differential equation such as (4.2.6) is expressed in finite differences by discretizing in time and space (the x-coordinate). This means that functions (in this case topographic height and sediment transport) are calculated over a number N of equidistant intervals Δx on each time step Δt until the total time of simulation T is reached. For this, an initial condition describing the physical phenomenon at the start (t=0) of the experiment and at least one boundary condition describing the physical nature of the problem at the boundary (x=0) are also needed.

4.5.1 Choice of numerical method

The easiest way to solve Eq. (4.1.1) is to calculate the solution at each time step from the solution at the previous time step by:

$$h_{x,\,t+\Delta t} = h_{x,\,t} - \frac{q_{x,t} - q_{x-\Delta x,t}}{\sigma\ \Delta x}\,\Delta t \qquad (4.5.1)$$

This is called the Euler scheme. As the initial condition for the original topography any function can be chosen; for instance a sine, a cosine or a starting dune. However, Eq.(4.5.1) is not an accurate solution, and other choices have to be made for the time-advancing scheme and the boundary conditions.

There is a great number of other numerical methods that can be considered for solving systems of equations. They can be divided in explicit, implicit and predictor-corrector methods.
Explicit methods calculate the function at each point x, at a given time step t, based on the solution of previous time steps. These methods are usually straightforward to apply, but it can be troublesome to obtain stable solutions and therefore sometimes very small time steps have to be taken.
Implicit methods calculate the solution at a certain point x at time t based also on the solution for other points at that same time step t. This cannot be done straightforwardly, and a matrix equation needs to be solved. Implicit methods have the advantage that they are always stable. They can best be used, however, for linear equations with one

dependant variable (i.e. the topographic height h in Eq. (4.2.6)), which means that they are not easily applicable if we introduce nonlinear transport equations. Implicit methods are not very flexible because the system of equations determines the matrix to be solved, and changing the transport equation changes the whole matrix.

Predictor-corrector methods are those where the solution at each point and time is calculated explicitly in several steps, each step being a corrected estimate of the solution. They have the simplicity of explicit methods, but are more accurate for a given time step, and also more flexible than implicit methods, because the equations of the system are not necessarily coupled in the programme. In the present study, one of the most popular predictor-corrector methods has been used, which is Runge-Kutta 4th order. It is given by:

$$h_{x,t+\Delta t} = h_{x,t} + \frac{1}{6}\left(k_1 + 2k_2 + 2k_3 + k_4\right) \tag{4.5.2a}$$

where:

$$k_1 = \Delta t\, f'\left(t, h_{x,t}\right) \tag{4.5.2b}$$

$$k_2 = \Delta t\, f'\left(t + \frac{\Delta t}{2},\ h_{x,t} + \frac{k_1}{2}\right) \tag{4.5.2c}$$

$$k_2 = \Delta t\, f'\left(t + \frac{\Delta t}{2},\ h_{x,t} + \frac{k_1}{2}\right) \tag{4.5.2d}$$

$$k_4 = \Delta t\, f'\left(t + \Delta t,\ h_{x,t} + k_3\right) \tag{4.5.2e}$$

In these expressions f' represents the derivative of a function to x. The error of this Runge Kutta scheme is of the order $(\Delta x)^5$ .The Runge-Kutta scheme requires four evaluations (k_1, k_2, k_3 and k_4) of the right side of Eq. (4.1.1), per time step. The first evaluation (k_1) is the prediction of the topography from the sediment transport $q_1(x)$:

$$k_1 = -\frac{1}{\sigma}\left(\frac{\Delta q_1}{\Delta x}\right)\Delta t \tag{4.5.3a}$$

With this prediction a new topography ($h_{x,t} + 0.5k_1$) is calculated, which in turn results in a new sediment transport $q_2(x)$. This gives the first correction:

$$k_2 = -\frac{1}{\sigma}\left(\frac{\Delta q_2}{\Delta x}\right)\frac{\Delta t}{2} \qquad (4.5.3b)$$

The next corrections are determined in a similar way, according to:

$$k_3 = -\frac{1}{\sigma}\left(\frac{\Delta q_3}{\Delta x}\right)\frac{\Delta t}{2} \qquad (4.5.3c)$$

$$k_4 = -\frac{1}{\sigma}\left(\frac{\Delta q_4}{\Delta x}\right)\Delta t \qquad (4.5.3d)$$

Where $q_3(x)$ and $q_4(x)$ are determined for the topographies $(h_{x,t} + 0.5k_2)$ and $(h_{x,t} + k_3)$. A combination of the prediction and the three corrections according to (Eq. (4.5.2a)), gives the topography for the next time step. For the spatial derivative of the sediment transport a central difference scheme has been used:

$$\left(\frac{\Delta q}{\Delta x}\right)_i = \frac{q_{i+1} - q_{i-1}}{2\Delta x} \qquad (4.5.4)$$

The error is of the order (Δx^2)

4.5.2 Choice of boundary conditions

It has been mentioned that conditions must be defined at, at least, one boundary. In this case, since a central difference scheme is being used for the spatial derivative (Eq. (4.5.4)) conditions need to be defined at both boundaries. To solve the system of Eqs. (4.1.1) and (4.1.2). the boundary conditions should be given for $q(x,t)$ (i.e. $q(0,t)$ and $q(N+1,t)$). If a PDE as Eq. (4.2.6) were to be solved, the boundary conditions should be given for $h(x,t)$ (i.e. $h(0,t)$ and $h(N+1,t)$). Several types of boundary conditions can be considered:
Dirichlet conditions: or boundary conditions of the first kind; when the function is given at the boundary.
Neumann conditions: or boundary conditions of the second kind; when the derivative of the function is given at a boundary.
Cauchy conditions: or boundary conditions of the third kind, sometimes also called mixed boundary conditions; when a relationship between the variable and its derivative is given at a boundary.

These three types of boundary conditions are adequate if we have a problem in a bounded domain, or if special conditions occur at either extreme (an example for a Dirichlet condition is a specified influx of sediment, e.g. $q(0,t) = 0$; an example of a Neumann condition is that the slope at the extreme remains constant, e.g. $dh(0,t)/dx = 0$).

For infinite domains the following boundary conditions can be defined:
Non-reflective conditions: when no value of any kind is specified at the boundary. Physically, it is required that the outgoing wave is not reflected back into the domain again. It is implemented with numerical schemes that use only internal points. This condition is often used for wave phenomena.
Periodic conditions: the domain is assumed to repeat itself periodically, and the waves going out of the domain at the right side enter it again at the left side. The solution applied in chapter 5 requires periodic boundary conditions. These have been implemented in the computer programme.

4.5.3 Testing the numerical method

The simple wave model (Eq. (4.2.6)) is very appropriate for testing and evaluating the computer programme. Numerical errors are introduced by the numerical method Eq. (4.5.2) and by the space difference scheme Eq. (4.5.4). A good way of evaluating a time-advancing scheme of a numerical method is by calculating the amplitude and phase errors of a periodic function (e.g. a sine) after a number of time steps (e.g. 1000).

The amplitude of a sine is the wave height. As the wave height in the simple-wave equation does not change through time, any change in amplitude is caused by the numerical scheme. The phase indicates the position of the wave at a given time. It is best evaluated by comparing the theoretical wave velocity[2] to the numerical wave velocity. The difference indicates that there is a shift in phase due to the numerical method. Both phase and amplitude errors should be evaluated for different grid spacing, time steps, and for waves of different wave number. The amplitude error is particularly affected by the number of discretization intervals, while the phase error is largely affected by the wave number.

A sine-shaped wave has been taken as an example to evaluate the numerical scheme. Amplitude and phase errors have been evaluated for two different grids (64 and 128 intervals) and two different wave numbers. An amplitude of 1 m has been chosen.

---

[2] It has already been indicated that in a morphodynamical context the wave velocity is equal to the migration rate. However in this section, which treats generally applicable numerical aspects, the term wave velocity will be maintained.

The data of Table 4.4.1 together with Eq. (4.4.4), would give the following linear equation for the sediment transport:

$$q_l(x,t) = 0.0709 + 0.0188h(x,t) \tag{4.5.5}$$

so that according to Eq. (4.2.6a) the theoretical wave velocity (c_t) , for any type of wave form, is equal to:

$$c_t = \frac{0.0188}{\sigma} m \cdot s^{-1} = 1.123\ 10^{-5} m \cdot s^{-1} = 0.0404 m \cdot h^{-1} \tag{4.5.6}$$

For periodic functions, the difference between the theoretical and the numerical wave velocity (c_n) can be expressed as a shift of the phase per unit of time:

$$\frac{\text{phase-shift}}{\text{time}} = (c_t - c_n)\frac{2\pi}{L} \tag{4.5.7}$$

The results for a simulation of 1000 hours (equal to 1000 iterations), for two different grid intervals and two different wave numbers [3] are shown in Table 4.5.1. These results show that the numerical errors in all cases are very small, so that it can be concluded that the numerical time-advancing scheme is adequate.

Table 4.5.1 *Wave velocity, phase shift, amplitude and amplitude error for numerical simulations with varying wave number (k_n) and number of intervals (N) after 1000 hours of simulation.*

		N=64	N=128
theoretical value	wave velocity [$m \cdot h^{-1}$]	0.0404	0.0404
	amplitude [m]	1.0	1.0
k_n=1 wave length = $N \cdot \Delta x$	wave velocity [$m \cdot h^{-1}$]	0.041	0.0405
	phase shift [$° \cdot h^{-1}$]	$3.375 \cdot 10^{-3}$	$0.5625 \cdot 10^{-3}$
	amplitude [m]	0.99905	0.99995
	amplitude error [%]	0.095	0.005
k_n=2 wave length = $N \cdot \Delta x/2$	wave velocity [$m \cdot h^{-1}$]	0.040	0.0405
	phase shift [$° \cdot h^{-1}$]	$4.50 \cdot 10^{-3}$	$1.125 \cdot 10^{-3}$
	amplitude [m]	0.99750	0.99954
	amplitude error [%]	0.25	0.046

[3] The mathematical definition of the wave number is given in Appendix I and an explanation of the term can also be found in the glossary.

Chapter 5

Bedform migration and growth

5.1 Introduction

In the previous chapter it was shown that dune migration is a result of the increase and decrease of wind velocity caused by the topography. The non-linear relationship between wind velocity and sediment transport causes deformation of the topography into shapes resembling a dune. The growth of a bedform, however, can be explained only with a more accurate calculation of the flow than in the previous models. In this chapter a more detailed flow model will be combined with Bagnold's linearized sediment-transport equation. An analytical solution is developed for a sine-shaped topography of a particular wave number, and expressions are obtained for the shear stress, the sediment transport, the erosion and deposition, the topography and the growth and migration of the bedform. This is essentially relevant for the two-dimensional schematization of a transverse dune; and gives a better understanding of the behaviour of the dune. The flow model that will be used is an analytical model developed by Jackson and Hunt (1975). A derivation of the equations is given in Appendix II, but the underlying ideas will be summarized briefly here.

5.2. Background of the flow model

Jackson and Hunt (1975) developed a two-dimensional analytical model for a turbulent wind-flow over a low hill. They divided the profile into an inner region close to the surface and an outer region further away from the surface (Fig. 5.2.1). Outside the outer region the flow is undisturbed by the topography. They assumed that in a first approximation the velocity in the inner region has the logarithmic profile of the turbulent boundary layer over a flat surface of constant roughness (see section 3.3). However, the topography causes a vertical displacement of air with a certain vertical velocity. Sufficiently far above the topography, the horizontal velocity should be equal to the undisturbed velocity, and the vertical velocity should be zero. This implies that in the outer region (i.e. between the inner region and the undisturbed region) there is a perturbation of the horizontal velocity, which also leads to a perturbation of the pressure in the outer region. This pressure perturbation affects the pressure of the inner region,

which in turn affects the local horizontal and vertical velocities in the inner region. Jackson and Hunt deduced corrections for the pressure, and for the vertical and horizontal velocities in the inner and outer regions. The corrections were based on a perturbation approximation, so that the solutions have the form of an infinite summation of linear terms of the topography. For the theory developed in this chapter, only the first of these correction terms was used, higher order terms being considered small and negligible. Henceforth, the logarithmic profile will be called the zero-order approximation, and the correction term will be called the first-order approximation.

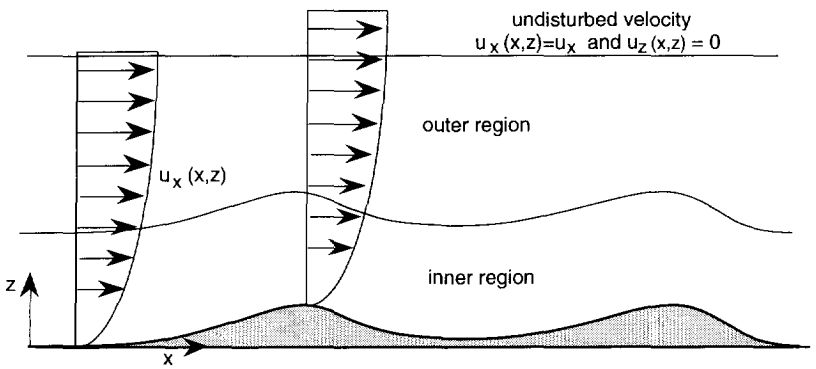

Fig. 5.2.1 *Schematic representation of Jackson and Hunt's flow model (1975), with the logarithmic velocity profile that corresponds to the zero order solution (after Jackson and Hunt, 1975).*

Jackson and Hunt's model is an analytical model that is easily implemented and involves little computational effort when compared to numerical flow models. To apply it for the simulation of sedimentation processes, some observations need to be made.

The most important assumption in the theory is that the relationship between shear stress and the turbulent profile remains unchanged over the whole topography. This means that the same zero-order velocity profile (i.e. the logarithmic velocity profile) applies over the whole topography. This can be justified considering that it takes some time for the flow profile to adapt to a change. It is thus assumed that changes in the velocity profile occur on a larger horizontal scale (which remains outside the considerations of this work) than the changes in the flow due to the topography perturbation.

A further consideration concerns the effect of saltation on the velocity profile (which was indicated in chapter 3). Bagnold modelled

this as an "extra" roughness (Eq. (3.4.1)) and included the effect of the threshold velocity. The effects of saltation should also be accounted for in Jackson and Hunt's model by assuming, like Bagnold, an appropriate surface roughness. Bagnold's formula, as used in this study, is a function of the shear velocity so it is not affected by the threshold velocity. An implicit condition is that saltation should occur constantly, as a change from saltation to non-saltation would also lead to a change in velocity profile. This is a reasonable assumption if considered that, once saltation has started, it quickly reaches a steady-state situation (Anderson and Haff, 1991). If the wind velocity were below threshold velocity, no sediment transport would occur and this again would affect the velocity profile.

The perturbation caused by the change in topography must be small, so that the dune height (H) should be much smaller than its length (L). Jackson and Hunt give a limit of $H/L < 0.05$. This means that the theory is only valid for very gentle topographies, as is the case of incipient dunes, long before separation of the boundary layer occurs and proper slipfaces with avalanching develop.

Comparisons of Jackson and Hunt's (1975) theory to actual measurements (Bradley, 1980 and Gong and Ibbetsen, 1989) generally agree that it gives satisfactory predictions of the mean flow on the upwind side of hills. The theory was extended to three dimensions (Mason and Sykes, 1979 and Walmsley et al., 1982). Further refinement of the model concerns a generalization for a wider range of conditions, such as changes in thermal stratification of the air (which affect the velocity profile) and in surface roughness (Hunt et al., 1988).

The solution of the flow, according to Jackson and Hunt's (1975) model, is expressed in Fourier Transforms. The theory of Fourier transformation is based on the fact that any function (e.g. a topography) can be written as a sum of sines and cosines. For the convenience of the reader the theory of Fourier Transforms necessary for this chapter, has been included in Appendix I. A more extensive explanation of the principles is given in Rikitake et al. (1987) and of its practical applications in Ferziger (1981).

5.3 Development of an analytical solution

The expression of the shear stress of the velocity in terms of Fourier Transforms of the topography, makes it adequate for the development of an analytical solution. The analytical solution becomes simpler if only one wave number is considered, so that the summations in the Fourier series are reduced to only one term. The general line is

analoguous to the development of the simple and kinematic wave equations in sections 4.2 and 4.3. The continuity equation is:

$$\frac{\partial h^*(x^*,t)}{\partial t} = -\frac{1}{\sigma^*}\frac{\partial q(x^*,t)}{\partial x^*} \qquad (5.3.1a)$$

Dimensionless coordinates have been used (indicated by an asterisk *), so that:

$$x^* = \frac{x}{L} \quad [-] \qquad (5.3.1b)$$

$$h^*(x^*,t) = \frac{h(x^*,t)}{H} \quad [-] \qquad (5.3.1c)$$

$$\sigma^* = \sigma H L \quad [kg \cdot m^{-1}] \qquad (5.3.1d)$$

where:

H = maximum topographic height [m]

An expression for the spatial derivative of the sediment transport has to be substituted in the continuity equation. A linearization of Bagnold's sediment-transport formula will be used (this was referred to in section 4.2). This can be justified by considering that Jackson and Hunt's (1975) solution results from a linear approximation of the equations of motion of a fluid, and that non-linear terms have been neglected (Appendix II). A linearized transport equation would be consistent with this approximation. It is difficult to give an estimate of the error involved with Jackson and Hunt's model. The approximation can be estimated by comparison to full numerical simulations, as has been done by Hunt et al. (1988). They indicated that the key features of their model were comparable with the numerical results. The error involved with the linearization of Bagnold's formula is minor in comparison with the simplifications of the flow model. An estimate of this error has been given in section 4.4.

For the linearization it has to be considered that the shear stress $(\tau(x^*,t))$ results from Prandtl's logarithmic profile (τ_0) with Jackson and Hunt's (1975) dimensionless first-order correction $(\tau_1(x^*,t))$ according to:

$$\tau(x^*,t) = \tau_0\left(1 + \varepsilon\, \tau_1(x^*,t)\right) \qquad (5.3.2)$$

Bagnold's linearized sediment-transport formula (according to Eq. (4.4.4)) then becomes:

$$q_l(x^*,t) = C_B \tau_0^{3/2} \left(1 + \frac{3}{2}\varepsilon \tau_1(x^*,t)\right) \tag{5.3.3}$$

where:

τ_0 = shear stress from logarithmic profile [Pa]
τ_1 = first order correction to the shear stress from the logarithmic profile [dimensionless]
ε = perturbation factor. This is a dimensionless number smaller than 1. The exact expression is given in Appendix II.

Differentiation of the linearized transport equation to the dimensionless coordinate x^* gives:

$$\frac{\partial q_l(x^*,t)}{\partial x^*} = \frac{3}{2} C_B \varepsilon \tau_0^{3/2} \frac{\partial \tau_1(x^*,t)}{\partial x^*} \tag{5.3.4}$$

To develop this equation, Jackson and Hunt's (1975) expression for the correction of the shear stress (see Appendix II) can be used. Expressed as a Fourier Transform $\hat{\tau}_l(k^*,t)$ the shear stress correction is:

$$\hat{\tau}_1(k^*,t) = \kappa |k^*| \hat{h}^*(k^*,t) z_k e^{i\phi} \frac{K_1\left(z_k e^{i\phi}\right)}{K_0\left(z_k e^{i\phi}\right)} \tag{5.3.5a}$$

with:

$$z_k = 2\sqrt{\frac{z_r |k^*|}{l}} \tag{5.3.5b}$$

and:

$$\begin{aligned} \phi &= \pi/4 \quad if \quad k^* > 0 \quad \text{(positive wave numbers)} \\ \phi &= -\pi/4 \quad if \quad k^* < 0 \quad \text{(negative wave numbers)} \end{aligned} \tag{5.3.5c}$$

In these formulae:

l = thickness of the inner region [m]
K_0 = Modified Bessel function of the zero-order
K_1 = Modified Bessel function of the first-order
k^* = dimensionless wave number. It should be noted that by introducing the dimensionless coordinate $x^*=x/L$, the maximum wave length (λ) has become equal to one and therefore the wave number ($k=2\pi/\lambda$) has become dimensionless also.

For small arguments, the Modified Bessel functions can be approximated with the following functions (Abramowitz and Stegun, 1972, p. 375):

$$K_0\left(z_k\, e^{i\phi}\right) = -\, ln\, \left(z_k\, e^{i\phi}\right) = -ln\,(z_k) - i\,\phi \tag{5.3.6a}$$

$$K_1\left(z_k\, e^{i\phi}\right) = \frac{1}{z_k\, e^{i\phi}} \tag{5.3.6b}$$

With this approximation, Eq.(5.3.5a) can be written as:

$$\widehat{\tau_1}(k^*,t) = -\,\kappa\,|k^*|\,\widehat{h}^*(k^*,t)\;\frac{1}{ln\, z_k + i\phi} \tag{5.3.7}$$

Which can be developed further to:

$$\widehat{\tau_1}(k^*,t) = -\,\kappa\,|k^*|\,\widehat{h}^*(k^*,t)\;\frac{ln\, z_k - i\phi}{(ln\, z_k)^2 + \phi^2} \tag{5.3.8}$$

Equation (5.3.8) can be substituted in the spatial derivative of the sediment-transport equation (5.3.4) (using Eq. A-I.8 in Appendix I) giving:

$$\widehat{\frac{\partial q_1(x^*,t)}{\partial x^*}} = -\,\frac{3}{2}\,C_B\,\varepsilon\,\tau_0^{3/2}\,\kappa\, ik^*|k^*|\,\widehat{h}^*(k^*,t)\,\frac{ln\, z_k - i\phi}{(ln\, z_k)^2 + \phi^2} \tag{5.3.9}$$

Substituting Eq. (5.3.9) in the continuity equation (5.3.1a), results in:

$$\frac{\partial \widehat{h}^*(k^*,t)}{\partial t} = \frac{3}{2}\,\frac{C_B}{\sigma^*}\,\varepsilon\,\tau_0^{3/2}\,\kappa\, k^*\,|k^*|\,\widehat{h}^*(k^*,t)\,\frac{\phi + i\, ln\, z_k}{(ln\, z_k)^2 + \phi^2} \tag{5.3.10}$$

The above equation is a first order differential equation of the form:

$$\frac{\partial \widehat{h}^*(k^*,t)}{\partial t} = C_k\;\widehat{h}^*(k^*,t) \tag{5.3.11}$$

of which the solution is of the form:

$$\widehat{h}^*(k^*,t) = \widehat{h}^*(k^*,0)\, exp\,(C_k\, t) \tag{5.3.12}$$

The factor C_k [s^{-1}] is a complex number, determined by both Bagnold's (1941) sediment-transport formula and by Jackson and Hunt's (1975) flow model:

$$C_k = C_\tau \left(\phi + i\, ln\, z_k\right) \tag{5.3.13a}$$

where C_τ has the dimension [s^{-1}] and is:

$$C_\tau = \frac{\frac{3\,C_B}{2\,\sigma^*}\,\varepsilon\,\tau_0^{3/2}\,\kappa\,k^*|k^*|}{\left(ln\, z_k\right)^2 + \phi^2} \tag{5.3.13b}$$

Equation (5.3.12) represents a moving wave. This can be more easily seen if written as:

$$\hat{h}^*(k^*,t) = \hat{h}^*(k^*,0)\, exp\left(C_{Re}t\right) exp\left(i\, C_{Im}t\right) \tag{5.3.14a}$$

with:

$$C_{Re} = C_\tau \phi \tag{5.3.14b}$$

$$C_{Im} = C_\tau\, ln\left(z_k\right) \tag{5.3.14c}$$

The imaginary exponential represents a wave migrating in time. The phase (C_{Im}) of the exponential gives the shift of the wave in time. By dividing this phase shift for the wave number (2π), the wave velocity is obtained:

$$c^* = \frac{C_{Im}}{k^*} = \frac{\frac{3\,C_B}{2\,\sigma^*}\,\varepsilon\,\tau_0^{3/2}\,\kappa\,|k^*|}{\left(ln\, z_k\right)^2 + \phi^2}\, ln\left(z_k\right) \tag{5.3.15}$$

The wave velocity of Eq. (5.3.15) is the normalized migration rate of the bedform, defined for one wave number (k^*), as a function of time. It can be seen that this migration rate is constant through time, so the bedform will migrate at a constant velocity. This is a consequence of the linearized sediment transport (Eq. (5.3.3)). Equation (5.3.15) shows that bedform migration is determined by C_τ/k^* , which is a factor dependent on the magnitude of the wave number $|k^*|$. This means that the migration rate will be larger for higher wave numbers. Smaller bedforms will therefore have higher migration rates.

Table 5.3.1 *Summary of analytical formulae for bedform morphodynamics, using an approximation of Jackson and Hunt's (1975) flow model for small bedforms.*

	Eq. no.	Equation
sediment continuity	5.3.1a	$\frac{\partial h^*(x^*,t)}{\partial t} = -\frac{1}{\sigma^*}\frac{\partial q(x^*,t)}{\partial x^*}$
shear stress [Pa]	5.3.2	$\tau(x^*,t) = \tau_0\left(1 + \varepsilon\,\tau_1(x^*,t)\right)$
sediment transport [kg·m^{-1}·s^{-1}]	5.3.3	$q_l(x^*,t) = C_B\,\tau_0^{3/2}\left(1 + \frac{3}{2}\varepsilon\,\tau_1(x^*,t)\right)$
perturbation factor [dimensionless]	A-II.3	$\varepsilon = \frac{H\,\ln^2(L/z_r)}{L\,\kappa\,\ln(l/z_r)}$
thickness inner region l [m]	A-II.4	$\frac{l}{z_r} = \frac{1}{3}\left(\frac{L}{z_r}\right)^{0.9}$
factor z_k (dimensionless)	5.3.5b	$z_k = 2\sqrt{\frac{z_r\lvert k^*\rvert}{l}}$
factor ϕ (dimensionless)	5.3.5c	$\phi = \pi/4 \quad if \quad k^* > 0$ $\phi = -\pi/4 \quad if \quad k^* < 0$
shear stress first order correction [dimensionless]	5.3.8	$\widehat{\tau_1}(k^*,t) = -\kappa\lvert k^*\rvert\,\widehat{h}^*(k^*,t)\,\frac{\ln z_k - i\phi}{(\ln z_k)^2 + \phi^2}$
spatial derivative of sediment transport [kg·m^{-2}·s^{-1}]	5.3.9	$\widehat{\frac{\partial q_l(x^*,t)}{\partial x^*}} = -\frac{3}{2}\,C_B\,\varepsilon\,\tau_0^{3/2}\,\kappa\,k^*\lvert k^*\rvert\,\widehat{h}^*(k^*,t)\,\frac{\phi + i\ln z_k}{(\ln z_k)^2 + \phi^2}$
sedimentation per unit of time [m·s^{-1}]	5.3.11 with 5.3.13a	$\frac{\partial \widehat{h}^*(k^*,t)}{\partial t} = C_\tau\,\widehat{h}^*(k^*,t)\left(\phi + i\ln z_k\right)$
factor C_τ [s^{-1}]	5.3.13b	$C_\tau = \frac{\frac{3\,C_B}{2\,\sigma^*}\,\varepsilon\,\tau_0^{3/2}\,\kappa\,\lvert k^*\rvert\,k^*}{(\ln z_k)^2 + \phi^2}$
topography [m]	5.3.14a	$\widehat{h}^*(k^*,t) = \widehat{h}^*(k^*,0)\,exp\left(C_{Re}t\right)\,exp\left(i\,C_{Im}t\right)$
growth factor [s^{-1}]	5.3.14b	$C_{Re} = C_\tau\,\phi$
normalized migration rate [s^{-1}]	5.3.15 with 5.3.14c	$c^* = \frac{C_\tau\,\ln(z_k)}{k^*}$

The dimensionless amplitude $A^*(t)$ of the wave is given by:

$$A^*(t) = \hat{h}^*(k^*,0)\, exp\,(C_{Re}t) \qquad (5.3.16)$$

Equation (5.3.16) gives the height of the bedform through time, the coefficient of the real exponent (C_{Re}) being the growth factor. It can be seen from the exponent (Eqs. (5.3.13b) and (5.3.5c)) that this factor is always positive for all wave numbers k^* (both positive and negative). For positive wave numbers, k^* will be positive, so will ϕ, and consequently C_{Re}. For negative wave numbers, k^* will be negative as will ϕ, which again gives a positive C_{Re}. The positive coefficient C_{Re} indicates that there will always be growth, not decay. According to Eq. (5.3.14a), the growth of a bedform will be exponential. It has to be noted here that this is only acceptable with regard to the limitations of Jackson and Hunt's flow model, where low topographies are assumed. It is probably also a consequence of the linear treatment of the model. When a bedform grows further, other processes not included in this model (increased vorticity, avalanching) will counter this effect. The bedform growth is also determined by C_τ, so that bedform growth will also increase with the wave number.

The main analytical formulae are summarized in Table 5.3.1. It must be noted that where applicable, they are given in complex Fourier notation as in Eq. (A-I.4a). A Fourier series as in Eq. (A-I.1) can be obtained by means of Eq. (A-I.5ab).

5.4 Interpretation of the analytical model: an example

The analytical equations developed in the previous section serve two main purposes: firstly for a qualitative understanding of the behaviour of the system and, secondly, to check the computer programme used in Chapter 6. A numerical example of a sine topography will be developed here.

The example that will be developed is for a single sine. This dimensionless topography is described by:

$$h^*(x,0) = sin\left(\frac{2\pi x}{L}\right) \qquad (5.4.1)$$

which in complex Fourier notation (Eq. (A-I.3ab)) is written as:

$$h^*(x,0) = -\frac{1}{2}\, i\, exp\left(\frac{2\pi x i}{L}\right) + \frac{1}{2}\, i\, exp\left(-\frac{2\pi x i}{L}\right) \qquad (5.4.2)$$

Table 5.4.1 *Assumed values for the development of an analytical example of a sine-shaped topography, rounded off to two significant decimals*

description	assumed values	eq. no.	calculated value
num. of intervals interval length max. top. height	N=128 Δx = 1 m $L = N \cdot \Delta x = 128\ m$ z_r/l = 0.001m H= 1 m	5.3.5b	z_k =0.063
roughness length	from z_r/l = 0.001m	A-II.4	z_r =0.0059 m
thickness inner region	from z_r/l = 0.001m and z_r = 0.0059m		l =5.9 m
shear velocity air density	(1) $u*$ = 0.686 m·s^{-1} ρ = 1.2 kg·m^{-3}	3.3.3	τ_0 = 0.565 Pa
magnitude velocity perturbation		A-II.3	ε = 0.572

(1) This corresponds to a wind velocity of 10 m·s^{-1} measured at 2 m height

Table 5.4.2 *Resulting expressions for a sine-shaped topography. The number of the corresponding equation is also indicated. In the cases where this referred to a dimensionless Fourier equation, the final expressions are given as a function of the x-coordinate and have been written in dimensional form. Values have been rounded off to two significant decimals.*

description	eq. no.	calculated function
initial topography [m]	5.3.1	$h(x,0) = 1 \cdot sin(0.049x)$
shear stress correction [-]	from 5.3.8	$\tau_1(x,t) = 0.134\ cos(0.049x)$ - $0.038\ sin(0.049x)$
linearized sediment transport [kg·m^{-1}·s^{1}]	from 5.3.3	$q_1(x,t) = 0.0509 + 0.0017\ cos(0.049x)$ - $0.0058\ sin(0.049x)$
increase in topographic height [m·s^{-1}]	from 5.3.10	$\partial h(x,t)/\partial t = -1.712 \cdot 10^{-7}\ cos(0.049x) +$ $4.85 \cdot 10^{-8}\ sin(0.049x)$
topography [m]	5.3.14a	$h(x,t) = sin(0.049x)\ \ exp(6.8 \cdot 10^{-8}\ t)$ $exp(i\ 2.4 \cdot 10^{-7}\ t)$
growth factor [s^{-1}]	5.3.14b	$C_\tau \cdot \phi = 6.8 \cdot 10^{-8}$
migration rate [m·h^{-1}] (1)	5.3.15	c = 0.0176

(1) a dimension of [m·h^{-1}] has been used instead of the S.I unit [m·s^{-1}], as this gives a more reasonable quantity.

The example will be developed with the numerical values from Table 5.4.1. The resulting expressions for the shear stress, the linearized sediment transport, the increase of topographic height in time and of the topography as a function of time are given in Table 5.4.2. The values of the migration rate and growth factor have also been given. These equations and values have been expressed in x-coordinates instead of Fourier coordinates, so that they can be easily compared to their graphical representation. The Fourier equations referred to in the table can easily be expressed into x-coordinates by using Eq. (A-I.2).

The equations in Table 5.4.2 have also been expressed in dimensional coordinates (x instead of x^*), which can be obtained with Eqs. (5.3.1b,c and d).

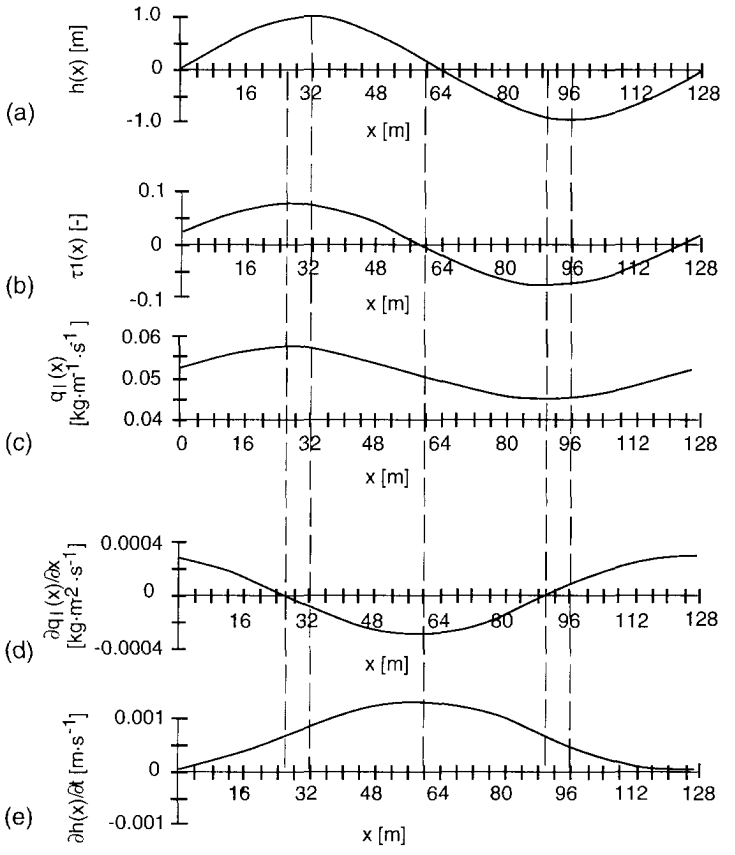

Fig. 5.4.1 *Results of the analytical solution for a sine-shaped topography at t=0; (a) topographic height h(x) = 1·sin(2π x/L) [m]; (b) first-order correction for the shear-stress $\tau_1(x)$ [-]; (c) linearized sediment-transport capacity q(x) [kg·m^{-1}·s^{-1}]; (d) spatial derivative of the sediment-transport capacity ∂q/∂x [kg·m^{-2}·s^{-1}]; (e) rate of increase in topographic height ∂h/∂t [m·s^{-1}].*

5.4.1 Analysis of the results

The expressions given in Table 5.3.2 have been shown graphically in Fig. 5.4.1 for $t=0$. These functions clearly show the general characteristics of the solutions. The topography ($h(x,t)$) starts as a sine (Fig. 5.4.1a). The correction of the shear stress $\tau_1(x,t)$ is a sinusoidal

function slightly out of phase with regard to the topography. This can be seen because its maximum and its minimum are slightly shifted to the left (Fig. 5.4.1b) with regard to the maximum and minimum heights. The sediment transport is also a sinusoidal function, in phase with the shear stress (Fig. 5.4.1c). Therefore the maximum and minimum sediment transport will occur at the same point as the maximum and minimum shear stress.

It is the fact that topography and shear stress are out of phase (the maximum and minimum shear stress occurring before the maximum and minimum topographic heights) that causes growth of the bedform. Erosion occurs up to the point of maximum shear stress and deposition occurs from the point of maximum shear stress onward. Therefore deposition also occurs at the point of maximum topographic height, so that the bedform grows. If the maximum would occur exactly at the peak (as in the models of chapter 4), the bedform would simply migrate without growing. This phase difference has al o been oberved in field measurements of velocity profiles over dunes (Arens, 1994).

The derivative of the transport capacity $(\partial q_l(x) / \partial x)$ is shown in Fig. 5.4.1d. It changes its phase by 90 degrees with respect to the sediment transport (as the sine and cosine functions are each other's derivatives). This means that at the points of maximum and minimum sediment transport, $\partial q_l(x) / \partial x = 0$. The derivative of the transport capacity is the opposite function of the erosion or deposition $(\partial h(x,t)/\partial t)$. We see in Fig. 5.4.1e that $\partial h(x,t)/\partial t$ is negative where $\partial q_l(x) / \partial x$ is positive and vice versa. Erosion occurs until slightly before the point of maximum height, and deposition after this point, until slightly before the point of minimum height. At the point of maximum shear stress, the sedimentation is zero.

Finally, a diagram of the sine topography through time, migrating at a constant rate and growing exponentially through time, is shown in Fig. 5.4.2.

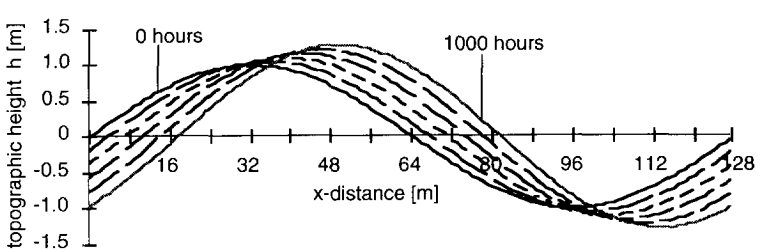

Fig. 5.4.2 *Growth and migration of a sine-shaped topography. The topography is shown in time-steps of 200 hours, for 1000 hours of simulation.*

5.5 Effects of wind velocity, roughness length and wave number

The advantage of analytical expressions as have been developed in this section, is that they allow a clear understanding of the influence of different terms (i.e. wind velocity, the surface roughness and the wave number) on the topography. The behaviour of the topography is best analysed by the change in the growth factor and the normalized migration rate (Eqs. (5.3.14b) and (5.3.15) respectively). Both of these are determined mainly by the factor C_τ given by Eq. (5.3.13b). This section will treat the effect of wind velocity, surface roughness and wave number on the growth fator and the migration rate, and on the factor C_τ.

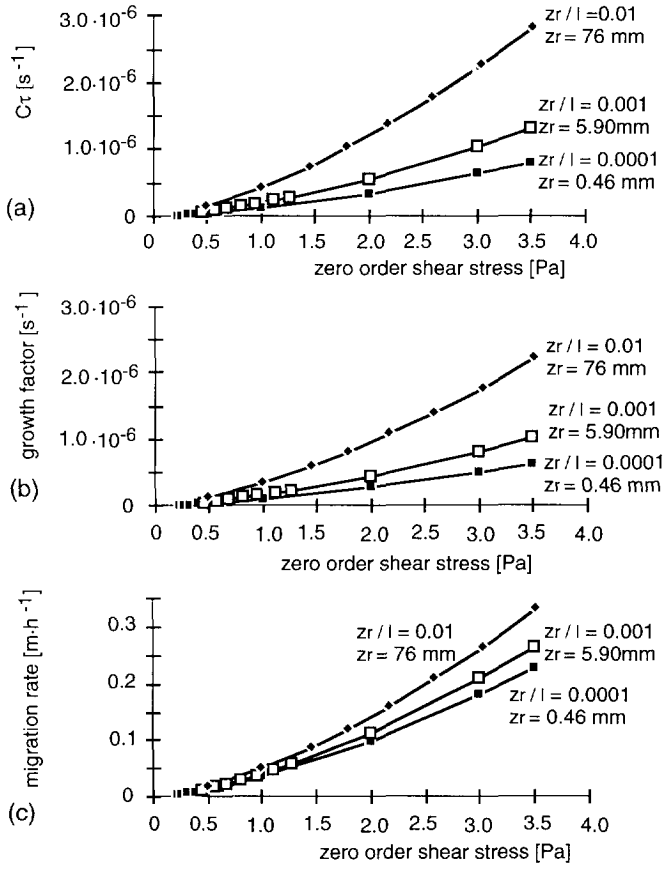

Fig. 5.5.1 *Influence of wind velocity and surface roughness on the bedform behaviour; (a) the coefficient C_τ; (b) the growth factor; (c) the migration rate. For convenience the migration rate has been given in [m·h^{-1}] instead of [m·s^{-1}].*

5.5.1 Effect of the wind velocity on growth factor and migration rate

The magnitude of the wind velocity is given by the uncorrected shear stress (τ_0). Equation (5.3.14b) shows that the growth factor is determined by C_τ (Eq. (5.3.13b)) and therefore directly dependent on the shear stress to the power 3/2. This means that a higher shear stress (i.e. wind velocity) will directly increase the growth factor. The migration rate is determined by the same factor, C_τ, and is therefore affected in the same way by the shear stress. A higher shear stress results in a higher migration rate, which can intuitively be accepted. Figure 5.5.1a shows how the factor C_τ increases with increasing shear stress. Figures 5.5.1b and 5.5.1c show the growth factor and migration rate for increasing shear stress, confirming that a higher wind velocity increases both.

5.5.2 Effect of the roughness length on growth factor and migration rate

The roughness length z_r is contained in the term z_k , which is directly proportional to its square root. The logarithm of this term is included in the denominator of the factor C_τ (Eq. (5.3.13b)). As z_k is usually a number smaller than 1, its logarithm will be a negative number, of which the absolute value decreases with increasing surface roughness. Therefore C_τ will increase with increasing surface roughness, as is shown in Fig. 5.5.1a. This means that the growth factor will be higher when the surface roughness is higher, as is shown in Fig. 5.5.1b. Finally, regarding the migration rate, the logarithm of z_k also appears in the numerator. However, the influence of the denominator is more important, so that it may be concluded that the migration rate will also increase with increasing surface roughness, as is illustrated in Fig. 5.5.1c. A cautioning comment should be added when applying this conclusion directly to actual measurements. The increase of the growth factor and of the migration rate with the surface roughness is obtained directly from Eqs. (5.3.13b), (5.3.14b) and (5.3.15), where the zero-order shear velocity (τ_0) has been maintained constant. Figures 5.5.1a,b and c result from the fact that an increased surface roughness would increase the first-order correction of the shear stress. In practice the corresponding wind velocities that would be measured (with constant zero-order shear stress) would increase with the increasing surface roughness. The reason for this is that according to Eq. (3.4.1) an increase in surface roughness reduces the wind velocity measured at a certain height (see Fig. 3.4.2). Therefore if a constant shear stress is maintained, the wind velocity measured at a datum height must necessarily increase with the surface roughness.

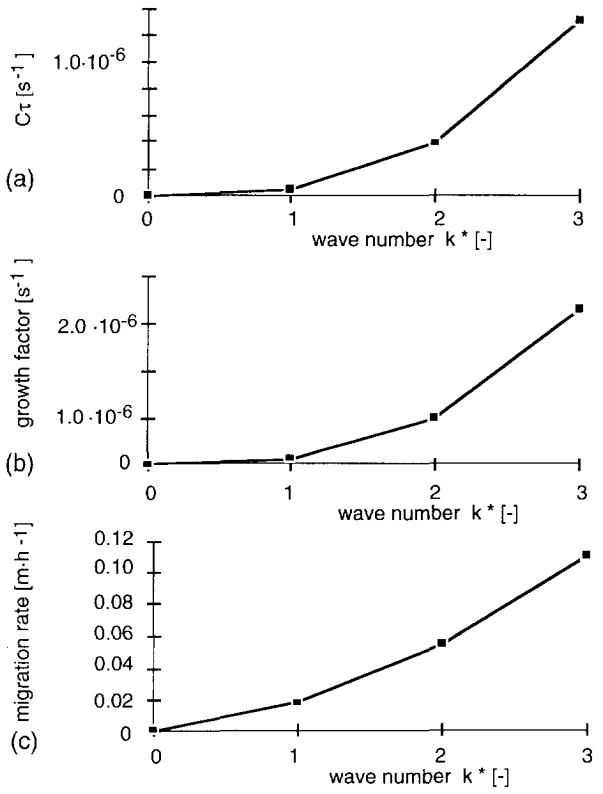

Fig. 5.5.2 *Influence of the wave number on the bedform behaviour. In these graphs* $\tau_0 = 0.565$ *Pa and* $z_r/l = 0.001$*; (a) the coefficient* C_τ*; (b) the growth factor; (c) the migration rate. For convenience the migration rate has been given in* $[m \cdot h^{-1}]$ *instead of* $[m \cdot s^{-1}]$*.*

5.5.3 Influence of the wave number on growth factor and migration rate

Equations (5.3.14b) and (5.3.15) permit us to work out the growth and migration rates for different wave numbers k^*. The influence of the wave number on the factor C_τ is shown in Fig. 5.5.2a. There it can be seen that C_τ increases for increasing wave number. This same behaviour is shown for the growth factor and migration rate (Fig. 5.5.2b,c). It can be clearly seen that the migration rate increases for larger wave numbers (i.e. for smaller wave lengths). It supports mathematically the observation that small dunes migrate faster than large dunes and ripples faster than dunes and draas. The growth factor is also higher for higher wave numbers. It must be noted that this model for growth and migration is valid only in the first stages of bedform formation, where Jackson and Hunt's model still applies. As bedforms grow it will no

longer be possible to neglect the non-linear terms in the flow equations. In a much later stage flow separation occurs and a wake zone with eddies will form, where avalanching will occur.

5.5.4 An example of migration rates of dunes from Salton Sea (California)

There are few published studies that monitor dune dynamics over a longer time period which can be used to analyse the type of relationships that have been developed in the preceding sections. One study that could be used in this sense, was published by Long and Sharp (1964). It analysed the movement of 47 barchan dunes in Salton Sea (California), by comparing their change in position from maps dating from different periods. They published the crest height, length with and without horns, width, and the movement in two different time periods: from 1941 to 1956 (15 years) and from 1956 to 1963 (7 years). These two time periods were considered separately as the authors observed a difference in the average movement of the dunes, which they attributed to an increase in sediment supply. The data (all the dimensions indicated in Fig. 5.5.5) and the migration rates for the seven year period, which was the most recent period are complete for 27 of the dunes, and are given in Table 5.5.1. The dunes are all barchans, formed in a mainly uni-directional wind regime. Their heights range from 2.74 to 12.2 m. As all the dunes have been subjected to the same wind regime, this is an interesting data set for a quick test of some of the ideas forwarded in the preceding section.

A graph of the wave numbers of the dunes against their migration rates can be compared with the theoretical relationship found in the previous section (Fig. 5.5.2c). The longest wave was considered to have the smallest wave number ($k^*=1$), and the rest of the wave lengths were expressed as a ratio of this one. Figure 5.5.3 shows this relationship for the 27 dunes. Dunes of smaller wave length have higher migration rates, and the relationship is somewhat similar to the theoretical one shown in Fig. 5.5.2c. Cautioning comments need to be added to this example. Data of three-dimensional reality are being compared with two-dimensional simulations. In Fig. 5.5.3 some points have been marked that do not fit very well within the general trend. These points correspond to dunes of high length relative to their width, in other words dunes that can less easily be considered as two-dimensional (they have also been marked in Table 5.5.2). The real migration rates are approximately ten times lower than the theoretical ones. However no importance should be given to this, considering that the theoretical migration rates are instantaneous values, while the real migration rates are resultant values over a period of 7 years. The wind did not blow constantly during 7 years and no calibration of average wind regime,

surface roughness and grain size has been done. Also the real dunes have avalanching slip-faces, while in the theoretical relationship no avalanching occurs. This should not be considered as a simulation of the Salton Sea dunes, even though the trend does fit reasonably well with the theory and this can be considered a promising result.

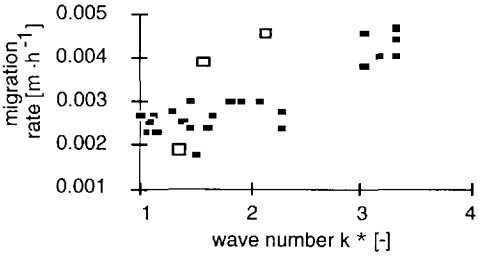

Fig. 5.5.3 *Relationship between the wave number of the dunes and their migration rate, shown for 27 dunes from Salton Sea (California). The data for this graph was taken from Long and Sharp (1964). Three dunes have been marked differently. The ratio between length and width is the highest for these dunes, therefore they have the strongest three-dimensional character (see Table 5.5.2). For convenience the migration rate has been given in [m·h⁻¹] instead of [m·s⁻¹].*

Long and Sharp (1964) assumed an inverse relationship between dune height and migration rate (Fig. 5.5.4). It has always been reasoned that the bigger the bedform, the more sediment is involved when it advances, so that its migration is slower. This need not contradict the conclusion on the relationship between migration rate and wave number as it seems reasonable to assume that longer waves (i.e. smaller wave numbers) will also be higher. Table 5.5.2 gives the ratio of the height and length of the 27 dunes. The ratio has been calculated both with the length including horns (abbreviated as Le in Fig. 5.5.5) and without horns (abbreviated as le in Fig. 5.5.5). The averages and standard deviations support this hypothesis. It can be considered that the relationship expressed in Fig. 5.5.3 gives a slightly better fit than the relationship of Fig. 5.5.4, given by Long and Sharp (1964).

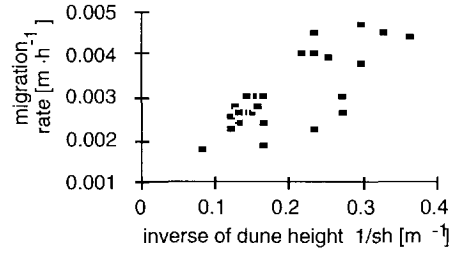

Fig. 5.5.4 *Long and Sharp's (1964) relationship between the inverse of the dune height (1/sh) and the migration rate, shown for 27 dunes from Salton Sea (California). For convenience the migration rate has been given in [m·h⁻¹] instead of [m·s⁻¹].*

Table 5.5.1 *Dimensions of 27 barchan dunes, measured in Salton Sea (California) by Long and Sharp (1964)*

length [m] (le) *	length including horns [m] (Le) *	width [m] (w) *	slipface height [m] (sh) *	distance migrated in 7 years [m]
79.04	121.6	197.6	7.904	152
76	144.4	152	6.992	182.4
68.4	136.8	152	6.08	144.4
97.28	186.96	129.2	6.688	159.6
33.44	88.16	45.6	2.736	266
103.36	168.72	106.4	4.256	136.8
48.64	82.08	212.8	7.904	167.2
48.64	156.56	115.52	7.6	144.4
33.44	65.36	50.16	3.344	281.2
72.96	212.8	197.6	12.16	106.4
53.2	109.44	85.12	6.384	182.4
60.8	103.36	56.24	6.08	182.4
69.92	91.2	45.6	3.952	235.6
110.96	193.04	121.6	3.648	159.6
85.12	136.8	114	6.384	167.2
66.88	176.32	167.2	7.296	159.6
36.48	66.88	51.68	3.344	228
100.32	164.16	152	8.208	152
33.44	71.44	60.8	4.56	243.2
95.76	179.36	109.44	8.208	136.8
51.68	91.2	42.56	4.256	273.6
107.92	185.44	250.8	7.6	159.6
36.48	65.36	41.04	3.04	273.6
76	144.4	83.6	6.08	144.4
82.08	112.48	68.4	6.08	114
57.76	80.56	53.2	3.648	182.4
34.96	62.32	54.72	4.256	243.2

* abbreviations correspond to Fig. 5.5.5

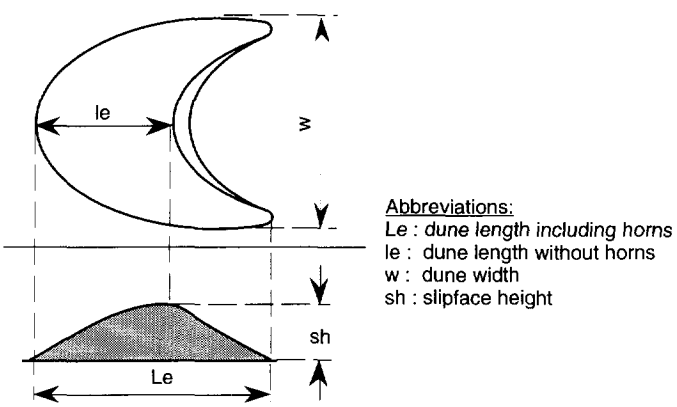

Fig. 5.5.5 *Sketch showing plan and side view of a dune with the dimensions measured in Tables 5.4.1 and 5.4.2, as given by Long and Sharp (1964).*

Table 5.5.2 *Relations between dune height, length, width and the migration rate averaged over the seven year period, for the dunes from Long and Sharp (1964)*

height/length sh/le [-]	height /length sh/Le [-]	length/width le/w [-]	average migration rate [m·h^{-1}]	
0.1	0.065	0.400	0.0025	
0.092	0.048	0.500	0.0030	
0.089	0.044	0.450	0.0024	
0.069	0.036	0.753	0.0026	
0.082	0.031	0.733	0.0044	
0.041	0.025	0.971	0.0023	
0.163	0.096	0.229	0.0028	
0.156	0.049	0.421	0.0024	
0.100	0.052	0.667	0.0046	
0.167	0.057	0.369	0.0018	
0.120	0.058	0.625	0.0030	
0.100	0.059	1.081	0.0030	
0.057	0.043	1.533	0.0039	*
0.033	0.019	0.913	0.0026	
0.075	0.047	0.747	0.0028	
0.109	0.041	0.400	0.0026	
0.092	0.050	0.706	0.0038	
0.082	0.050	0.660	0.0025	
0.136	0.064	0.550	0.0040	
0.086	0.046	0.875	0.0023	
0.082	0.047	1.214	0.0045	*
0.070	0.041	0.430	0.0026	
0.083	0.047	0.889	0.0045	
0.080	0.042	0.909	0.0024	
0.074	0.054	1.200	0.0019	*
0.063	0.045	1.086	0.0030	
0.122	0.068	0.639	0.0040	
0.093	0.049	mean		
0.033 ≈ 35%	0.014 ≈ 28%	standard deviation		

* these dunes have been marked in Fig. 5.5.4. Their length/width relationship is the largest of all (>1.2), therefore they have the most notable three-dimensional character.

Chapter 6

Applying the theory to a computer model of non-sinusoidal bedforms

6.1 Introduction

In the previous chapter a series of analytical expressions was developed to calculate the behaviour (migration and growth) of a sinusoidal bedform. The underlying theory combined a wind flow model (Jackson and Hunt, 1975) with a linearized sediment transport formula (Bagnold, 1941). By means of a Fourier Transform (Appendix I) any function can be decomposed in a sum of sines and cosines, so that the theory can be generalized to calculate the evolution through time of a bedform of any shape. To simplify the calculations a computer programme called EOLSIM has been developed (for more details see Appendix III). This chapter will treat the computational problems that appear with the generalization of the analytical theory.

According to the theory of the preceding chapter, the growth of a sine-shaped bedform is exponential, and faster for higher wave numbers. This means that in a topography composed of several wave numbers, the highest wave numbers will grow the fastest, and will dominate over the smaller wave numbers. In reality, dunes reach an equilibrium state in which they migrate without changing shape. In this chapter the reasons for this equilibrium are considered and avalanching has been taken as the most important mechanism in this equilibrium.

6.2 Problems with application to non-sinusoidal bedforms

To generalize the theory, a computer algorithm has been developed. However, in this respect there are several sources of numerical errors that need to be considered, because they can lead to instability of the programme. These numerical errors can be caused by: i) the appearance of artificial wave numbers; ii) the numerical interaction of different wave numbers in a linear model; iii) the problems of including the non-linear sediment-transport formula.

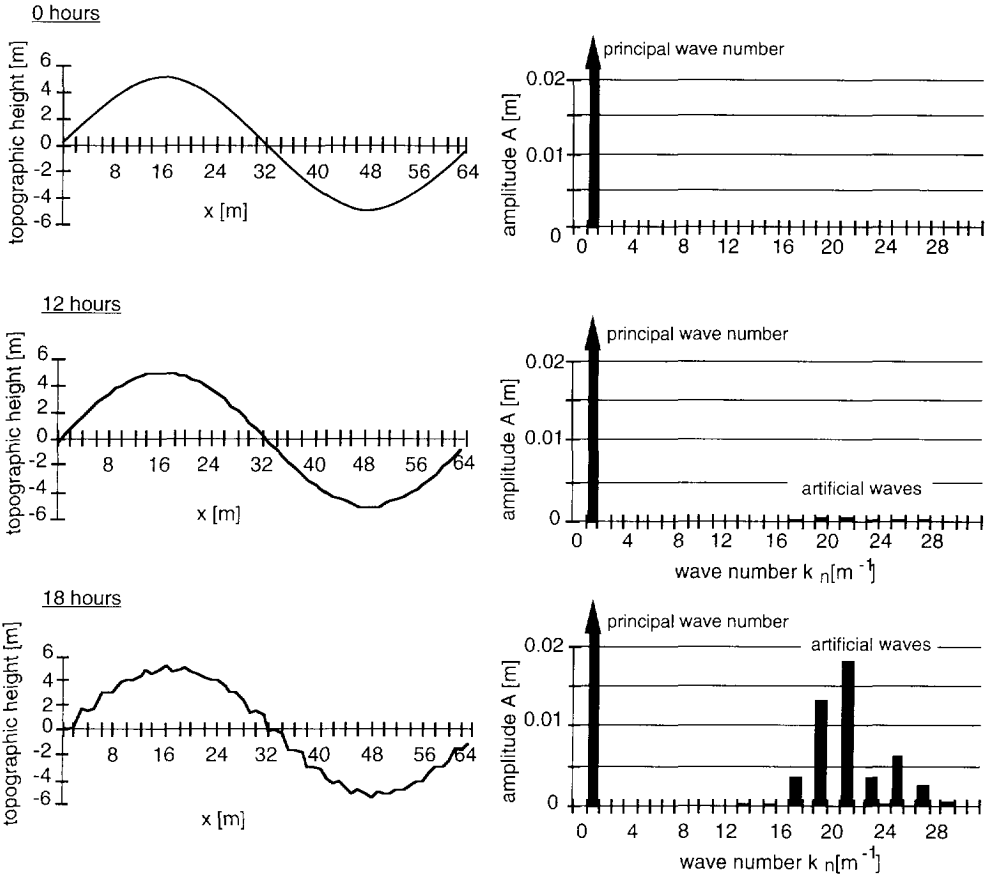

Fig. 6.2.1 *Effect of the artificial wave numbers on the evolution of a sine topography through time. The corresponding spectrum of the topography, showing the amplitudes of the principal and the artificial wave numbers, is given on the right. The spectrum is given by the quadratic mean of the amplitudes of the real and imaginary components of the wave number* k_n *(see Eq.(A-1.10)).*

6.2.1 Growth of artificial wave numbers

The FFT (Fast Fourier Transform) decomposition used in EOLSIM, will give small, non-zero values for the amplitude of all the wave numbers of the spectrum. These wave numbers (the so-called artificial wave numbers) are a result of rounding errors and machine accuracy and do not belong to the spectrum at all. These artificial waves will be amplified, resulting in a disproportionate growth, which is more pronounced for higher wave numbers. The effect of this problem has been illustrated in Fig. 6.2.1 which shows a sine bedform through time. The spectrum shows the growth of the artificial wave numbers that cause the solution to become unstable after only a few iterations (18

hours). The large impact of high wave numbers of the spectrum of the topography on the air flow of Jackson and Hunt's (1975) model has already been observed by other authors, such as Walmsey et al. (1982), but it is more pronounced in combination with the sediment-transport model, because of the high amplitude-growth of the higher wave numbers.

The problem can be solved by filtering out the wave numbers that do not belong to the actual spectrum. This is easy in the case of a single sine or cosine function which only has one wave number, because all other wave numbers can be filtered out by equaling them to zero. However, any other mathematical function, and also a natural dune, will have a spectrum with an infinite realm of wave numbers and it becomes impossible to distinguish between the real Fourier coefficients with very small amplitudes and the numerically introduced Fourier coefficients. In the programme all wave numbers with small amplitudes, both real and artificial, have been filtered out. This means that if the amplitude with a certain wave number is smaller than a certain minimum (an arbitrary value of 0.0015 has been chosen), the influence of that wave number on the topography has been disregarded. For non-sinusoidal bedforms this will generally (though not necessarily) imply that the high wave numbers will be filtered out, because in that case their initial contribution to the spectrum is usually small. If the high wave number contributes significantly to the spectrum (which means its amplitude is higher than the chosen minimum) this filtering will not happen.

6.2.2 Numerical interaction of different wave numbers

The model that has been treated up to this point is a linear model because all the equations are linear or have been linearized. A linear problem can be solved by subdividing it into independent subproblems, and adding the solutions of the subproblems. The topography is a superposition of different wave numbers. At each time step, the topography can be obtained by considering the waves of the spectrum independently and each wave should migrate and grow without affecting the other waves.

It appears, however, that in a FFT decomposition, the amplitudes of the different waves influence each other. The spectrum that results from calculating each wave separately and summing the results, is different from the one that results from calculating the different waves together (see Fig. 6.2.2). This is caused by the growth of the waves at each time step, which changes the topography. At each time step the FFT routine decomposes the new topography in the different wave numbers, so that they interact slightly with each other. The amount of

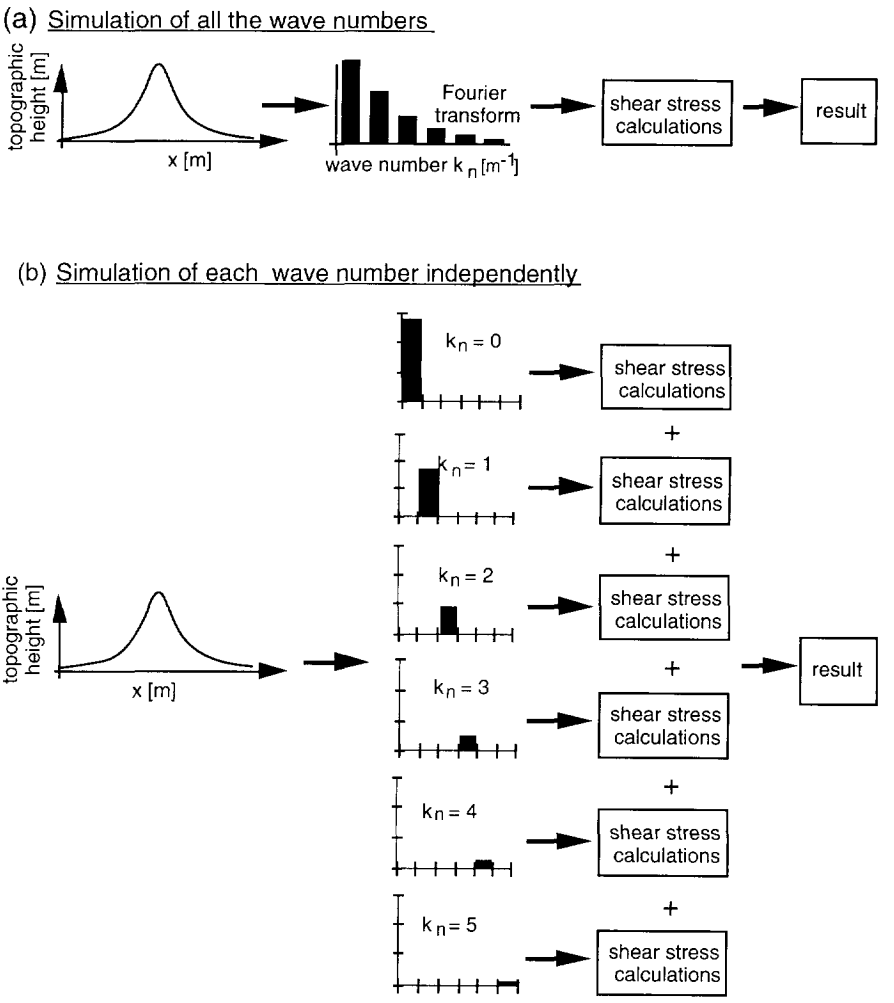

Fig.6.2.2 *Scheme of two different simulation approaches: (a) simulation of the whole spectrum of the function; (b) simulation of each wave number k_n independently.*

interaction between the different wave numbers has been evaluated by a simulation of 100 time steps of a Gaussian topography (each time step was of one hour). The six lowest wave numbers (k_n=0,1..5) have been considered, as they gave the most important contribution to the total spectrum. The difference between a simulation of the six lowest wave numbers separately and together, has been expressed as a percentage of the squared mean of all six amplitudes at each time step, according to:

$$E_n = \frac{\sqrt{\left(Re\left(\hat{f}_n'\right)\right)^2 + \left(Im\left(\hat{f}_n'\right)\right)^2} - \sqrt{\left(Re\left(\hat{f}_n\right)\right)^2 + \left(Im\left(\hat{f}_n\right)\right)^2}}{\sum_{n=0}^{6} \sqrt{\left(Re\left(\hat{f}_n\right)\right)^2 + \left(Im\left(\hat{f}_n\right)\right)^2}} \qquad (6.2.1)$$

where:

E_n = error for wave number k_n in the case of a simulation of all the wave numbers together

$Re\left(\hat{f}_n\right)$, $Im\left(\hat{f}_n\right)$ = amplitudes of the real and imaginary components of wave number k_n, in the case where each wave number is simulated separately

$Re\left(\hat{f}_n'\right)$, $Im\left(\hat{f}_n'\right)$ = amplitudes of the real and imaginary components of wave number k_n, in the case where all the wave numbers are simulated together

The error is shown in Fig. 6.2.3. It can be seen that after 100 time steps the maximum error is approximately 1.8%. This difference is hardly noticeable in the wind velocity calculations or in the topography itself. A correct algorithm would calculate the migration and growth of each component of the spectrum separately and sum the results, as this would avoid the numerical interaction. However, the error when the whole spectrum is calculated together is very small. As this results in a more efficient algorithm, it has been implemented in this way in EOLSIM.

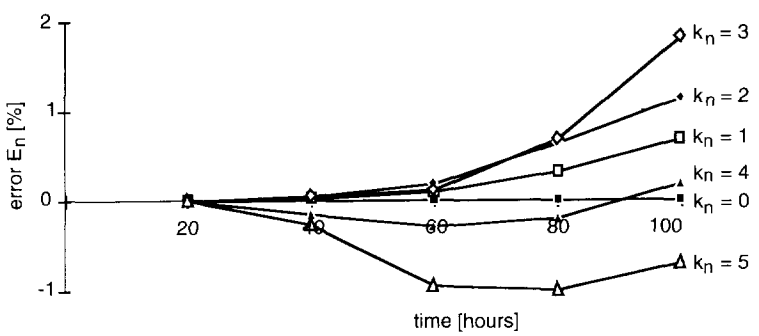

Fig. 6.2.3 Error of the interaction of different wave numbers in a linear model.

6.2.3 Non-linearity

If the full nonlinear sediment-transport equation is used (e.g. Bagnold's Eq. (3.4.4)) the different waves will cause higher wave numbers to appear. This is illustrated in Fig. 6.2.4, which compares the spectrum of a single sine for the linearized transport formula and for the non-linearized model. Though these wave numbers appear as a result of the physical process they cannot be distinguished from the artificial wave numbers, so that it is generally not possible to avoid them being filtered out together with the artificial waves. As has already been noted in section 4.2. the linearization of the sediment-transport formula is a very good approximation, so that the difference with a non-linear calculation is barely noticed. From a computational point of view, it is clearer to use a linearized model and filter out all small and artificial wave numbers, than to use a non-linear model without control on the growth of the artificial wave numbers. Therefore, EOLSIM uses the linearized model.

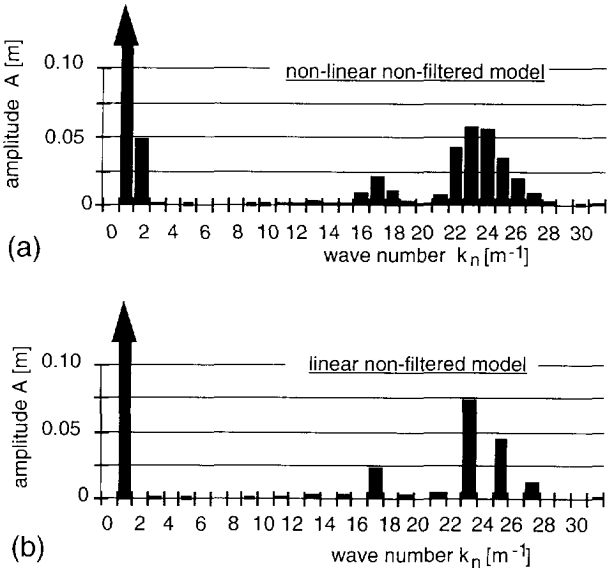

Fig. 6.2.4 *Comparison of the spectra of the amplitudes of a sine-shaped topography after 10 iterations with: (a) the non-linear non-filtered model; (b) the linear non-filtered model. Note the extra wave numbers that appear in (a) as a consequence of the non-linearity. These are difficult to distinguish from the artificial wave numbers that appear in (b), and which in turn also give extra wave numbers in the non-linear simulations.*

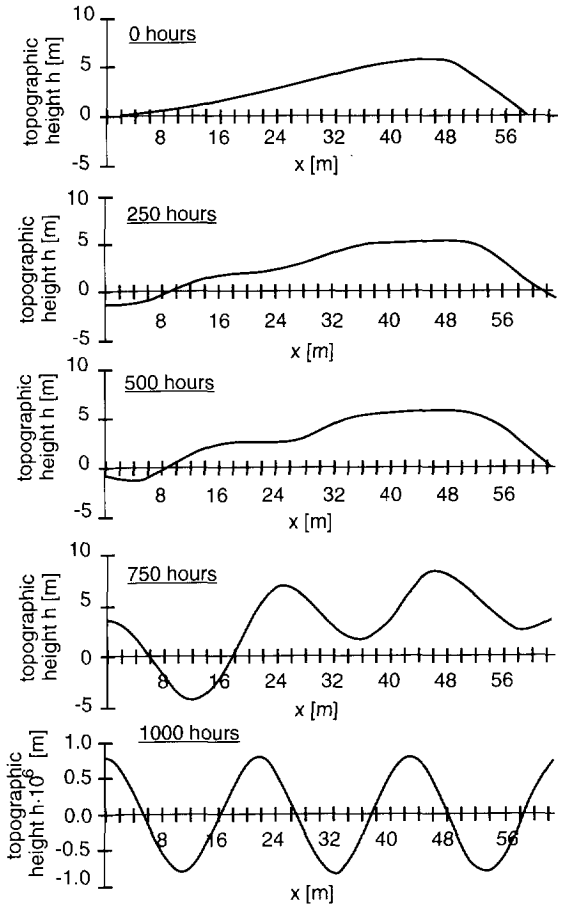

Fig. 6.3.1 Evolution of a dune through time. The simulation shows how the high wave numbers that are not filtered out start dominating the topography. At the last time step the topography is unstable because the amplitude of the highest wave number grows disproportionately (note the different vertical scale of the last time step). This means that other processes should be considered to model the dynamic equilibrium of a bedform.

6.3 Application to non-sinusoidal bedforms; bedfom stability

The application of the theory to a dune topography is shown in Fig. 6.3.1. The somewhat schematized topography of a dune, published by Howard et al. (1978), has been taken as an example. The artificial wave numbers and the wave numbers of small amplitude, referred to in the previous section, have been filtered out. However, it can be seen that after several time steps the topography deforms completely and the original dune ceases to be recognizable. This is caused by the growth of the higher wave numbers that belong to the spectrum of the toporaphy,

which, after several time steps, dominate the topography. Figure 6.3.1 shows clearly that the exponential growth leads to unstable bedforms, while it is known that bedforms reach a stable equilibrium where they migrate without changing shape. It is therefore necessary to analyse the physical reasons for this instability more closely.

The exponential form of the growth is a consequence of the linearity of the model. A similar linearised model was developed for subaqueous bedforms by Kennedy (1969), who used a flow model based on potential flow and included a lag effect. This lag was an uncertainty factor, which accounted for both the phase-difference between the topography and the flow, and between the flow and the sediment transport. The model resulted in an expression where the bedform amplitude grows or decays exponentially. Jackson and Hunt's (1975) boundary-layer model gives a more accurate flow description than the potential-flow model, as it includes friction effects. This is the fluid-dynamic reason for the maximum shear stress to occur upstream of the maximum height.

As a bedform grows, the boundary layer separates (see Chapter 3) and a wake forms. This process is not correctly described by Jackson and Hunt's (1975) first-order correction. A first approach that could be considered is to add higher-order terms to the first-order solution. The second-order term of the shear stress is, however, much smaller than the first-order correction (Jackson and Hunt, 1975) and it is questionable if it would be significant enough to result in bedform stability (a proper analysis of the higher-order terms in Jackson and Hunt's solution would be necessary to confirm this). A second approach that could be taken is to develop another flow model to determine the turbulent flow in a fully developed wake. McLean (1990) indicates some of the effects of the flow separation in subaqueous dunes, considering them important in adjusting the phase of the shear stress relative to the topography. The separation zone creates a high shear zone which extracts momentum from the flow. Moreover, the wake structure imposes a different flow behaviour than the boundary-layer model, where the flow is more topographically controlled. The calculation of turbulent flow in wakes, however, is one of the most complicated subjects in fluid mechanics and goes beyond the scope of this study. Moreover, it can generally be considered that the boundary-layer model (such as that of Jackson and Hunt, 1975) is still a good approximation of the flow up to the point of separation.

Summarizing, it is clear that the fluid-dynamic processes after flow separation affect bedform stability. Furthermore, mechanisms such as a lag between surface shear stress and sediment transport have also been considered to affect bedform stability. A mechanism that has not been

considered in the above discussion, which is not affected by the flow conditions and which plays an important role in aeolian dunes, is avalanching. Avalanching has been discussed in literature as a process in itself, but publications on bedform stability (Kennedy, 1969, McLean, 1990) have not considered its role in bedform stability. This possibility will be worked out further in this study.

6.4 Avalanching

Avalanching occurs when the slope at some point becomes too steep, and the force of the gravity component along the topography becomes higher than the shear stress of the sand grains maintaining them in position. Part of the dune slides down the slipface, depositing a long narrow tongue of sand that lies conformably over the deposits underneath (as can be seen in Fig. 2.4.5 on page 34). The angle at which avalanching begins is called the angle of initial yield (approximately 34°). A grain avalanche will descend the slope from the place where this angle is first exceeded, leaving all or part of the surface inclined at a lower angle called the angle of repose (approximately 30° to 32°). Avalanches generally start close to the crest of the dune. As the avalanche moves down the slipface, it destabilizes the slope further down, so that the avalanching progresses downwards.

Jackson and Hunt's (1975) flow model has been maintained in this study, and a simple avalanching routine was added. Beside the justification of the physical aspects that has been given in the previous section, it has the advantage of an analytical flow-model versus a numerical model. This advantage leads to clearer relationships between different physical variables, and to calculations that are generally less cumbersome and require less computer time. Flow has been calculated over the whole bedform using Jackson and Hunt's model (1975), while, wherever the slope became too steep, the deposited sediment was redistributed by the avalanching process. It was considered that in this way the flow behaviour is still reasonably correctly calculated, while avalanching as the main process occurring in the wake zone, is also included. The objective is to see whether avalanching could indeed be an important mechanism limiting dune growth.

6.4.1 Avalanching routine

An avalanching routine has been developed for EOLSIM. The amount of sediment that avalanches and the topography after avalanching is modelled geometrically. It should be noted that the routine necessarily simplifies the process described in the previous section. The routine is based on the following points (see Fig. 6.4.1):

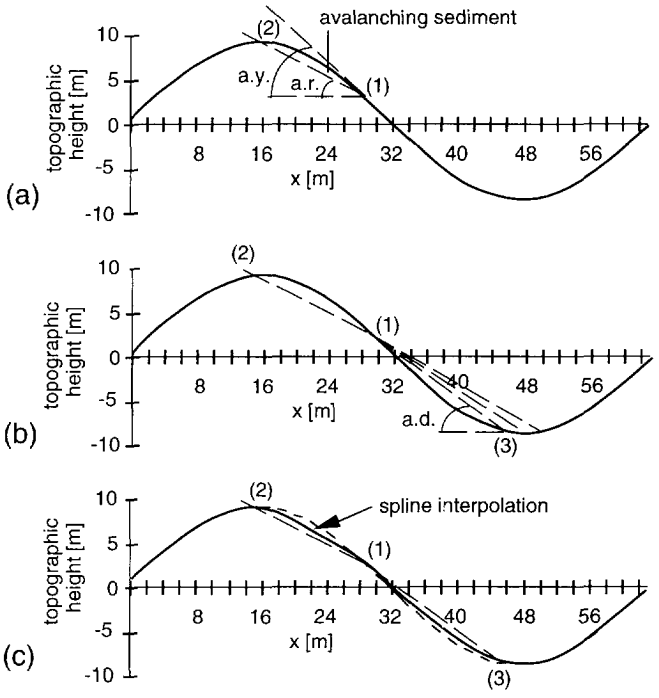

Fig. 6.4.1 *Schematization of the avalanching routine (a) Determination of the amount of sediment that will avalanche; (b) Determination of the angle at which the sediment will deposit. Different angles of deposition are calculated iteratively until the avalanching volume equals the deposited volume (c) The final topography after avalanching is determined by interpolation with a cubic spline between points (1), (2) and (3).*

i) The migration and growth of the dune through time is simulated according to the model that results from combining Bagnold's linearized sediment-transport formula with Jackson and Hunt's flow model.

ii) At each time step, the slope over the whole topography is checked on both the stoss and lee sides. Wherever the angle of initial yield is exceeded the avalanching routine will be called. It is convenient to use a small time step of simulation. This does not affect the flow simulations directly, but causes the avalanching to be a more continuous process, which is more in agreement with reality.

iii) The procedure of checking the slope is done from the apex onward, first down the stoss side and then down the lee side. In this way avalanching will first be initiated at points close to the crest of the dune (Allen, 1984, p.150B). A complete check of the slopes at a given time steps will therefore lead to several single avalanches; in between each of them the topography is readjusted. The final topography after this slope-check results from all the individual avalanches.

iv) The volume that will slide down in an individual avalanche is the volume contained between the lines at the angle of initial yield and the angle of repose (Fig. 6.4.1a). In EOLSIM both the angle of initial yield and of repose are maintained constant. The angle of initial yield has been taken at 30° and the angle of repose at 25° (Fig. 6.4.1a).

v) Deposition of an individual avalanche will occur downslope from the point where avalanching started, which is the point where the angle of initial yield was surpassed. The angle at which the sediment deposits is determined iteratively until the deposited volume equals the avalanched volume (Fig. 6.4.1b). The angle at which the avalanched sediment will rest at the foot of the bedform is defined by EOLSIM as the angle of deposition. It is determined by the volume of the sediment that slides down the slope, and varies every time the avalanching routine is called.

vi) The topography after an individual avalanche is therefore characterized by three points, (see Fig. 6.4.1c). These points are: the point where avalanching started (1), the point on the slope where the angle of repose intersects the original topography (2) and the point at which the angle of deposition intersects the original topography (3).

vii) The final topography after an individual avalanche results from an interpolation between these three points. In a first approach, this interpolation has been done with a cubic spline. Other interpolation functions that could be considered are: (a) a linear interpolation; (b) a Langrange interpolation with the polynomial of lowest possible degree, in this case a quadratic polynomial. The linear interpolation would be quite realistic. The quadratic interpolation could tend to oscillate unrealistically between the given points. Both these interpolation procedures result in discontinuities in either the topography or in the slope of topography, which will cause difficulties in the Fourier Transform (see Appendix I). Interpolation with a spline function garantees smoothness up to some order of the derivative of the function, and therefore avoids these discontinuities. The cubic-spline function has been chosen as it is the one most frequently used. The resulting topography is continuous through the second derivative. A standard routine was used (Press et al. 1988). The cubic spline is calculated from the

three points in Fig. 6.4.1. and the derivatives of the topography at the first and last points of the interpolation interval (points 2 and 3 in Fig. 6.4.1c).

viii) It is also important to note that the topography after avalanching should observe the periodic boundary conditions necessary for applying the FFT.

6.4.2 Application to a sine bedform

Figures 6.4.2a and 6.4.2b compare the simulation of a sine topography with and without the avalanching routine. The initial sine topography has an amplitude of 5 m. The same simulation conditions as in section 5.3 were maintained: $u*$=0.686 m·s^{-1} (or u=10 m·s^{-1} measured at 2 m height) and z_r/l=0.001 which gives a surface roughness of z_r=0.0059 m. The topography was given at 64 points (numbered from 0 to 63) resulting in 63 intervals of 1m. A total of 1000 hours was simulated. The simulation without avalanching (Fig. 6.4.2a) shows the bedform migrating and growing through time. As has already been noted in the analytical developments in Chapter 5, the growth of the amplitude is exponential. The simulation that includes avalanching shows the sine bedform migrating much more slowly, while approximately keeping its shape.

The effect of the avalanching routine can be seen by comparing the the spectrum of the topography from both simulations (Fig. 6.4.3). The spectrum of the topography without avalanching shows the wave number of the sine growing. We know from Eq. (5.2.14a) that this growth is exponential. The spectrum of the simulation with avalanching shows that the wave number of the original sine reaches a certain value, and that additional wave numbers appear.

Figures 6.4.4 and 6.4.5 show the effect that avalanching has on respectively the migration and the growth of the bedform. Avalanching occurs for the first time after 159 hours, so that the effects of avalanching start to become visible after this time step. Figure 6.4.4 shows the location of the apex of the sine-shaped bedform during a 1000 hour simulation, both with and without avalanching. It can be seen that initially the bedform with avalanching advances faster than the bedform without avalanching. The initial increase of the migration rate should probably be attributed to numerical reasons rather than to a physical cause. It has already been mentioned that the avalanching routine is only a first simple approximation and indicative of a general trend. After the initial increase, the advance of the dune with avalanching is clearly much lower, indicating a decrease of the migration rate caused by the

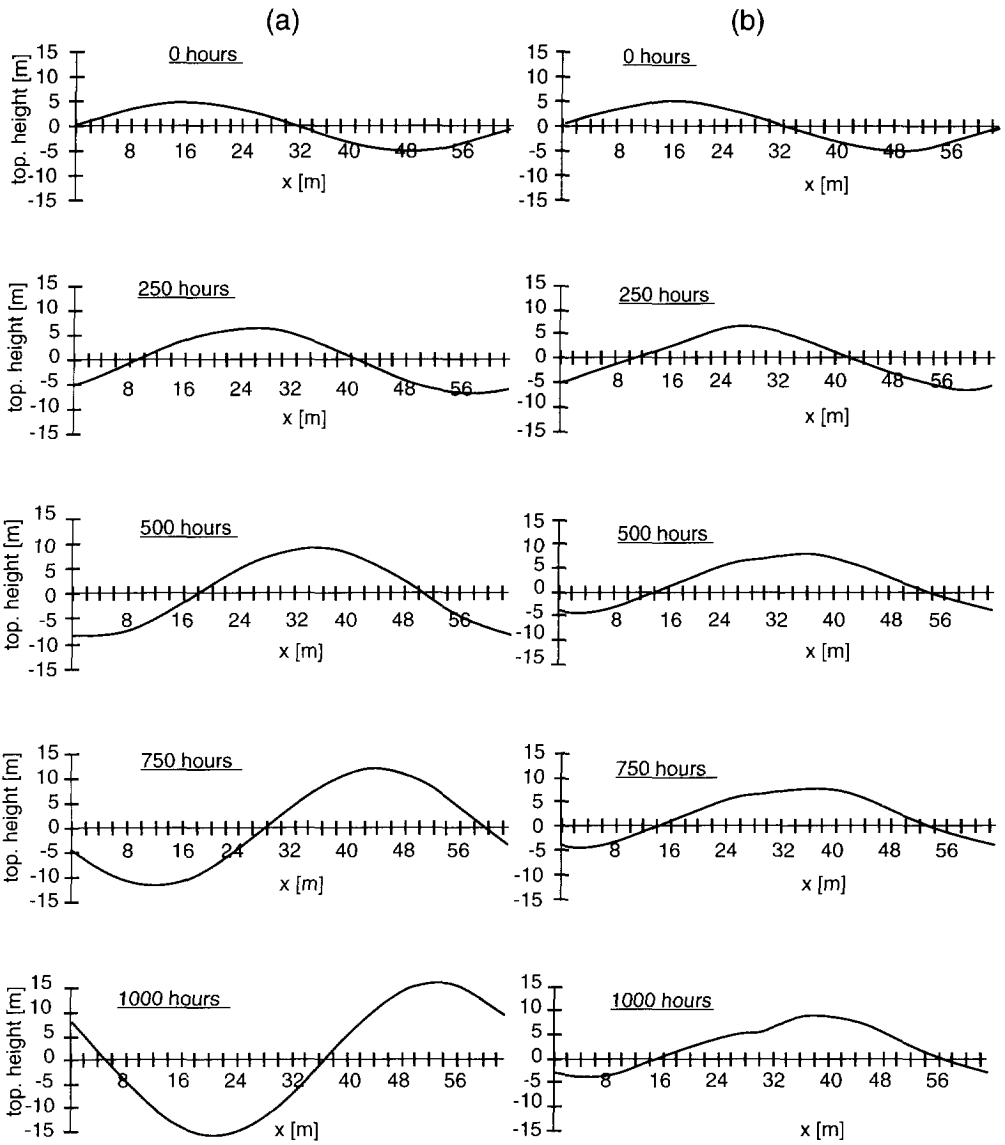

Fig. 6.4.2 *Simulation of a sine-shaped bedform (a) without avalanching; (b) with avalanching.*

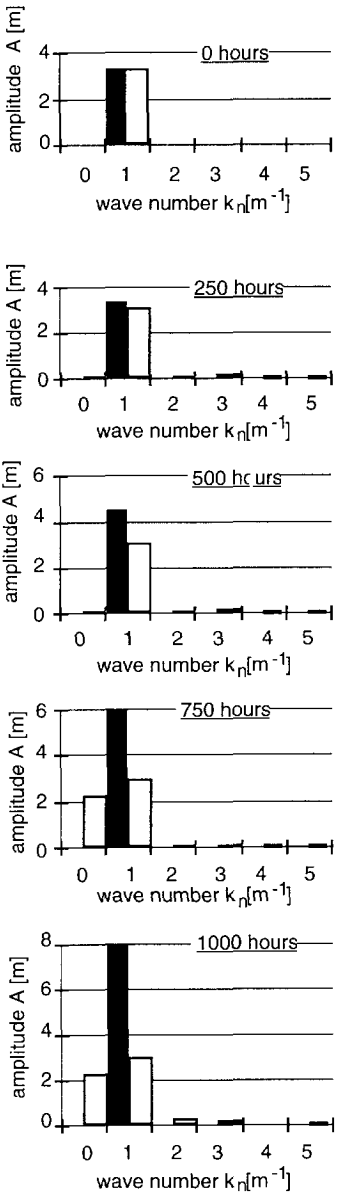

Fig. 6.4.3 *Evolution of the spectrum of a sine-shaped bedform through time. Black bars indiate simulation without avalanching. White bars indicate simulation with avalanching.*

avalanching. Figure 6.4.5 shows the height of the apex during a 1000 hour simulation with and without avalanching. It can be seen that, once avalanching starts, the increase in height is much smaller, until finally the height tends to remain constant. This indicates that avalanching is an important process in limiting bedform growth.

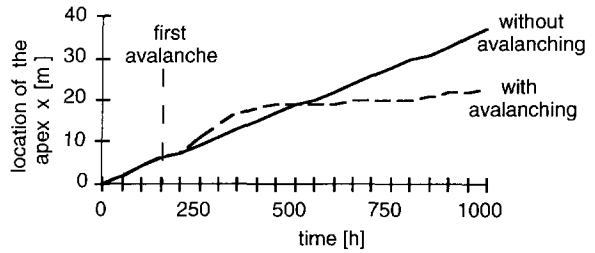

Fig. 6.4.4 Effect of the avalanching routine on the migration of a sine-shaped bedform. The graph shows the location of the apex of the bedform throughout the simulation.

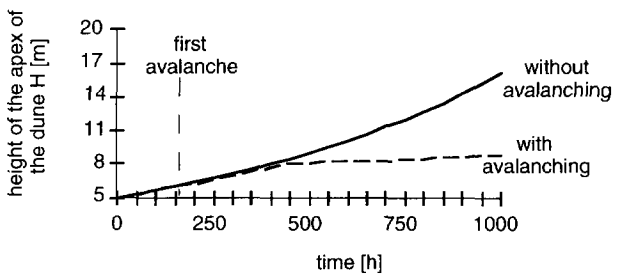

Fig. 6.4.5 Effect of the avalanching routine on the growth of a sine-shaped bedform. The graph shows the height of the apex of the bedform throughout the simulation.

6.4.3 Application to a dune

The effect of applying EOLSIM with an avalanching routine on a dune topography is shown in Figs. 6.4.6a and b. The simulation was done with the same conditions of wind velocity and surface roughness as in the previous example of a sine-shaped dune. Though there is still deformation of the dune, this is considerably less than in the simulation without avalanching. Moreover, after 1000 hours, the simulation without avalanching gives an unstable topography, dominated by a sine of unrealistically high amplitude, which corresponds to the highest wave number that is allowed to pass the filter. The simulation that includes the avalanching routine limits this growth and leads to more stable solutions (even though at first sight the topography seems more irregular).

Figure 6.4.7 shows the effect of avalanching on the spectrum of the topography. Only the first five wave numbers are shown, as higher wave numbers have very small coefficients. It can be seen that in the simulation without avalanching, the higher wave numbers grow excessively. In the simulation with avalanching this growth is limited. It could even be observed that some components of the spectrum decrease in amplitude, though simulations with a refined avalanching routine would be necessary to judge whether this has a physical cause.

6.4.4 Evaluation

The previous simulations have shown the effect of including an avalanching routine in EOLSIM. The avalanching routine is a first simple approach, so that only general behaviour should be analysed and no physical reasons should be given to local trends in growth and migration. From analyses of the spectrum of the bedforms, it can clearly be seen that avalanching limits the growth of the wave numbers. In the case of a sine-shaped bedform it can be seen that the growth of the principal wave number stops and that other wave numbers appear in the spectrum. In the case of a dune-shaped topography, with an infinite spectrum, it can be seen that avalanching effectively limits the growth of all the wave numbers.

The effect of avalanching on the topography is that the sine-shaped bedform advances at a much lower rate while maintaining approximately its initial shape. The simulation of a dune-shaped topography still shows some deformation of the original shape, but this is significantly less than shown by a simulation without avalanching. In the latter simulation, the highest wave number allowed to pass by the filter, will grow to disproportionate amplitudes, dominating completely the whole topography. This is a strong indication that avalanching is an important mechanism in bedform stability and the first simulations with an avalanching routine show promising results.

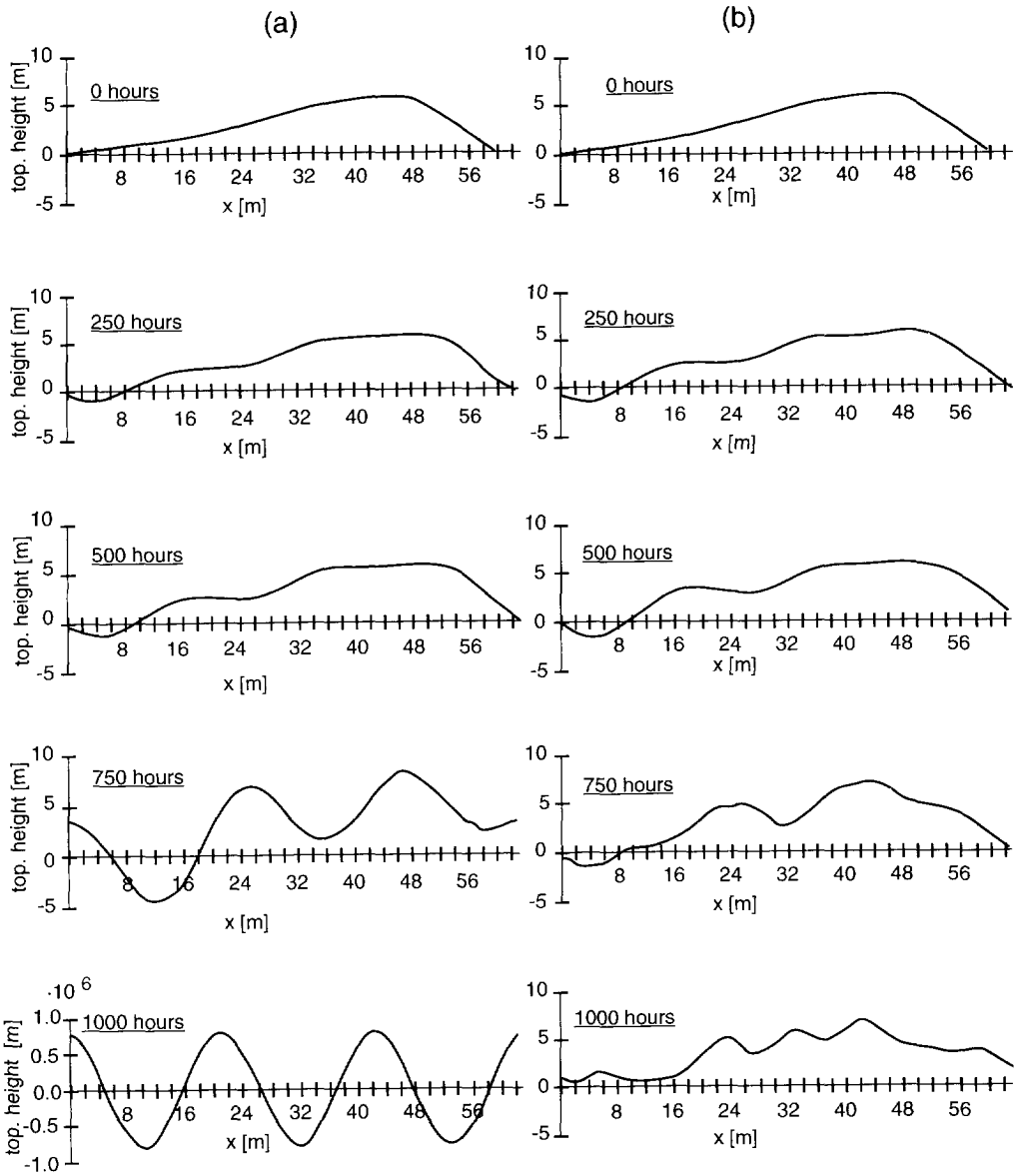

Fig. 6.4.6 *Simulation of a dune (a) without avalanching; (b) wih avalanching.*

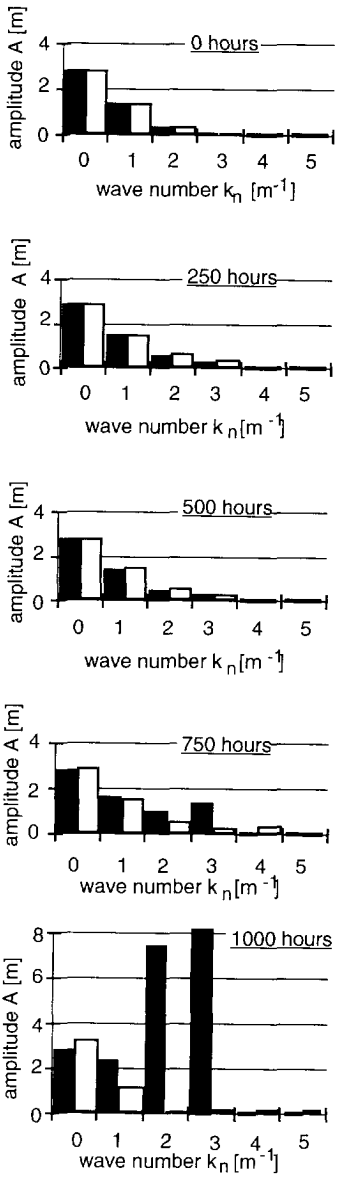

Fig. 6.4.7 *Evolution of the spectrum of a dune through time. Black bars indicate simulation without avalanching. White bars indicate simulation with avalanching.*

Chapter 7

Conclusions, discussion and recommendations

7.1 Conclusions and discussion

The study has presented the results of modelling the dynamics of aeolian bedforms. A fluid-flow model has been combined with a sediment-transport formula in a mathematical computer model. Flow of a certain velocity has a certain sediment transport capacity for a particular grainsize. The bedform affects the flow velocity (and related parameters like the shear stress), which differs notably from the logarithmic velocity profile. The variation of the flow velocity over the bedform causes changes in sediment transport capacity. Erosion or deposition occurs, as the flow seeks to re-establish its transport capacity. The following conclusions summarize the results of this work:

7.1.1 On the modelling of bedform dynamics

i) The most important factor that determines the dynamics of bedforms is the flow behaviour of the fluid. This is the main control of bedform dynamics. Although aeolian sedimentation is affected by many complicating factors (e.g. humidity of the air and of the sand, grain size, vegetation, groundwater level) that make interpretations difficult, the basic physical process can be modelled by combining an adequate flow model with a sediment-transport equation.

7.1.2 On the sediment-transport equation

ii) Regarding the sediment transport, many equations have been published, the best-known is Bagnold's (1941). All of them develop roughly similar relations between the sediment transport capacity and the wind velocity. However, there is a large variation between the sediment transport calculated by the different equations, and there are no clear arguments or experiments favouring any specific equation.

iii) From a fluid dynamic point of view it is preferable to use a transport equation expressed as a function of shear velocity instead

of the wind velocity. The main reason for this is that the shear velocity is a characteristic parameter of the flow, independent of the height of measurement. The shear velocity is defined as a function of the shear stress, which is the main force maintaining sediment transport (by the process known as saltation).

7.1.3 On the flow model

iv) The boundary-layer model for turbulent flow, developed by Jackson and Hunt (1975), is a good approximation of the flow variation over a low hill. It reproduces the main characteristics that can be expected: flow acceleration at the stoss side and deceleration at the lee side. The flow pattern over the hill is asymmetric, due to the effect of the shear stress. A further characteristic feature is that the maximum velocity occurs slightly upstream from the topographic maximum. Being a boundary-layer model, it calculates flow where the boundary layer remains attached to the surface. The flow in the wake of a fully developed dune, where the boundary layer has separated from the surface, is much more difficult to determine.

v) Simulation of flow where the boundary layer remains attached to the surface, is relevant for sedimentological studies. Wilson (1972) and Kocurek et al. (1992) describe how dunes originate from protodunes that migrate and grow. Flow behaviour in this stage is accurately described by Jackson and Hunt's (1975) model.

vi) Jackson and Hunt's (1975) model can also serve to simulate approximately the further stages of dune evolution, when a wake zone forms and a proper slipface with avalanching develops. In this case it should be considered that boundary-layer models give a good description of the flow characteristics upstream of the point of flow separation. Downstream from the point of flow separation, in the wake, the main sedimentary process is avalanching, which is determined by slope instability and not by the flow itself.

7.1.4 On the modelling results for bedform dynamics

vii) By combining Jackson and Hunt's (1975) flow model and a linearization of Bagnold's sediment-transport equation, an analytical solution for dune dynamics was developed. Analytical expressions for the shear stress, the sedimentation rate, the topography through time, the migration rate and the growth were developed for a sine-shaped dune.

viii) These expressions show that there is a phase difference between the shear stress and the topography, so that the maximum shear stress (therefore also the maximum shear velocity) occurs before the maximum height and the minimum shear stress occurs before the trough. This is the reason for bedform growth (as has been pointed out by Kennedy, 1969 and McLean, 1990). Because of this phase difference, deposition will occur downstream of the maximum shear velocity, therefore also at the location of the maximum height.

ix) The model appears to indicate that, under constant wind velocity, bedforms migrate at a constant rate through time. This is due to a simplification of the flow model, where only first-order terms have been taken into account and higher-order terms have been neglected.

x) Migration and growth rates are higher for higher wind velocities. This is a calculated result that intuitively can be expected.

xi) Under constant shear stress, migration rate and growth factor are higher for higher surface roughness. It should be noted, however, that a constant shear stress with an increasing surface roughness will result in higher wind velocities being measured. There are no published observations on the relationship between migration rates and surface roughness, so this conclusion has not yet been supported by observations.

xii) The migration rate is higher for higher wave numbers (i.e. smaller wave lengths). Comparison with migration rates published by Long and Sharp (1964) seems to support this conclusion. This trend suggests that smaller dunes will migrate over large ones, and therefore the large bedforms (draas and large dunes) will be preserved under the smaller dunes. This has been observed in modern desert deposits (Pugh et al., 1993) as well as inferred from ancient aeolian formations (Weber, 1987). There are many other factors affecting the preservation of aeolian sediments (the main one being basin subsidence), and it is too premature to relate the theoretical results to these observations because there are many aspects that require further research (see section 7.3). However, it can be stated at this point that the theory does not conflict with the observations.

xiii) The growth rate is also higher for higher wave numbers. There are no published observations to confirm this, although McLean (1990) reached the same conclusion from theoretical fluid-dynamic

considerations. It seems plausible that ripples grow faster than dunes, and dunes faster than draas.

xiv) The expressions show that the growth of a bedform is exponential through time. This may be so in an initial stage of a protodune, but does not hold as a dune evolves. It is likely however, that the exponential growth is due to the linearity of the model. In a later stage of dune evolution, an equilibrium is reached, where a dune migrates without changing its shape.

7.1.5 On the equilibrium of bedforms

xv) From the previous conclusion we can infer that after the initial period of growth, either the growth rate decreases, or other processes occur that counteract the growth. This would imply that:
- As a dune evolves, the flow pattern and the topography change progressively until they are in phase. This possibility could be studied by carrying out simulations with a more detailed flow model or by detailed experimental measurements (e.g. in wind tunnels).
- There is a process that counteracts the phase difference between shear stress and topography. The process that has been considered in this study is avalanching. Another possibility is that the transport rate and the shear stress are also out of phase, as suggested by McLean (1990). In this way the transport rate does not respond immediately to the changes in shear stress. However in that case one has to explain why this lag appears in the equilibrium phase and not during the evolution of the protodune.

xvi) Avalanching has been considered as a process that balances bedform growth. Including a simple avalanching routine shows that bedforms grow until a certain stage, after which the growth rate slowly decreases and the bedform continues to migrate. This first experiment indicates that avalanching plays a key role in dune equilibrium.

xvii) Avalanching affects the migration rate, which becomes smaller. Again there is no published data on migration rates of protodunes versus fully developed dunes, so this conclusion has still to be supported by actual observations.

7.2 Applications and recommendations for further research

This research is a step towards understanding the physics of bedforms. It opens many subjects, of both a theoretical and an

experimental nature that would be interesting to consider for further study. It also gives a good basis for concrete studies directed towards simulating subsurface structures for reservoir engineering applications, which was the general purpose for which this research was formulated.

i) Jackson and Hunt's model, being an analytical model, is more practical to use for simulations because it requires less computer time and, because of the analytical expressions developed in this study, the relationships between different parameters are clearer to understand. Conclusions (iv), (v) and (vi) indicate that it is important to determine the accuracy of Jackson and Hunt's flow model. This can be done by doing simulations with a more detailed numerical calculation and comparing with characteristic trends (e.g. location and magnitude of maximum and minimum velocities etc.).

ii) Conclusion (xvi) indicates that it would be recommendable to improve the avalanching routine. This would permit a more trustworthy comparison of migration rates, with and without avalanching, for different wave lengths, as is noted in conclusion (xvii). This also makes it possible to determine the proportions of grain-flow strata (resulting from the avalanching process) and grain-fall strata (resulting from the saltation process) depending on wave length, wind velocity etc. Such simulations would be more comparable with actual reservoir samples (i.e. cores). This is of particular interest for the prediction of good hydrocarbon reservoirs in aeolian deposits, where the grain-flow strata form the better reservoirs.

iii) It would be of interest to consider the effect of the variation of wind velocity through time. Daily variations of wind regime could be considered but also seasonal effects (e.g. the shamal in Arabia) and effects on a longer time scale (e.g. the strong winds in the Pleistocene forming single dunes of 100 m height, whereas today's winds form much smaller dunes, see Glennie, 1984).

iv) Further extensions that can be considered include the effects of different grain sizes, of a variable sand supply, of the influence of the ground-water table and of the possibility of immobilization of the surface (caused by e.g. the growth of vegetation). Simulation of different grain sizes would constitute a feature that is easier to compare with reservoir data such as core samples.

v) It is always important to develop and understand the implications and effects of a two-dimensional model before developing a three-dimensional model. Once the two-dimensional model is fully

understood, the logical extension to a three-dimensional model can be considered. The extension of Jackson and Hunt's model to three dimensions has already been done (Mason and Sykes, 1979). A three-dimensional aeolian model based on the extended Jackson and Hunt theory (1975) and including a three-dimensional avalanching routine would permit modelling variable wind direction, and assess the effect on the dune morphology. This can reinforce the empirical observations of Fryberger (1979) and the experimental results of Rubin and Ikeda (1990).

vi) It would be of interest to compare the theory with field measurements. In order to make relevant morphological field studies, dune geometries (height, width and length), migration rates, and detailed annotation of the wind regime (i.e. velocity and height of measurements for the whole observation time), should be registered. There are many aeolian studies of deserts and beaches, however there is little complete and consistent data published with which to test the theory. Many studies only publish sand roses, which only serve as a global indication of the wind direction but cannot be used for quantitative conclusions.

List of symbols

symbol	concept	unit	dimension
$a_{0..m}$ =	amplitude of the cosine components of the Fourier series of a function	same as the function	
A =	amplitude	m	L
A^* =	dimensionless amplitude	-	-
A_t =	constant for threshold shear velocity	-	-
$A_{1,2..}$ =	general constants used in linearizations	-	-
$b_{0..m}$ =	amplitude of the sine components of the Fourier series of a function	same as the function	
c =	migration rate, sometimes also called wave velocity or celerity	$m \cdot s^{-1}$	$L \cdot T^{-1}$
c^* =	normalized migration rate	s^{-1}	T^{-1}
$c_{0..m}$ =	coefficient of the complex form of the Fourier series of a function	same as the function	
c_n =	numerical wave velocity	$m \cdot s^{-1}$	$L \cdot T^{-1}$
c_t =	theoretical wave velocity	$m \cdot s^{-1}$	$L \cdot T^{-1}$
C =	general constant in sediment transport formulae	depending on the formula	
C_1 =	empirical constant in Bagnold's sediment-transport formula as a function of the shear velocity	-	-
C_2 =	empirical constant in Bagnold's sediment-transport formula as a function of the velocity	-	-
C_B =	constant derived from Bagnold's sediment-transport formula	$s^2 \cdot m^{1/2} \cdot kg^{-1/2}$	$T^2 \cdot L^{1/2} \cdot M^{-1/2}$
C_{Im} =	coeficient of the imaginary exponential of the topography equation, related to the dune migrating rate	s^{-1}	T^{-1}

C_{Re}	=	coeficient of the real exponential of the topography equation, related to the dune growth	s^{-1}	T^{-1}
C_k	=	complex factor related to the migration rate and growth factor of a sine-shaped bedform	s^{-1}	T^{-1}
C_τ	=	factor containing the physical parameters related to migration rate and growth factor of a sine-shaped bedform	s^{-1}	T^{-1}
d	=	grain diameter	m	L
D	=	grain diameter of a standard 0.25 mm sand	m	L
E_n	=	error for wave number k_n in the case of a simulation of all the wave numbers together	-	-
f	=	general function		
Fr	=	Froude number	-	-
g	=	gravitational acceleration	$m \cdot s^{-2}$	$M \cdot T^{-2}$
h	=	topographic height	m	L
h^*	=	dimensionless topographic height	-	-
H	=	maximum topographic height	m	L
k	=	wave number	m^{-1}	L^{-1}
k^*	=	dimensionless wave number	-	-
k_n	=	wave number for the discreet Fourier Transform	-	-
L	=	characteristic length	m	L
l	=	thickness of the inner region	m	L
$_n$	=	subindex indicating the wave number coorresponding to a discreet Fourier transform	-	-
N	=	number of intervals in the x-direction	[-]	[-]
p	=	fluid pressure	Pa	$M \cdot L^{-1} \cdot T^{-2}$
p_1	=	first order correction for the pressure	-	-
q	=	sediment-transport capacity	$kg \cdot m^{-1} \cdot s^{-1}$	$M \cdot L^{-1} \cdot T^{-1}$
Q	=	sediment-transport capacity per surface unit	$kg \cdot m^{-2} \cdot s^{-1}$	$M \cdot L^{-2} \cdot T^{-1}$
q_0	=	constant basic sediment-transport capacity	$kg \cdot m^{-1} \cdot s^{-1}$	$M \cdot L^{-1} \cdot T^{-1}$
q_x	=	sediment-transport capacity in the x-direction per unit length in the y-direction	$kg \cdot m^{-1} \cdot s^{-1}$	$M \cdot L^{-1} \cdot T^{-1}$

q_y	=	sediment-transport capacity in the y-direction per unit length in the x-direction	$kg \cdot m^{-1} \cdot s^{-1}$	$M \cdot L^{-1} \cdot T^{-1}$
q_l	=	Bagnold's linearized sediment-transport capacity	$kg \cdot m^{-1} \cdot s^{-1}$	$M \cdot L^{-1} \cdot T^{-1}$
Re	=	Reynolds number	-	-
t	=	time	s	T
u	=	flow velocity, sometimes wind velocity is specified	$m \cdot s^{-1}$	$L \cdot T^{-1}$
u_1	=	first order correction for the flow velocity	-	-
u_*	=	shear velocity, friction velocity or drag velocity	$m \cdot s^{-1}$	$L \cdot T^{-1}$
u'_*	=	saltation shear velocity	$m \cdot s^{-1}$	$L \cdot T^{-1}$
u_{thr}	=	threshold velocity of a given grain size	$m \cdot s^{1}$	$L \cdot T^{-1}$
u_{*thr}	=	threshold shear velocity of a given grain size	$m \cdot s^{1}$	$L \cdot T^{-1}$
U	=	flow velocity at the upper edge of the boundary layer	$m \cdot s^{1}$	$L \cdot T^{-1}$
x	=	Cartesian coordinate	m	L
x^*	=	dimensionless Cartesian coordinate	-	-
y	=	Cartesian coordinate	m	L
z	=	Cartesian coordinate	m	L
z_k	=	factor dependent on the wave number	-	-
z_r	=	roughness length	m	L
z'_r	=	roughness length during saltation	m	L
γ	=	general argument of the Modified Bessel functions	-	-
ε	=	perturbation factor according to Jackson and Hunt (1975)	-	-
κ	=	Von Kármán constant	-	-
λ	=	wave length	m	L
ν	=	kinematic viscosity	$m^2 \cdot s^{-1}$	$L^2 \cdot T^{-1}$
ρ	=	fluid density, generally air density is specified	$kg \cdot m^{-3}$	$M \cdot L^{-3}$
ρ_s	=	grain density	$kg \cdot m^{-3}$	$M \cdot L^{-3}$
σ	=	sediment density	$kg \cdot m^{-3}$	$M \cdot L^{-3}$
σ^*	=	normalized sediment density	$kg \cdot m^{-1}$	$M \cdot L^{-1}$
τ	=	shear stress	Pa	$M \cdot L^{-1}T^{-2}$
τ'	=	shear stress due to the saltation	Pa	$M \cdot L^{-1}T^{-2}$
τ_0	=	shear stress from logarithmic profile	Pa	$M \cdot L^{-1}T^{-2}$

τ_1	=	first order correction to the shear stress from the logarithmic profile	-	-
υ	=	order of the Modified Bessel function	-	-
ϕ	=	$\pi/4$ for positive wave numbers	-	-
		$-\pi/4$ for negative wave numbers	-	-

operators

d	=	differential
∂	=	partial differential
Δ	=	increment
$\hat{}$	=	Fourier Transform

functions

kei_0, ker_0	=	Kelvin functions of the zero order
kei_1, ker_1	=	Kelvin functions of the first order
K_0	=	Modified Bessel function of the zero-order
K_1	=	Modified Bessel function of the first order

Glossary of geological terms

In this study, terminology from different disciplines has been used. This glossary has been included for the convenience of the reader who might not be acquainted with some of these specific terms. Most of the geological definitions have been taken from Visser (1980). Some specific aeolian terms have been taken from Glenn (1979). Cross-references to other terms in this glossary are indicated in italics.

allocyclical processes. Processes resulting from changes external to the sedimentary unit, such as uplift, subsidence, climatic variation or *eustatic* change.

alluvial fan. River deposit in the form of a fan or cone, usually flanking a mountain or a mountain range.

amplitude. Half the distance between the maximum and the minimum of the cycle of a periodic phenomenon in space or time (Fig. 1).

angle of deposition. Term used in this study to indicate the inclination angle at which avalanched sediment will deposit at the toe of the dune.

angle of initial yield. Inclination angle at which the slope is unstable in the gravity field and sediment starts to avalanche (Allen, 1984, vol B, p.149).

angle of repose, angle of rest. The residual angle, lower than the *angle of initial yield*, at which a slope is left after avalanching has occurred (Allen, 1984, vol B, p.149).

anisotropic. A mass or body is anisotropic when its properties differ in different directions.

apex. See *crest* .

arroyo. Channel of an ephemeral or intermittent stream (spanish term).

autocyclical processes. Processes that are generated within the sedimentary unit, such as channel migration (Selley, 1978, p.19).

avalanche slope. See *slipface*.

barchan. Crescent shaped sand *dune*, which migrates downwind in the direction of its *horns*.

bedform. Surface shape of the structure formed at the interface of water (or air) currents and sediment bed.

brink. The top of the *slipface* of a *dune*. It may coincide with the *crest* or *apex* (Fig. 2).

crest. *Dune* summit, the highest natural point of a *dune* (Fig. 2).

cross-bedding. The arrangement of beds (thicker than 1 cm) at one or more angles to the general *dip* of the formation.

cross-stratification. The arrangement of beds (thicker than 1 cm) or laminae (thinner than 1 cm) at one or more angles to the general *dip* of the formation.

diagenesis. All mechanical, chemical, mineralogical and biological processes and changes in a sediment and its interstitial water after its deposition; e.g. compaction, cementation, pressure solution etc.

dip. The angle which a planar feature makes with the horizontal plane, as measured in a plane normal to the *strike*.

draa. Very large sand *dune*, with a height in excess of 60m and a width of 500m or more. It may carry *dunes* of normal size on its gently sloping side and form part of a regular series.

dune. Accumulation of wind-blown sand possessing one or more *slipfaces*.

erg. An extensive region of sand *dunes* and *interdune* areas. Sometimes the *dunes* are so close together that the *interdunes* can be absent (North African term).

eustatic. Pertaining to a simultaneous, world-wide change in sea-level

festoon cross-bedding. Cross-stratification pattern that results from successive erosion and filling of plunging troughs. The filling of the troughs occurs by thin concave upward layers. The festoon pattern is most conspicuous on vertical faces cut at right angles to the longitudinal axes in a series of superimposed troughs plunging in the same direction.

fluid threshold velocity. The velocity at which sand movement starts by the action of the fluid (Bagnold, 1941, p.89).

foreset laminae/bed. Series of parallel, inclined laminae or beds of a *cross-bedded* unit, deposited by water or wind, the layers or laminae dipping in the direction of the flow.

grading. The gradual reduction of grain sizes in a given direction within a layer of granular material.

homogeneous. A mass or body is homogeneous when samples from different locations but of the same size and orientation have the same properties.

horns. The pointed ends of a *dune*, especially the forward extensions of a *barchan dune*.

impact threshold velocity. The lowest velocity at which sand movement by *saltation* is maintained by the action of the fluid. This is lower than the *fluid threshold velocity* (Bagnold, 1941, p.104).

inhomogeneous. A mass or body is inhomogeneous when samples from different locations but of the same size and orientation have different properties.

interdune Relatively flat areas between *dunes*.

inverse grading. The decrease in grain size of the *grading* goes from fine at the base to coarse at the top.

isotropic. A mass or body is isotropic when its properties are the same in all directions.

lee side. Downstream side of a *dune* (Fig. 2).

linear dune, longitudinal dune or seif. Parallel straight *dune* with *slipfaces* on both sides of its *crestline*. Its long axis is parallel to the *dune*-forming wind.

model. Simplification of the actual conditions and concentration on the essential aspects of a phenomenum.

normal grading. The decrease in grain size of the *grading* goes from coarse at the base to fine at the top.

playa, playa lake. Dried-up desert lake; generally non-saline.

protodune. *Bedform* that will develop into a *dune*. A protodune has migrated away from its initial deposition site, but has not yet developed a *slipface* with *avalanching*.

reservoir. Porous body of rock containing an accumulation of hydrocarbons or water.

ripple. A small scale, rythmic relief pattern, formed on the surface of an unconsolidated sediment under the influence of flow of water or air.

sabkha, sebkha. A flat area of clay, silt or sand, with saline incrustations that forms, for instance, at the borders of desert lakes. They may also obtain their moisture from proximity to the water table.

salina. Semi-permanent salt lake that may form in a desert.

saltation. Jumping transport of bottom particles, whereby they are intermittently thrown upward into flowing air or water and moved downcurrent a short distance until they land again on the bottom.

sand sea. See *erg*.

sand sheet. Accumulation of sand in essentially flat laminae forming a sheetlike or blanketlike deposit. It has no *slipfaces*, but has distinct geographic boundaries.

sandstone. A consolidated arenaceous rock, having a dominantly siliceous composition.

slipface. Steep face on the *lee* side of a *dune* usually at the *angle of repose* of dry sand.

star dune. A piramidal *dune*, roughly star shaped with three or more arms with *slipfaces*, extending in various directions. It is thought to form where seasonal winds are strongly oblique to each other. May also result by modification of parts of older transverse or linear *dunes*.

strike. The line formed by the intersection of an inclined planar feature with a horizontal plane.

stoss side. The upstream side of a *dune* or *ripple*, facing the dominant wind direction from which the *dune* has migrated and opposite to the *lee side* (Fig. 2).

stratum. Unit layer in a stratified rock sequence that is lithologically distinguishable from other layers above and below.

transverse dune. Asymmetric sand ridge, with a gentle *stoss* slope and a steep *lee* slope, in which the length dimension is perpendicular to the dominant wind direction. It has one *slipface* .

wadi. See *arroyo* (arabic term).

wave length. The length of a complete cycle of a periodic phenomenon in space or time (Fig. 1).

wave number. The number of complete cycles of a periodic phenomenon in a unit of space. When the phenomenon is periodic in time this is called the frequency.

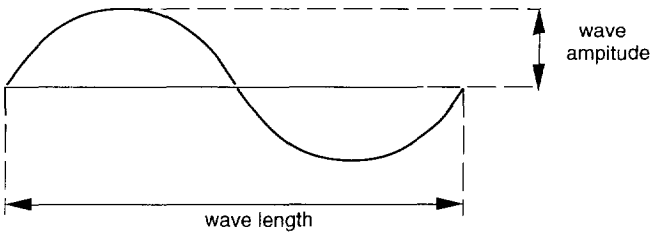

Fig. 1 *Scheme of a wave and its parts*

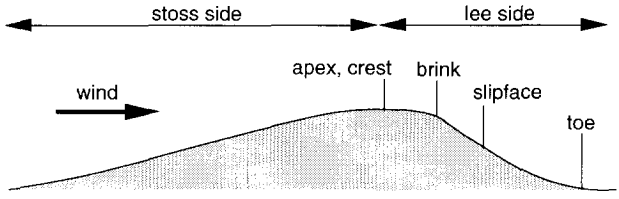

Fig. 2 *Scheme of a transverse dune and its parts.*

Appendix I

Fourier series, Transforms and discrete Fourier Transforms

The Fourier series

Any function $f(x)$ on $0 < x < L$ can be written as a sum of sine and cosine functions by a Fourier series:

$$f(x) = \frac{a_0}{2} + \sum_{m=1}^{\infty} \left(a_m cos \left(\frac{2\pi m x}{L} \right) + b_m sin \left(\frac{2\pi m x}{L} \right) \right) \quad \text{(A-I.1a)}$$

where the coefficients a_0 , a_m and b_m are given by:

$$a_0 = \frac{2}{L} \int_0^L f(x)\, dx \quad \text{(A-I.1b)}$$

$$a_m = \frac{2}{L} \int_0^L f(x)\, cos \left(\frac{2\,\pi\, m\, x}{L} \right) dx \quad \text{(A-I.1c)}$$

$$b_m = \frac{2}{L} \int_0^L f(x)\ sin \left(\frac{2\,\pi\, m\, x}{L} \right) dx \quad \text{(A-I.1d)}$$

In these expressions:

x	=	the horizontal coordinate [m]
L	=	the total length of the domain [m]
m	=	a natural number (1,2,3...∞)

The idea has been illustrated in Fig. A-I.1 where a dune-shaped topography can be seen decomposed in its Fourier series.

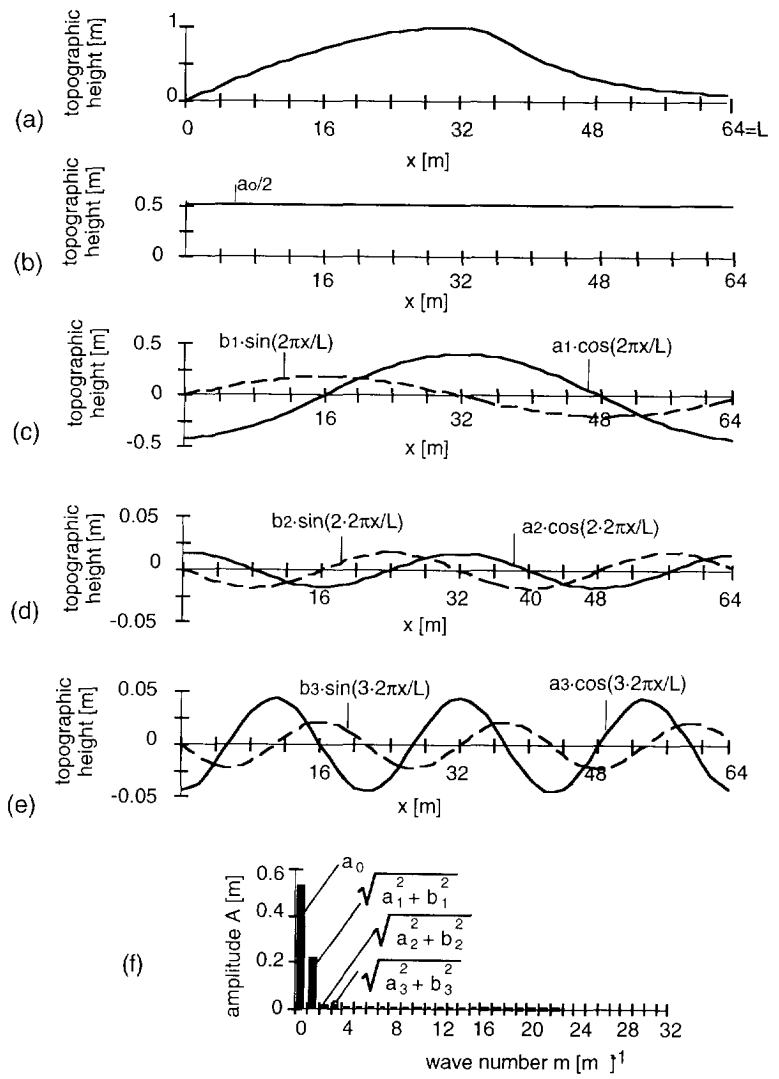

Fig A-1.1 *Fourier decomposition of a dune shaped topography according to:*

$$h(x) = \frac{a_0}{2} + \sum_{m=1}^{\infty}\left(a_m \cos\left(\frac{2\pi m x}{L}\right) + b_m \sin\left(\frac{2\pi m x}{L}\right)\right)$$

(a) topography; (b) contribution of the zero-wave number; (c) contribution of the first wave number; (d) contribution of the second wave number; (e) contribution of the third wave number; (f) spectrum showing the relative contribution of each wave-number.

The following concepts can then be defined:

The wave length [1]:	$\lambda = L/m$	[m]
The wave number:	$2\pi/\lambda = 2\pi m/L$	[m^{-1}]

It should be noted that the maximum wave length is L, which corresponds to the minimum wave number (m=1)

Making use of the following relationships:

$$e^{iy} = cos\ y + i\ sin\ y \qquad \text{(A-I.2)}$$

and:

$$cos\ y = \frac{1}{2}\left(e^{iy} + e^{-iy}\right) \qquad \text{(A-I.3a)}$$

$$sin\ y = \frac{1}{2i}\left(e^{iy} - e^{-iy}\right) \qquad \text{(A-I.3b)}$$

Eq. (A-I.1a) can be expressed as:

$$f(x) = \sum_{m=-\infty}^{+\infty} c_m exp\left(\frac{i\,2\pi m x}{L}\right) \qquad \text{(A-I.4a)}$$

where

$$c_m = \frac{1}{L}\int_0^L f(x)\, exp\left(-\frac{i\,2\pi m x}{L}\right) dx \qquad \text{(A-I.4b)}$$

This is the complex form of the Fourier series. Note that due to the positive and negative sign of the exponentials in Eqs. (A-I.3a,b), the summation goes from -∞ to +∞ instead of from 0 to +∞ as in Eq. (A-1.1a). Equaling (A-1.1a) and (A-1.4a) it can easily be seen that the following relationship holds between c_m and a_m and b_m :

$$c_m = \frac{1}{2}\left(a_m - ib_m\right) \quad if\ m > 0 \qquad \text{(A-I.5a)}$$

$$c_m = \frac{1}{2}\left(a_m + ib_m\right) \quad if\ m < 0 \qquad \text{(A-I.5b)}$$

$$c_0 = \frac{a_0}{2} \quad if\ m = 0 \qquad \text{(A-I.5c)}$$

---

[1] In practice the half-wave length is also used because it resembles more real-life situations. Often the term "half" is then dropped and the term "wave-length" is used. This can cause confusion, and therefore this has been avoided here.

The Fourier transformation

A Fourier series defines a function on an interval $0 < x < L$ and is assumed to repeat itself periodically for $x > L$ and $x < 0$, that is on $(-\infty, \infty)$. Most functions however, that describe real situations are not periodic. An analogous representation of Eqs. (A-1.4ab) can then be given by:

$$f(x) = \int_{-\infty}^{\infty} \hat{f}(k)\, exp\,(i\, k\, x)\, dk \qquad \text{(A-I.6a)}$$

with:

$$\hat{f}\,(k) = \frac{1}{2\pi} \int_{-\infty}^{\infty} f(x)\, exp\,(-i\, k\, x)\, dx \qquad \text{(A-I.6b)}$$

$\hat{f}(k)$ is called the Fourier Transform of $f(x)$. Applying Eq. (A-I.6b) to a function is called the Fourier transformation, and applying Eq. (A-I.6a) the inverse Fourier transformation. Slightly different conventions are sometimes used regarding the sign of the exponent or in the factor 2π. The Fourier Transform represents a function in a continuous resolution of wave numbers k, defined from $-\infty < k < +\infty$.

The discrete Fourier transformation

For practical application of Eqs. (A-I.6ab) a discrete version of the Fourier transformation, on a finite length, is needed. The x-coordinate is discretized into N intervals of Δx length, denoted as x_j $(j=0....N)$. Discreet values for the wave number k_n $(n=0....N)$ also have to be taken. Since the function is defined on N mesh points, only N Fourier coefficients are needed. This means that there are as many Fourier coefficients as discretization intervals (N), but different indices are used for each (subindex $_j$ for the x-coordinate and subindex $_n$ for the wave number). In this way Eqs. (A-I.6a and b) become:

$$f\,(x_j) = \sum_{n=0}^{N} \left(\hat{f}_n\, exp\,(i\, k_n\, x_j)\right) \qquad \text{(A-I.7a)}$$

and

$$\hat{f}_n = \frac{1}{N} \sum_{j=0}^{N} \left(f(x_j)\, exp\,(-i\, k_n\, x_j)\right) \qquad \text{(A-I.7b)}$$

which are the discrete Fourier transformation (Eq. A-I.7b) and the inverse discrete Fourier transformation (Eq. A-I.7a). Note that the term 2π becomes N in the discrete Fourier Transform. A practical set of values for the discreet wave number k_n is given by:

$$k_n = 2\pi n/N\Delta x \qquad \text{with } n=0,\ 1,\ 2...N$$

It is important to note that in this convention the x-axis starts at $j=0$ and that for even N:
n =0,1,2...$^1/_2N$-1 corresponds to positive wave numbers
n =$^1/_2N$+1, $^1/_2N$+2...N corresponds to negative wave numbers
n =$^1/_2N$ corresponds to the zero wave number.
A convention with a centred x-axis (from j= -$^1/_2N$ to +N) can also be used. In that case:
n = 1,2....$^1/_2N$ corresponds to positive wave numbers
n = -1,-2....-$^1/_2N$ corresponds to negative wave numbers
n = 0 corresponds to the zero wave number.

Again periodic extension of that function is assumed. In this case again, care must be taken that $f(0) = f(N\Delta x)$ so that periodicity of a smooth function is ensured (discontinuities cannot be represented by a finite sum).

If we differentiate Eq. (A-I.7a) (with a continuous variable x instead of the discrete variable x_j), we would obtain

$$\frac{df(x)}{dx} = \sum_{n=0}^{N} \left(i\, k_n \widehat{f}_n exp\left(i\, k_n x\right) \right) \qquad \text{(A-I.8)}$$

which implies that obtaining the derivative of a function is the same as multiplying the Fourier Transform by ik_n; which is a convenient way of calculating the derivative of a function $f(x)$.

Both the function $f(x_j)$ and the Fourier Transforms $\widehat{f}_n(k_n)$ can be complex. However, if the function expressed in Eq. (A-I.7a) is real, all the imaginary terms should eliminate each other. This can happen only if the N Fourier Transforms are symmetric and conjugate around $N/2$, so that in the summation (Eq. A-I.7a) the imaginary terms will add up to zero.

It is practical to note that, considering Eq. (A-I.2.2), the Fourier Transform can be expressed in its modulus and phase:

$$\widehat{f}_n = \left|\widehat{f}_n\right| \; exp \; (i \; \eta_n) \tag{A-I.9}$$

where the modulus is calculated from

$$\left|\widehat{f}_n\right| = \sqrt{\left(Re \; \left(\widehat{f}_n\right)\right)^2 + \left(Im \left(\widehat{f}_n\right)\right)^2} \tag{A-I.10}$$

and the phase from:

$$arctan \left(\frac{Im \left(\widehat{f}_n\right)}{Re \left(\widehat{f}_n\right)}\right) \tag{A-I.11}$$

The modulus defines the frequency spectrum of that component. It represents the contribution of a wave, with wave number k to the whole function. The behaviour of a phenomenon can be understood by the behaviour of its frequency spectrum, and it is very useful to help identify the problems that arise when using Fourier methods. The phase of a wave number indicates the shifting of that wave along the x-coordinate.

Appendix II

Calculation of the flow field according to Jackson and Hunt

Underlying ideas

Jackson and Hunt (1975) developed a two-dimensional analytical model for a turbulent wind flow over a low hill. They divided the profile in an inner region close to the surface and an outer region further away from the surface (Fig. 5.2.1). Outside the outer region the flow is undisturbed by the topography. They assumed that in a first approximation the velocity has the logarithmic profile of the turbulent boundary layer over a flat surface of constant roughness. However, the topography causes a vertical displacement of air with a certain vertical velocity. Sufficiently far above the topography, above the outer region, the horizontal velocity should be equal to the undisturbed velocity and the vertical velocity should be zero. This implies that in the outer region (i.e. between the inner region and the undisturbed region) there is a perturbation of the horizontal velocity, which also leads to a perturbation of the pressure in the outer region. This pressure perturbation affects the pressure of the inner region which in turn affects the local horizontal and vertical velocities in the inner region. For the purpose of this study we are mainly interested in the flow close to the surface, where the sediment transport occurs through saltation, therefore this appendix will concern the inner region.

Assumptions

It is assumed that the flow occurs over a hill of length L and maximum topographic height H, where the height is much smaller than the length and the slope is small everywhere. In a first approximation the velocity has the logarithmic profile. If the slopes of the hill are small enough, the topography causes a perturbation of the logarithmic profile. The horizontal velocity can then be written as:

$$u(x,\Delta z) = \frac{u_*}{\kappa} ln\left(\frac{\Delta z}{z_r}\right) + \varepsilon\, u_* u_1\left(\frac{x}{L},\frac{\Delta z}{l}\right) \qquad \text{(A-II.1)}$$

with:

$$u_* = \sqrt{\frac{\tau_0}{\rho}} \qquad \text{(A-II.2)}$$

where:

u_1 = dimensionless perturbation velocity [-]

ε = perturbation factor [-]
equal to:

$$\varepsilon = \frac{H \ ln^2(L/z_r)}{L \ \kappa \ ln(l/z_r)} \qquad \text{(A-II.3)}$$

l = thickness of the inner region, which, for $10^4 < \frac{L}{z_r} < 10^7$

can be approximated to within 4 percent with:

$$\frac{l}{z_r} = \frac{1}{8}\left(\frac{L}{z_r}\right)^{0.9} \qquad \text{(A-II.4)}$$

Jackson and Hunt developed their equations for velocity and pressure over a topography with dimensionless length and height (x/L and $h(x)/H$ respectively). The effect of the actual slope is then accounted for by the magnitude of the perturbation factor ε. Fig. (A-II.1) shows ε according to Eq. (A-II.3) as a function of the slope (h/L) for different roughness lengths (z_r) given by Eq. (A-II.4). Three roughness lengths have been taken: 0.001m, which would correspond to the roughness caused by surface grains, 0.01m which would correspond to the roughness caused by ripples, and 0.1m, which would correspond to the roughness caused by shrubbery. Fig. (A-II.1) shows that Jackson and Hunt's corrections have a greater weight for steeper slopes and for an increased roughness length.

The shear stress at the surface, which is the parameter necessary for calculating sediment transport, is given by Jackson and Hunt as:

$$\tau(x) = \tau_0 + \varepsilon \ \tau_0 \ \tau_1(x) \qquad \text{(A-II.5)}$$

The shear-stress correction is finally calculated from the correction of the horizontal component of the velocity according to:

$$\tau_1 = 2 \ \kappa \Delta z \frac{\partial u_1}{\partial z} \qquad \text{(A-II.6)}$$

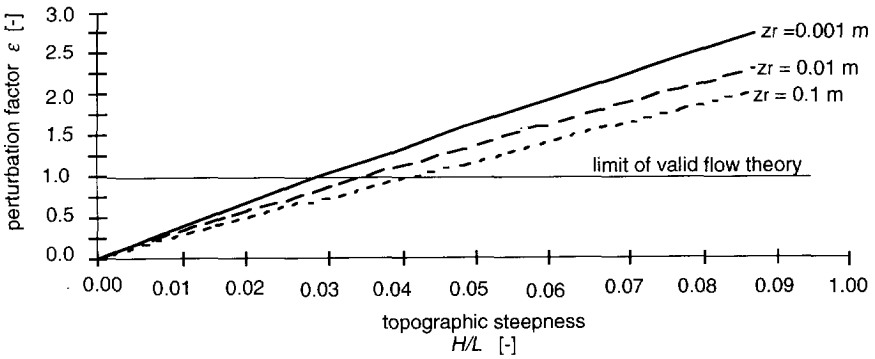

Fig A-II.1 *Variation of perturbation factor ε with topographic steepness (H/L), for different roughness lengths z_r. The perturbation factor ε should be smaller than 1. It determines the weight of the correction of Jackson and Hunt's theory (1975) in relation with Prandtl's logarithmic profile. This graph has been calculated by taking a fixed H=1m and varying L.*

Equations for the inner region

For the inner region Jackson and Hunt start from the equations of motion of a boundary layer, in which they substitute the expressions for the perturbed horizontal and vertical velocities and for the pressure. By ignoring the non-linear terms in ε they develop a system of equations for the velocities and pressure. The solutions for the first order correction for the velocity and the pressure in the inner region, are finally given as:

$$i\,k^*\,\widehat{u_1} = -i\,k^*\,\widehat{p_1} + \frac{\partial}{\partial\left(\frac{\Delta z}{l}\right)}\left(\frac{\Delta z}{l}\,\frac{\partial\widehat{u_1}}{\partial\left(\frac{\Delta z}{l}\right)}\right) \qquad \text{(A-II.7)}$$

$$\widehat{p_1} = -\,|k^*|\,\hat{h}^* \qquad \text{(A-II.8)}$$

$\widehat{p_1}$ = the Fourier Transform of the first-order correction for the pressure [-]

$\widehat{u_1}$ = the Fourier Transform of the first-order correction for the velocity [-]

$\widehat{h^*}$ = the Fourier Transform of the topography [-]. The topography has been normalized according to: $h^*(x)=h(x)/H$

k^* = wave number of the Fourier Transform. It should be noted that, contrary to the notation used in Appendix I, as Jackson and Hunt use dimensionless x coordinates (x/L) the wave number k^* becomes dimensionless.

Solutions for the horizontal velocity and shear stress

The combination of Eqs. (A-II.7) and (A-II.8), and rewriting the resulting expression, gives a non-homogeneous Modified Bessel function (Abramovitz and Stegun, 1972, p.374, formula 9.6.1). The solutions, in Fourier Transforms, that Jackson and Hunt give for the first order corrections of the velocity and the pressure are:

$$\widehat{u_1}(k^*,t) = |k^*|\,\widehat{h}^*(k^*,t)\left(1 - \frac{K_0\left(2\sqrt{\frac{\Delta z}{l}k^* i}\right)}{K_0\left(2\sqrt{\frac{z_r}{l}k^* i}\right)}\right) \qquad \text{(A-II.9)}$$

$$\widehat{p_1} = -\widehat{u_1} \qquad \text{(A-II.10)}$$

K_0 is the modified Bessel function of zero-order.

For our purpose, which will become evident further on, it is practical to write this as:

$$\widehat{u_1}(k^*,t) = |k^*|\,\widehat{h}^*(k^*,t)\left(1 - \frac{K_0\left(2\sqrt{\frac{\Delta z}{l}k^* i}\right)}{K_0\left(z_k e^{i\phi}\right)}\right) \qquad \text{(A-II.11a)}$$

Where

$$z_k = 2\sqrt{\frac{z_r}{l}|k^*|} \qquad \text{(A-II.11b)}$$

and

$$\begin{aligned} \phi &= \pi/4 \quad if\, k^* > 0 \\ \phi &= -\pi/4 \quad if\, k^* < 0 \end{aligned} \qquad \text{(A-II.11c)}$$

For this it should be noted that the sign of the wave number k^* has been included in the imaginary root so that :

$$\begin{aligned} &if\, k^* > 0 \quad \text{take} \quad \sqrt{i} = exp\left(\frac{i\pi}{4}\right) \\ &if\, k^* < 0 \quad \text{take} \quad \sqrt{-i} = exp\left(-\frac{i\pi}{4}\right) \end{aligned} \qquad \text{(A-II.11d)}$$

For the purpose of using Jackson and Hunt's model for simulating sediment transport, we need the shear stress at the surface. This is obtained applying Eq. (A-II.6) at $\Delta z = z_r$:

$$\frac{\partial \widehat{u_1}(k^*,t)}{\partial(\Delta z)} = |k^*|\ \widehat{h}^*(k^*,t) \sqrt{\frac{k^* i}{l}}\ (\Delta z)^{-1/2} \frac{K_1\left(2\sqrt{\frac{\Delta z}{l}}\, k^* i\right)}{K_0\left(z_k e^{i\phi}\right)} \qquad \text{(A-II.12)}$$

K_1 is the modified Bessel function of first order (and equal to minus the derivative of the modified Bessel function of zero-order; Abramovitz and Stegun, 1972, p. 376, formula 9.6.27). Equation (A-II-12) at $\Delta z = z_r$, multiplied with $2\kappa\Delta z$ and with the adequate substitutions using Eq. (A-II-11b) gives the following expression for the shear stress at the surface:

$$\widehat{\tau_1}(k^*,t) = \kappa\ |k^*|\ \widehat{h}^*(k^*,t)\, z_k e^{i\phi} \frac{K_1\left(z_k e^{i\phi}\right)}{K_0\left(z_k e^{i\phi}\right)} \qquad \text{(A-II.13)}$$

Applying an inverse Fourier Transform (Eq. A-1.6a) the expression for the shear stress in cartesian coordinates is obtained:

$$\tau_1(x) = \int_{-\infty}^{\infty} \kappa\ |k^*|\ \widehat{h}^*(k,t)\ z_k e^{i\phi} \frac{K_1\left(z_k e^{i\phi}\right)}{K_0\left(z_k e^{i\phi}\right)} e^{ikx}\, dk^* \qquad \text{(A-II.14)}$$

Calculation of the solution in the computer programme

In the computer programme developed in chapter 6, equation (A-II.14) has been solved using the Fast Fourier Transform (FFT) algorithm from Press et al. (1988). The Modified Bessel functions have been calculated with formulae from Abramovitz and Stegun (1972). As

the arguments of the Modified Bessel functions in Eq. (A-II.14) are complex numbers, their values are not directly tabulated but have to be determined in an indirect way. Two approaches have been used, one for small arguments ($\gamma<0.1$) using an asymptotic approximation and one for large arguments ($\gamma\geq0.1$) with the help of tabulated Kelvin functions.

For small arguments (γ) the modified Bessel functions can be solved with (Abramovitz and Stegun, 1972, p. 375, formulae 9.6.8 and 9.6.9):

$$K_0(\gamma) \approx -ln(\gamma) \qquad \text{(A-II.15a)}$$

$$K_1(\gamma) \approx \frac{1}{2}\Gamma(1)\frac{2}{\gamma} = \frac{1}{\gamma} \qquad \text{(A-II.15b)}$$

Applying this to Eq. (A-II.14) we obtain:

$$K_0\left(z_k e^{i\phi}\right) \approx -ln\left(z_k e^{i\phi}\right) = -ln(z_k) - ln\left(e^{i\phi}\right) = -ln(z_k) - i\phi \qquad \text{(A-II.16a)}$$

$$K_1\left(z_k e^{i\phi}\right) \approx \left(z_k e^{i\phi}\right)^{-1} \qquad \text{(A-II.16b)}$$

In equations (A-II.14):

$$z_k = 2\sqrt{\frac{z_r|k^*|}{l}} \qquad \text{(A-II.17a)}$$

and

$$\phi = +\pi/4 \; for \; k^* > 0$$
$$\phi = -\pi/4 \; for \; k^* < 0 \qquad \text{(A-II.17b)}$$

When the argument (γ) is large, the Bessel functions can be approximated with tabular values for Kelvin functions (Abramowitz and Stegun, 1972, p.379, formula 9.9.2) according to:

$$K_\upsilon\left(\gamma e^{i\pi/4}\right) = e^{i\upsilon\pi/4}\left(ker_\upsilon(\gamma) + i\, kei_\upsilon(\gamma)\right) \qquad \text{(A-II.18a)}$$

where υ is the order of the function. Considering also that according to Abramowitz and Stegun (p.376, formula 9.6.32) [1]:

$$K_\upsilon\left(\mathcal{C}(\gamma)\right) = \mathcal{C}\left(K_\upsilon(\gamma)\right) \qquad \text{(A-II.18b)}$$

---

[1] The symbol $\mathcal{C}$ denotes a complex conjugate

The Modified Bessel functions in Eqs. (A-II.13) and (A-II.14) can be solved by:

$$K_0\left(z_k\, e^{i\pi/4}\right) = ker\,(z_k) + i\; kei\,(z_k) \qquad \text{(A-II.19a)}$$

$$K_0\left(z_k\, e^{-i\pi/4}\right) = K_0\left[\mathbb{C}\left(z_k\, e^{i\pi/4}\right)\right] = \mathbb{C}\left(K_0^*\left(z_k\, e^{i\pi/4}\right)\right)$$
$$\mathbb{C}\left(ker\,(z_k) + i\; kei\,(z_k)\right) = ker\,(z_k) - i\; kei\,(z_k) \qquad \text{(A-II.19b)}$$

$$K_1\left(z_k e^{i\pi/4}\right) = e^{i\pi/2}\left\{ker_1(z_k) + i\; kei_1(z_k)\right\} = -kei_1(z_k) + i\; ker_1(z_k) \qquad \text{(A-II.19c)}$$

$$K_1\left(z_k\, e^{-i\pi/4}\right) = \mathbb{C}\left\{e^{i\pi/2}\left(ker_1\,(z_k) + i\; kei_1\,(z_k)\right)\right\} \qquad \text{(A-II.19d)}$$
$$K_1\left(z_k e^{-i\pi/4}\right) = e^{-i\pi/2}\left\{ker_1(z_k) - i\; kei_1(z_k)\right\} = -kei_1(z_k) - i\; ker_1(z_k)$$

Equations (A-II.16a,b) and (A-II.19a,b,c,d) have been used to calculate the Bessel functions for the solution of the shear stress (Eq. A-II.14) in the computer programme of chapter 6.

Appendix III

EOLSIM, a two-dimensional programme for simulating the dynamics of aeolian dunes

General approach

For the purpose of simplifying calculations in chapter 6, a computer programme called EOLSIM was developed. EOLSIM is a two-dimensional computer programme that models the deposition of aeolian dunes. It simulates the interaction between wind and topography, calculating where erosion, transport and deposition of sediment occur. Redistribution of sediment through avalanching is also accounted for.

Simulations concern a two-dimensional section, where the length forms the x-axis and where deposition occurs in the z-axis. A simulation is carried out in a number of successive time steps. At each time interval the shear stress at the surface is calculated for the whole section using Jackson and Hunt's (1975) analytical boundary-layer flow model. The sediment-transport capacity is then calculated with a linearization of Bagnold's (1941) sediment-transport formula. The sediment-transport capacity is considered as an equilibrium value, so that the wind either erodes or deposits sand to reach its sediment-transport capacity. The excess or deficiency of sediment-transport capacity is determined for every x-interval, and the amount of erosion or deposition is determined with the continuity equation. This results in a new topography, which is checked for slope instability. If at any point the slope is steeper than a given value (equal to the angle of initial yield) the sediment is redistributed by avalanching. The resulting topography determines a new velocity field, after which the cycle is repeated until the total simulation time has been reached.

Model input

Information required as input is itemized below. EOLSIM reads the input data from a standard file called input.d. An example of such a file is given in Table A-III.1.

Table A-III.1 *Example of an input file for EOLSIM. Lines starting with an asterisk are comments. They explain the meaning of the input data on the following line and are skipped by the programme.*

```
* title line
  Example input file for aeolian simulations
* name for output files for this experiment
  sine
* grid size [m] and number of rows
  1.0   64
* grain diameter [m]
  0.00025
* filename containing topographic elevations (extension *.top)
  sin.top
* datum wind velocity [m/s]  and height of measurement [m]
  10.0   2.0
* height [m] at which shear stresses are calculated
* and roughness length [m] (this allows for calculations at another
* height than the surface)
  0.00589   0.00589
* start of simulation [h], end of simulation [h], time per iteration [h]
* display time for dimensional parameters (short files) [h],
* display time for topographic results (long files) [h]
  0.0    1000.0   0.25   100.0   25
* symbol indicating end of input file
  #
```

i) Number of intervals and interval length: the number of grid points should be a power of 2 (to allow for the Fast Fourier Transform routine). In the simulations in this study, generally 64 grid points (equal to 63 intervals) have been taken, numbered from 0 to 63. This is a good compromise between the precision and the time required for computations.

ii) Average grain size: Aeolian deposits are characterized by clean, well-sorted and rounded grains with diameters between 0.1 and 1 mm. Deposition of the suspended load, which consists of the fraction smaller than 0.1 mm, is considered negligible (Bagnold, 1941; Illenberger and Rust, 1988) and not taken into account by the model.

iii) Topography at the outset: the topography should be a continuous and periodic function, to allow its Fourier Transform. This implies that there should be no discontinuities in the topography (i.e. no sudden changes in slope) and that the topographic height at the left boundary (x=0) should equal the topographic height at the right

boundary ($x=L$). The topography is given in a separate file, of which the filename is read from the input file. This allows the input file to be more compact while changes to the topography are less cumbersome.

iv) Datum wind velocity and height of measurement: wind is assumed to be constant and unidirectional during a simulation experiment. To allow for an eventual easier link with field measurements, EOLSIM calculates the shear stress from a datum wind velocity and height of measurement. These are read from the input file. Wind velocities in field measurements are generally taken at standard heights of 1, 1.5 or 2 m above the ground. Wind velocity and direction data are also recorded for meteorological purposes, in which case they are measured at a height of 10 m as specified by the World Meteorological Organization. Table A-III.2 gives an indication of different wind regimes. From observations in present deserts and arid environments (Kahlaf, 1989; Fryberger et al., 1984) it seems realistic to use wind velocities from 7 to 20 $m \cdot s^{-1}$ for simulating aeolian sedimentation. Normally very high wind velocities are accompanied by rain and aeolian transport ceases. However in arid environments, rain may not occur and very high winds, although sporadic, could produce high rates of aeolian transport.

Table A-III.2 *Wind regimes*

Beaufort scale	$km \cdot h^{-1}$	$m \cdot s^{-1}$	description
3 - 4	12.2- 25.2	3.4 - 7.4	weak
5 - 6	25.2 - 44.6	7.5 - 12.4	strong
7 - 8	44.6 - 65.5	12.5 - 18.2	very strong
9 - 10	65.5 - 90.4	18.3 - 25.1	storm
> 11	> 90.4	> 25.1	hurricane

v) Time parameters: start and end of simulation, time step of calculation and time intervals at which output files are to be printed. The implementation of an avalanching routine requires a small time step to be used (e.g. 0.25 hours). Two different time intervals are required for two different types of simulation results:

- A time interval for large files containing results at every x-interval (e.g. topography, sediment transport and shear velocity). As these files are generally large, it is convenient to take large intervals for storing this type of results (e.g. every 100 hours for a simulation of 1000 hours).
- A time interval for small files containing results that give general characteristics of the simulation (e.g. wave length, location of the apex, apex height). These results are more important for

monitoring and understanding a simulation and it is generally desirable to write these at a more frequent time interval (e.g. every 25 hours for a simulation of 1000 hours). As these files are smaller, this does not form a storage problem.

Programme functioning

After the initialization of the programme, a simulation is carried out in a successive number of time steps. At each time interval EOLSIM performs the following actions:

i) The shear stress over the topography is calculated using Jackson and Hunt's (1975) analytical model (see Appendix II) according to Eq. (A-II.14). For this, a Fast Fourier Transform routine from Press et al. (1988) is used. The Modified Bessel functions in Eq. (A-II.14) are calculated by a separate routine. For small values an asymptotic approach is used according to Eqs. (A-II.16 a and b). For larger values, tabulated Kelvin functions are used according to Eqs. (A-II.19a,b,c and d).
ii) The sediment transport is calculated over the topography using a linearization of Bagnold's formula (1941) according to Eq. (4.4.4).
iii) The sediment continuity equation (Eq. (4.1.1)) is solved using Runge Kutta's fourth-order numerical method, according to Eqs. (4.5.3a,b,c,d) and (4.5.4).
iv) The slope of the topography is checked. If at any point the slope exceeds the angle of initial yield the avalanching routine is called. Redistribution of the sediment through avalanching is modelled in a geometric way. The theoretical approach of the avalanching routine is given in section 6.4 and illustrated in Fig 6.4.1.
v) A mass balance of the sediment is computed as a check of the simulation. Also the general topographic parameters like wave length, height and location of the apex are calculated.

After a chosen time interval EOLSIM records the simulation results on separate files.

Programme output

At specified time intervals EOLSIM's results are written in files. The following output files record the results of simulations. By convention, output files have an extension of capital letters.

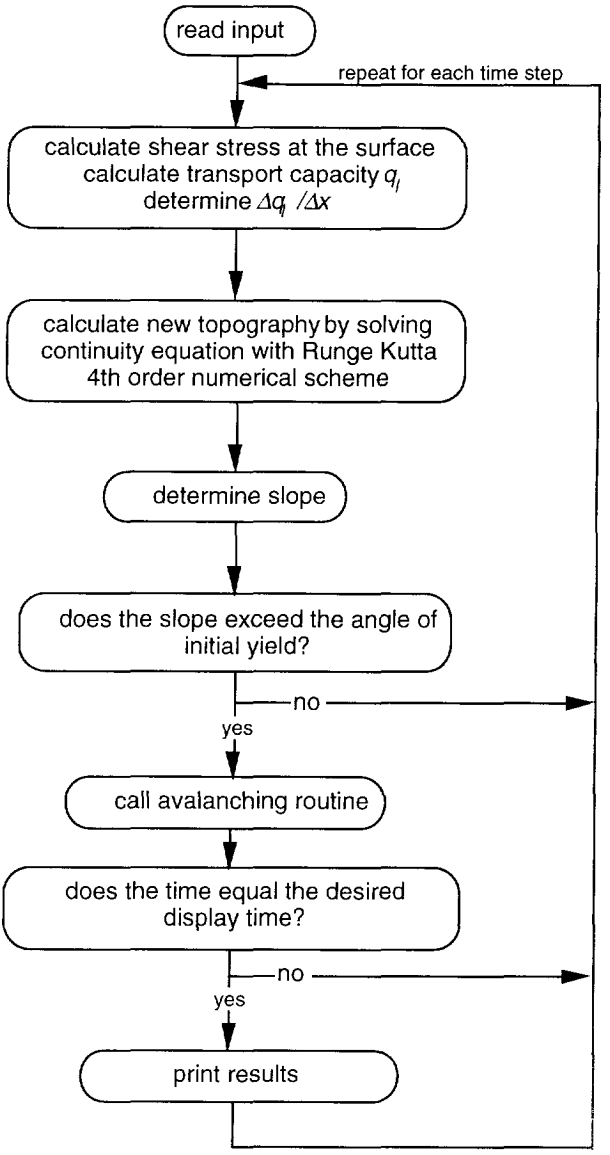

Fig A-III.1 *Structure diagram of EOLSIM, a programme for the two-dimensional simulation of dune migration and growth.*

Large output files recording results at each x-interval are:
*.SED: for the sediment deposited or eroded in a time interval.
*.SST: for the shear stress
*.STR: for the sediment transport and the spatial derivative of the sediment transport
*.TOP: for the topographic height

Small output files recording general characteristics to monitor the simulation behaviour are:
*.DIM: for the height and location of the apex and the half-wave length of the bedform
*.SMB: for the sediment mass balance
*.FFT: for the amplitude of the Fourier spectrum of the topography

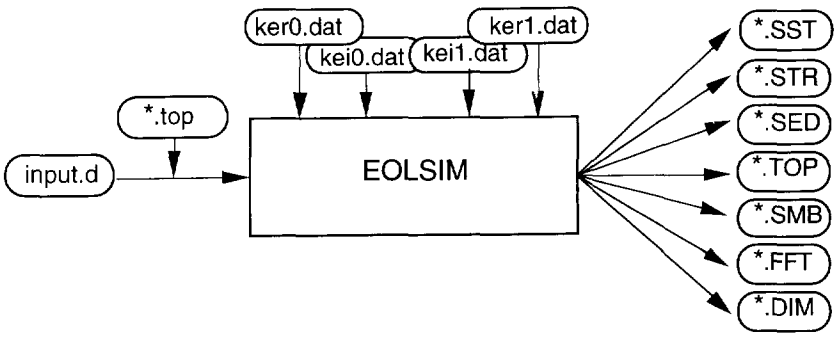

Fig A-III.2 *Diagram of input and output files related to EOLSIM.*

Programme structure

EOLSIM is written in ANSI standard C, compiled on a UNIX workstation. There is a Makefile for the compilation. The programme is written in a modular way, with different functions separated as much as possible in different subroutines. Comment lines are included in the code. A structure diagram of EOLSIM is given in Fig. A-III.1. A convention has been used where input and data files have an extension in small letters and output files have an extension in capital letters. A scheme of the input and output files is given in Fig. A-III.2. The programme itself is divided in the following main routines:

i) eolsim.c: the main driver of the programme, which controls the programme execution and calls the main subroutines.
ii) avalanche.c: calculates the avalanching.
iii) bessel.c: calculates the Modified Bessel functions.

---

* an asterisk denotes the characteristic name for the output files of a specific simulation. This name is chosen in the input file.

iv) four1.c: the subroutine from Press et al. (1988) that calculates the Fast Fourier Transform
v) init.c: an initialization subroutine that opens all output files and reads the four tabulated Kelvin functions (Abramowitz and Stegun, 1972, p.431) from the files called ker0.dat, ker1.dat, kei0.dat and kei1.dat .
vi) mathfuncts.c: contains small functions for performing specific mathematical operations such as calculating a derivative using a central difference scheme, determining the maximum and minimum of a function (e.g. the topography), calculating operations with complex numbers and the routine to calculate a cubic spline from Press et al. (1988)
vii) readin.c: reads the input from the data files input.d and *.top
viii) shear.c: calculates the shear stress over the topography.
ix) writeout.c: writes the large output files (i.e. shear stress, sediment transport and topography at every x-interval).

Appendix IV

Modelling permeability in imperfectly layered porous media II: A two-dimensional application of block-scale permeability

J.M.T. Stam and W. Zijl (1)

Abstract

In a previous paper (Zijl and Stam, 1992) a theory has been developed to calculate the nine components of the three-dimensional intrinsic permeability tensor on the scale of a grid-block from a local-scale, predominantly layered subsurface. The resulting block-scale expressions can be written as a perturbation series of which the first term, or zeroth-order solution, coincides with the conventionally applied arithmetic and harmonic averages over the layers of the subsurface. The derived expressions permit the calculation of the diagonal and off-diagonal terms of the permeability tensor. In the present paper these expressions will be applied in some numerical examples. Two basic two-dimensional hypothetical permeability distributions are adopted, and the various terms of the theoretical expressions are calculated. The results will be used to derive guidelines to discern the situations where higher order solutions can be neglected, and where conventional harmonic and arithmetic averages give a good estimate of the permeability on grid-block scale.

Introduction

Fluid flow simulation for oil and gas production or groundwater flow assessment requires an integration of the modelling of the geology of the subsurface on one hand, and of the techniques for the application of flow simulators for the calculation of fluid pressures, flow velocities

(1) The contents of this appendix have been published as an article in Mathematical Geology, 1992, v. 24, n. 8. It has been included in this thesis with its own list of symbols. The reason for this is that in some cases the same symbol has been used with a different meaning than in the rest of the thesis. As in both cases they were conventionally used symbols, and the meaning is always clear from the context, all the original symbols have been maintained. The references of this article have been included in the general references of the thesis.

and flow paths on the other. The difficulties of combining the qualitative geological models with the quantitative information required for the application of numerical flow models are countered by the development of tools for the computer simulation of facies distribution. These tools include stochastic techniques (Haldorsen and Lake, 1984) or process-based simulators (Bridge and Leeder, 1979 and Tetzlaff and Harbaugh, 1989).

One of the steps in this whole process is the quantification of the geological properties on the scale of grid-blocks that are currently used in fluid flow simulators. At some stage this requires the averaging of different parameter values to obtain one value attributable to the finite difference grid-block or the finite element. The parameter which is both most important and difficult to quantify is the intrinsic permeability. Permeability at each scale is a result of the distribution of heterogeneities at a smaller scale, so that the problem of understanding and upscaling permeabilities to obtain average values would have to be studied at each scale of the hierarchy of heterogeneities that occur in the subsurface (Weber, 1986). The problem of obtaining average permeability values is too complicated to warrant the use of a single straightforward method because it depends on the stratigraphical characteristics of the porous medium itself. However, in practice, straightforward methods are often used to obtain effective values for modelling problems: reservoir simulations and ground water flow calculations. Understanding when this is justifiable and what margin of error is being introduced can be very important.

The problem of correctly estimating average permeabilities has been treated, both from a theoretical and practical point of view, in geohydrology and in petroleum reservoir engineering. A distinction can be made between analytical and numerical approaches. The numerical approaches have been treated by White and Horne (1987). Analytical approaches can broadly be classified in three groups: algebraic, stochastic and the continuum mechanical approaches.

The first approaches evaluate simple algebraic averaging techniques of the different permeability values. Cardwell and Parsons (1945) concluded that average permeability would lie somewhere between the arithmetic and the harmonic averages, and closer to the arithmetic average. Warren and Price (1961) indicated that the geometrical average (which lies between a harmonic and an arithmetic average) was the most indicated method to use. These algebraic methods are hardly based on physical considerations of fluid flow, but their use can be justified in a statistical sense; as permeabilities in a facies are log-normally distributed (Freeze, 1975), they form a stochastic function, of which the expectation is a geometric average. More sophisticated

methods have also been developed, based on renormalization, for instance (King, 1989). Algebraic expressions based on the calculation of streamline lengths have been developed (Haldorsen and Lake, 1984; Begg and King, 1985) for specific deposits, e.g. sandy reservoirs with shaly permeability barriers. These are practical approaches that take into account the stratigraphic characteristics of the porous medium. However, they can be applied only when permeability contrast is sufficiently large to associate flow paths with sedimentary geometries. In sedimentology, this leads to the consideration and definition of flow units (Mijnssen et al.,1990). Finally, Kasap and Lake (1990) have developed algebraic expressions to calculate an average block-scale permeability, where the off-diagonal terms in the permeability matrix are caused by crossbedding angle. The physical origins of heterogeneity and the geological structure of the subsurface are not fully taken into account in these algebraic averaging techniques; however, they are easily applicable and widely used, and give a good estimate on the order of magnitude of the effective permeability.

Much work has been done on characterizing heterogeneity distributions with stochastic methods. These include geostatistical methods (Journel and Huijbregts, 1989) and fractal techniques (Jacquin and Adler, 1987). They have been termed as "sequence based methods" (Dubrule, 1989) because they incorporate information on the spatial distribution of properties at neighbouring locations. For averaging (i.e. upscaling) permeabilities to a block-scale (in statistics for obtaining a "best estimator" of a dataset), kriging is used (Journel and Huijbregts, 1989, p.304-443). A different statistical approach treats fluid flow itself from probability theory (Gelhar, 1986 and Dagan, 1989), and statistical properties (for instance stationarity) are then assumed for the porous medium.

Finally, continuum mechanical approaches are based on the equations governing fluid flow in porous media (Navier Stokes at pore scale, and Darcy at local scale) without assuming statistical properties of the porous medium. Whitaker (1986) develops expressions for a very general case, parting from the pore scale, to arrive at a homogenized local scale where Darcy's law can be applied. The macroscopization method is then applied (Quintard and Whitaker, 1987) to flow through larger areas, characterized by different grain sorting and packing. However, the resulting expressions for the block-scale Darcy's law tend to be of a very theoretical nature since the block-scale permeability is given in partial differential equations rather than in algebraic expressions. Therefore it is more difficult to gain insight in the effects in practical applications.

From the literature presented in this overview it can be seen that the most straightforward algebraic expressions for calculating an averaged block-scale permeability (the arithmetic average for horizontal permeability and the harmonic average for vertical permeability) apply to perfectly layered subsurfaces, and can be justified both from statistical considerations and from analytical reasoning. In practical studies, arithmetic averages are used for horizontal permeabilities of laterally continuous strata, while geometric means are used for less continuous strata. (Fogg, 1986).

In this paper, the continuum mechanical approach is applied by considering an analytical expression for the permeability tensor, as developed by Zijl and Stam (1992). The theory has been developed from the basic equations governing flow in porous media applied at local scale (i.e. the scale of several centimetres, which is the scale of the representative elementary volume and also the scale at which permeability measurements from e.g. core plugs would be obtained): the continuity equation, and Darcy's law with a local-scale, symmetrical, permeability tensor. From this, expressions are developed to calculate the permeability tensor at block-scale. To obtain expressions that are applicable in a relatively simple and straightforward way, thin blocks are considered in which the porous medium is simplified to a predominantly, but not perfectly, layered subsurface. In this way, permeability heterogeneities will be formed by an essentially stratified subsurface in which permeability can vary in the lateral direction along the layer ("imperfectly-layered porous media"). This represents the heterogeneities produced by a lateral succession of facies passing gradually into each other, in intra-facies sequences. Though the expressions have been developed in three dimensions, for purposes of insight they will be applied to two-dimensional hypothetical sections.

Theoretical basis

In single-phase fluid flow through a porous medium, the depth-averaged Darcy's law for flow in two dimensions can be written as:

$$\langle q_x \rangle = - \frac{\langle k_{xx} \rangle}{\mu} \frac{\partial \langle \phi \rangle}{\partial x} - \frac{\langle k_{xz} \rangle}{\mu} \frac{\partial \langle \phi \rangle}{\partial z} \qquad \text{(A-IV.1a)}$$

$$\langle q_z \rangle = - \frac{\langle k_{zx} \rangle}{\mu} \frac{\partial \langle \phi \rangle}{\partial x} - \frac{\langle k_{zz} \rangle}{\mu} \frac{\partial \langle \phi \rangle}{\partial z} \qquad \text{(A-IV.1b)}$$

where $<k_{xx}>$,$<k_{xz}>$, $<k_{zx}>$ and $<k_{zz}>$ are the four components of the depth-averaged two-dimensional permeability tensor. For imperfectly-layered subsurfaces, and assuming a coordinate system with the x-axis

parallel and the z-axis perpendicular to the layering, these components can be given by the following expressionsn (Zijl and Stam, 1992):

$$\langle k_{xx} \rangle (x) = \frac{t''(x,0)}{d} \qquad \text{(A-IV.2)}$$

$$\langle k_{zx} \rangle (x) = \frac{\partial}{\partial x} t''(x,0) \qquad \text{(A-IV.3)}$$

where:

$$t''(x,z) = \int_z^d k_h(x,z') \left\{ 1 + \frac{\partial \beta(x,z')}{\partial x} \right\} dz' \qquad \text{(A-IV.4a)}$$

$$\beta(x,z) = \int_0^z \frac{1}{k_v(x,z')} \frac{\partial t(x,z')}{\partial x} dz' \qquad \text{(A-IV.4b)}$$

$$t(x,z) = \int_z^d k_h(x,z')\, dz' \qquad \text{(A-IV.4c)}$$

and:

$$\langle k_{zz} \rangle (x) = \frac{d}{c''(x,d)} \qquad \text{(A-IV.5)}$$

$$\langle k_{xz} \rangle (x) = \frac{1}{c''(x,d)} \int_0^d k_h(x,z) \frac{\partial c''(x,z)}{\partial x} dz \qquad \text{(A-IV.6)}$$

where:

$$c''(x,z) = \int_0^z \frac{1}{k_v(x,z')} \left\{ 1 + \frac{\partial \alpha(x,z')}{\partial x} \right\} dz' \qquad \text{(A-IV.7a)}$$

$$\alpha(x,z) = \int_z^d k_h(x,z') \frac{\partial c(x,z')}{\partial x} dz' \qquad \text{(A-IV.7b)}$$

$$c(x,z) = \int_0^z \frac{1}{k_v(x,z')} dz' \qquad \text{(A-IV.7c)}$$

The above expressions for the components of the permeability tensor are depth-averaged over the grid-block depth *d*. They have been derived from asymmetrical boundary conditions (potential on top, flux at the bottom), and should be recalculated for reversed boundary conditions (flux on top, potential at the bottom) (Zijl and Stam, 1992). Resulting depth-averaged values are obtained as a combination of both.

Finally, a block-scale value for the permeability tensor is obtained by integrating over the horizontal dimension $2a$ according to:

$$\langle\langle \underline{k} \rangle\rangle = 2a \left\{ \int_{-a}^{a} \left[\underline{k} \ (x) \right]^{-1} dx \right\}^{-1} \qquad \text{(A-IV.8)}$$

The expressions (A-IV.2) and (A-IV.5) for the diagonal terms $<k_{xx}>$ and $<k_{zz}>$ are based on the calculation of $t''(x,0)$ and $c''(x,d)$, which are obtained from (A-IV.4a) and (A-IV.7a), respectively. We can see that both $t''(x,0)$ and $c''(x,d)$ are formed by two terms, which are the first two terms of a perturbation series that gives the correct solution for a porous medium with a predominantly, but not perfectly, layered structure (Zijl and Stam, 1992).

The first terms of expressions (A-IV.4a) and (A-IV.7a), at $z = 0$ and $z = d$ respectively, are basic terms (the zeroth-order solutions). For Eq.(A-IV.4a) this coincides with the well known arithmetic average of the permeabilities of a perfectly-layered subsurface (from which in geohydrology the transmissivity $\rho g t(x,0)/\mu$ is calculated). In the case of Eq.(A-IV.7a) the basic term is the well known harmonic average of the permeabilities of a perfectly-layered subsurface (from which in geohydrology the hydraulic resistance $\mu c(x,d)/(\rho g)$ is calculated).

The second terms of both the expressions (A-IV.4a) and (A-IV.7a) account for the lateral variations in permeability within each layer. An implicit condition is that lateral permeability heterogeneities occur gradually, so that the permeability can be considered as a sufficiently differentiable function. It has already been indicated that, in normal practice, the lateral heterogeneity occurring within layers is neglected, and the subsurface is frequently modelled as perfectly layered. In this case, $\partial c(x,z)/\partial x$ and $\partial t(x,z)/\partial x = 0$ so that $\alpha(x,z)$ and $\beta(x,z)$ are both zero, and the second terms of expressions (A-IV.4a) and (A-IV.7a) are also zero. In reality, a layer will not be perfectly homogeneous, therefore there will always be a correction on the basic harmonic and arithmetic mean value, and this can be considered as a measure of the lateral heterogeneity occurring in a layer. If variations are very slight, these terms will be so small as to be negligible. In that case, the conventional harmonic and arithmetic averages will be sufficiently good approximations of the block-scale permeability in the x- and z-direction of the domain.

It can easily be seen that, in a perfectly-layered structure where $\partial t''(x,z) / \partial x = 0$ and $\partial c''(x,z) / \partial x = 0$, the off-diagonal terms of the

permeability tensor $<k_{xz}>$ and $<k_{zx}>$ disappear. Lateral permeability variation is immediately expressed in the second terms of $<k_{xx}>$ and $<k_{zz}>$ which contain the second derivative of $t(x,z)$ and $c(x,z)$. As $<k_{xz}>$ and $<k_{zx}>$ contain third derivatives of $t(x,z)$ and $c(x,z)$, the influence of lateral heterogeneities may become significant in the first-order corrections of the diagonal terms before it becomes substantial in the off-diagonal terms of the tensor. It can also be observed that expression (A-IV.6) for the determination of $<k_{xz}>$ is very similar to expression (A-IV.7b) for the determination of $\alpha(x,z)$ while $<k_{zx}>$ is directly determined by differentiating $t''(x,z)$. The off-diagonal terms are clearly not equal to each other (the tensor is non-symmetric).

Examining expressions (A-IV.4a) and (A-IV.7a) it can further be concluded that the distance over the x-direction in which permeability variation occurs is of great influence. With the same variations over a larger x-distance, the terms $\partial t(x,z)/\partial x$, $\partial \beta(x,z)/\partial x$, $\partial c(x,z)/\partial x$ and $\partial \alpha(x,z)/\partial x$ will decrease (this is in accordance with the implicit condition of gradual variation of the permeability).

It can be noted from expression (A-IV.4b) that the depth-averaged $<k_{xx}>$ is inversely proportional to the local k_v. Expression (A-IV.7b) shows that the depth-averaged $<k_{zz}>$ is directly proportional to the local k_h.

Finally, some observations should be made to help understand expression (A-IV.8) to integrate the depth-averaged permeabilities in the lateral direction. It can be seen that the expression implies calculating a harmonic mean of the depth-averaged permeability matrix. This means that both $<<k_{xx}>>$ and $<<k_{zz}>>$, the diagonal terms of the block-scale permeability tensor, are obtained from a harmonic average of $<k_{xx}>$ and $<k_{zz}>$, which for the former seems more understandable than for the latter. This "paradox" can be understood because it is an average value for one grid-block in a whole domain. The flow through the block is determined by the flux surrounding it, and the resistance to flow is determined by the value of the permeability of all the grid-blocks in the domain, almost independently of the single grid-block under consideration.

Summarizing, it can be concluded from the above expressions that, if lateral heterogeneity within a layer is only very slight, the conventional arithmetic and harmonic average permeabilities give an accurate value for $<k_{xx}>$ and $<k_{zz}>$ (the diagonal terms of the permeability tensor), and that the influence of the lateral heterogeneity is larger for the diagonal terms of the permeability tensor than for the off-diagonal terms. These conclusions confirm knowledge from general practice; however, Eq.s (A-IV.2) to (A-IV.7a,b,c) enable us to quantify

the factors commonly known to affect permeability when it is calculated as a block-scale value from a local-scale permeability distribution. The expressions are restricted to the type of subsurface to which they can be applied; thin blocks with predominantly layered structure and with gradual permeability variations within each layer. This type of subsurface is frequently encountered in engineering practice. In oil and gas reservoir engineering these subsurfaces are typed as "layer-cake reservoirs" (Weber and Van Geuns, 1990). In geohydrology the underground can often be schematized as a layered succession of aquifers and aquitards.

Numerical examples

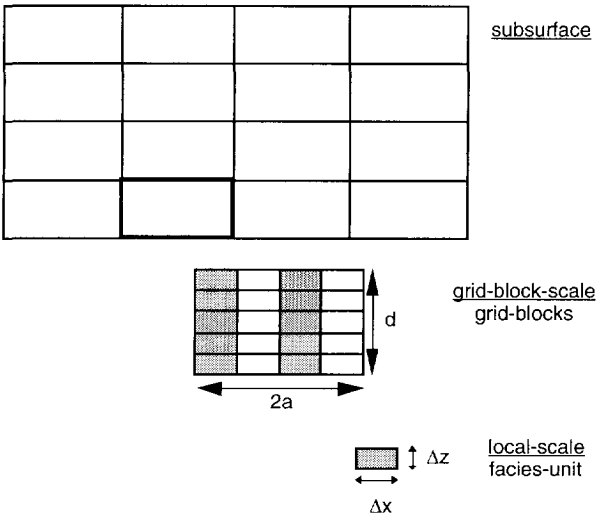

Fig A-IV.1 *Notation used for hierarchy of scales.*

From a geological point of view it is desirable that each facies unit is represented by a grid-block, in which case we would have to work with grid-blocks of 1 to 2 m in height, and of less than 100 m in width. However, conventional simulators work with grid-blocks of 5 m in height and 300 m in width (Weber and Van Geuns, 1990), so that block-scale permeability values have to be calculated from smaller scale units. These small-scale units can then be considered as the homogeneous facies with a local-scale, symmetrical permeability tensor, referred to in the introduction. A computer programme has been written that calculates each term of expressions (A-IV.2) to (A-IV.8) for any distribution of small-scale permeability units (Fig. A-IV.1). It is a Fortran computer code for two-dimensional computations, with a

finite-difference, block-centred approach. To understand the theory, expressions (A-IV.2) to (A-IV.8) are worked out in a series of numerical examples, with the idea of obtaining a block-averaged permeability as would be used in a conventional fluid-flow simulator. Two different local-scale permeability distributions of two different facies materials were adopted (designated by k_1 and k_2) as shown in Fig. (A-IV.2). The first local-scale permeability distribution (henceforth described as configuration A) shows a porous medium, with alternating units of relatively high and low permeability, representing a vertical succession with a preferential stacking. For this permeability distribution an analytical solution can be obtained as described in Appendix A. The second local-scale permeability distribution (configuration B) shows a block-scale isotropic "checkerboard" configuration. Although both distributions stretch the "stratified-medium-concept", for which the theory was originally developed, they represent extreme situations which will enable us to gain insight in the influence of the different terms of the theoretical expressions.

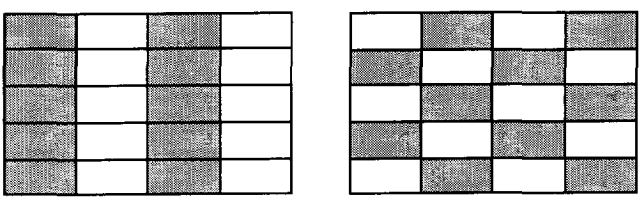

Fig A-IV.2 *Scheme of permeability distributions in grid-bocks as applied in numerical examples.*

The permeability distributions are repetitive in the z-direction, which implies that the two solutions for reversed boundary conditions (the top and bottom flux problems) are equal, so that the off-diagonal terms of the resulting depth-averaged tensor $\langle \underline{k} \rangle$ are zero. In the formulae, three essential parameters influence the results:

i) The contrast of the lateral permeability distribution, i.e. the factor k_1/k_2, where k_1 is the local-scale permeability of the well conducting facies unit, and k_2 the local-scale permeability of the poorly conducting facies unit.
ii) The facies geometry; i.e. the geometry of the small-scale units.
iii) The depth of the domain over which permeability will be averaged.

The first two factors are intrinsic to the characteristics of the porous medium itself, while the third factor is dependent on the

dimensions chosen for the grid-blocks, i.e. on the modelling approach. The influence of these three factors will be analyzed by considering the term $\partial\alpha(x,0)/\partial x$ and the block-scale value given by Eq. (A-IV.8). The terms $|\partial\alpha(x,0) / \partial x|$ and $|\partial\beta(x,d) / \partial x|$ are a measure for the correction to the basic zeroth-order solution for the average permeability. For $k_x = k_z$, $|\partial\alpha(x,0) / \partial x|$ and $|\partial\beta(x,d) / \partial x|$ give equal values in the case of the anisotropic configuration, and similar values in the case of the isotropic configuration, therefore only $\partial\alpha(x,0)/\partial x$ has been calculated. The results will serve to give insight in the influence of different modelling parameters on the resulting block-averaged permeability, and thus help to develop practical rules for the limitations in which traditional permeability averaging can still be used as a sufficiently accurate estimate of the block-scale permeability. The following assumptions have been made:

(i) In reality, the permeability variation from one facies into the other occurs gradually. However, for computational reasons, each layer is divided into blocks with homogeneous permeability, and the variation from one into another occurs with a step. For the mathematical justification and consequences of this, the reader is referred to Appendix B.
(ii) For reasons of insight it is assumed that the local-scale permeabilities k_x and k_z are equal to each other, though from a sedimentological point of view this is not realistic. This means that the local-scale anisotropy factor $k_x/k_z = 1$.
(iii) In the first numerical experiments the thickness of the block is chosen as five times the thickness of the facies unit, i.e. $d = 5\ \Delta z$. (In the experiments concerning the modelling parameters, the block depth was varied).

Table A-IV.1 *Orders of magnitude of intrinsic permeabilities for different types of facies (values taken from Dagan, 1989)*

material	Permeability [m^2]	Permeability [milli-Darcy (mD)]
Clay	10^{-17} to 10^{-15}	10^{-2} to 1
Sandstone	10^{-15} to 10^{-12}	1 to 10^3
sands	10^{-12} to 10^{-9}	10^3 to 10^6
Gravel	10^{-9} to 10^{-7}	10^6 to 10^8

Characteristics of the porous medium: facies geometry and permeability contrast

Lateral heterogeneities encountered in an essentially layered domain can be considered as permeability contrasts between facies within a layer. The effect of this on block-scale permeability was

assessed by increasing the ratios between the permeabilities of adjacent facies (i.e. adjacent small-scale units). Permeability ratios from 10 to 10^6 were considered. Permeability ratios of 10 occur between very similar facies; ratios of 10^6 can occur between materials like sand and clay. Orders of magnitude of the permeabilities of different materials are shown in Table (A-IV.1).

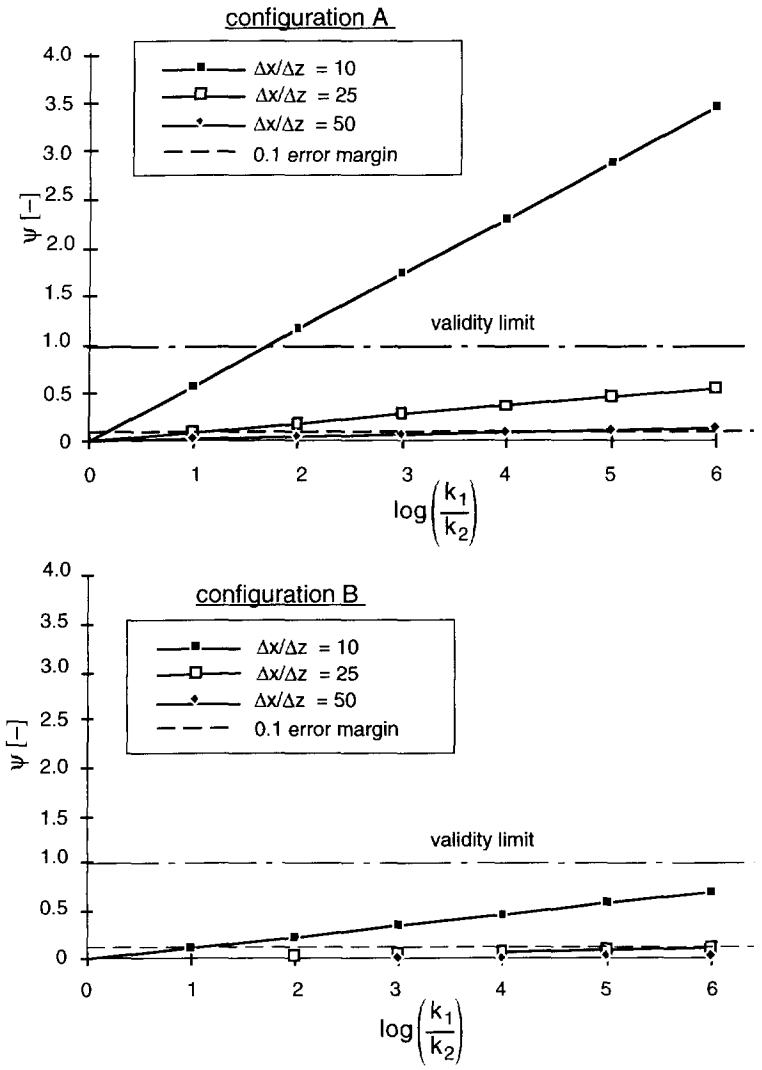

Fig A-IV.3 *Values of the correction factor* $\psi=|\partial\alpha\,(x,0)/\partial x|$ *for different aspect ratios and permeability values.*

The geometry of the facies units was varied by increasing the small-scale unit width from 10 m to 100 m while keeping a constant thickness of 1 m, so that the aspect ratio $\Delta x/\Delta z$ varied from 10 to 100. The influence of these factors for the two configurations A and B, expressed in the variation of $\psi = |\partial\alpha(x,0)/\partial x|$, are shown in Figure A-IV.3. In Fig. A-IV.3 it has been indicated for what geometries and permeability ratios the theory gives correct solutions. In relation to this, it should be noted that $\psi = |\partial\alpha(x,0)/\partial x|$ is the first correction term of an infinite series (Zijl and Stam, 1992). If $\psi>1.0$, this is an indication that more terms of the series should be included in the solution. Therefore the conclusions are valid only if $\psi<<1.0$, i.e. for lines lying well under $\psi=1$.

From Fig. A-IV.3 it can be seen that the term $\psi = |\partial\alpha(x,0)/\partial x|$ is directly proportional to the square of the aspect ratio $\Delta x/\Delta z$. This can be related back to the theory by observing that the term $\partial\alpha(x,0)/\partial x$ results from two derivatives in the x-direction, (and is therefore numerically divided twice by the x-dimension). A wide, thin facies geometry implies small $|\partial\alpha(x,0)/\partial x|$ and, therefore, a small correction to the basic term in expression (A-IV.7a) (a correction of the order of 0.1 in terms of ψ, has been considered as small). Facies geometry consequently has a large effect on the second term in expressions (A-IV.4a) and (A-IV.7a).

The second observation that can be made from Fig. (A-IV.3) is that $\partial\alpha(x,0)/\partial x$ is directly proportional to the decimal logarithm of k_1/k_2. For instance, increasing the permeability ratio by a factor 1000 means increasing $\partial\alpha(x,0)/\partial x$ by a factor 3.

Both these conclusions mean that the effect of facies geometry on $\partial\alpha(x,0)/\partial x$ is notably larger than the effect of the permeability ratio. If we consider a correction term of 0.1=10% as small, we could state that, in the case of a permeability distribution similar to configuration A, for an aspect ratio of minimally $\Delta x/\Delta z=25$ and a permeability ratio of maximally 10, a correction to the zeroth-order solution may be neglected. If the aspect ratio of the unit increases to $\Delta x/\Delta z=50$ (facies become thinner and longer), the permeability ratio may increase up to 10^3 to reach a correction term of 10%. Finally, if facies are thinner and longer so that $\Delta x/\Delta z=100$, permeability ratios may range up to 10^6 before reaching a correction term of 10%. This may seem very high, but not when we consider that this permeability varies gradually over a length scale of 100 times the facies thickness.

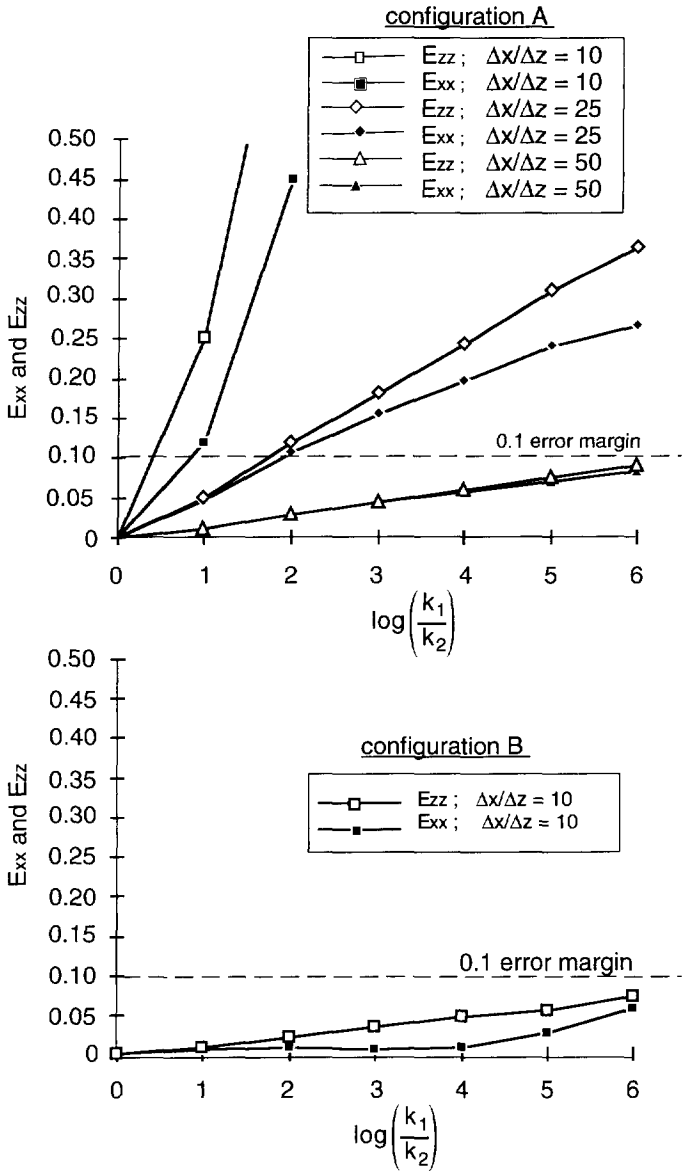

Fig A-IV.4 *Relative corrections to zero-order solutions as a function of $\log(k_1/k_2)$ for different aspect ratios and permeability ratios.*

$$E_{zz} = \frac{\langle\langle k_{zz}\rangle\rangle - \langle\langle k_z\rangle_0\rangle}{\langle\langle k_{zz}\rangle\rangle} \qquad \text{(A-IV.9b)}$$

For configuration B it can be seen that corrections are generally smaller. For $\Delta x/\Delta z>25$, accurate solutions are obtained for all permeability ratios. Aspect ratios of $\Delta x/\Delta z=10$ give accurate solutions for small permeability ratios ($k_1/k_2=10$).

These conclusions should also be evident in the block-scale permeabilities in x- and z-directions calculated over the total width $2a = 4\Delta x$, with expression (A-IV.8). This is shown for both configurations in Figure A-IV.4, where the relative corrections to the zeroth-order solutions $<<k_x>_0>$ and $<<k_z>_0>$ are plotted against aspect ratio and permeability contrasts. The relative corrections for $<<k_{xx}>>$ and $<<k_{zz}>>$ are calculated according to:

$$E_{xx} = \frac{\langle\langle k_{xx}\rangle\rangle - \langle\langle k_x\rangle_0\rangle}{\langle\langle k_{xx}\rangle\rangle} \qquad \text{(A-IV.9a)}$$

In the anisotropic configuration (Fig. A-IV.4, configuration A), both $<<k_{xx}>>$ and $<<k_{zz}>>$ are under-estimated by the zeroth-order permeability average (E_{xx} and E_{zz} are always positive). This under-estimation becomes more severe for increasing permeability contrasts or for smaller aspect ratios. The value of the relative correction for $<<k_{zz}>>$ is higher than for $<<k_{xx}>>$ ($E_{xx} < E_{zz}$). It can also be seen that slightly smaller aspect ratios and larger permeability ratios than in Fig. A-IV.3, still give a relative error margin of 10%.

If we repeat these calculations for the isotropic configuration, it can be seen that the corrections for all permeability ratios are very small, even for the lowest aspect ratio ($\Delta x/\Delta z$ = 10) wich is shown in Fig. A-IV.4. In Fig. A-IV.3, this still gave a correction larger than 10%. This can be ascribed to the isotropic character of the small-scale permeability distribution which becomes manifest in Eq. (A-IV.8).

Modelling parameters; block-scale depth

The theory has essentially been developed under the assumption that the modelling concerns thin grid-blocks. This limits the depth of the grid-block over which the average can be calculated (there is no limit to its width). This was examined by calculating the block-scaled average over a constant width of $2a = 4\Delta x$, and increasing the number of layers over which the average was calculated. The relative correction for both distributions is shown in Fig. (A-IV.5).

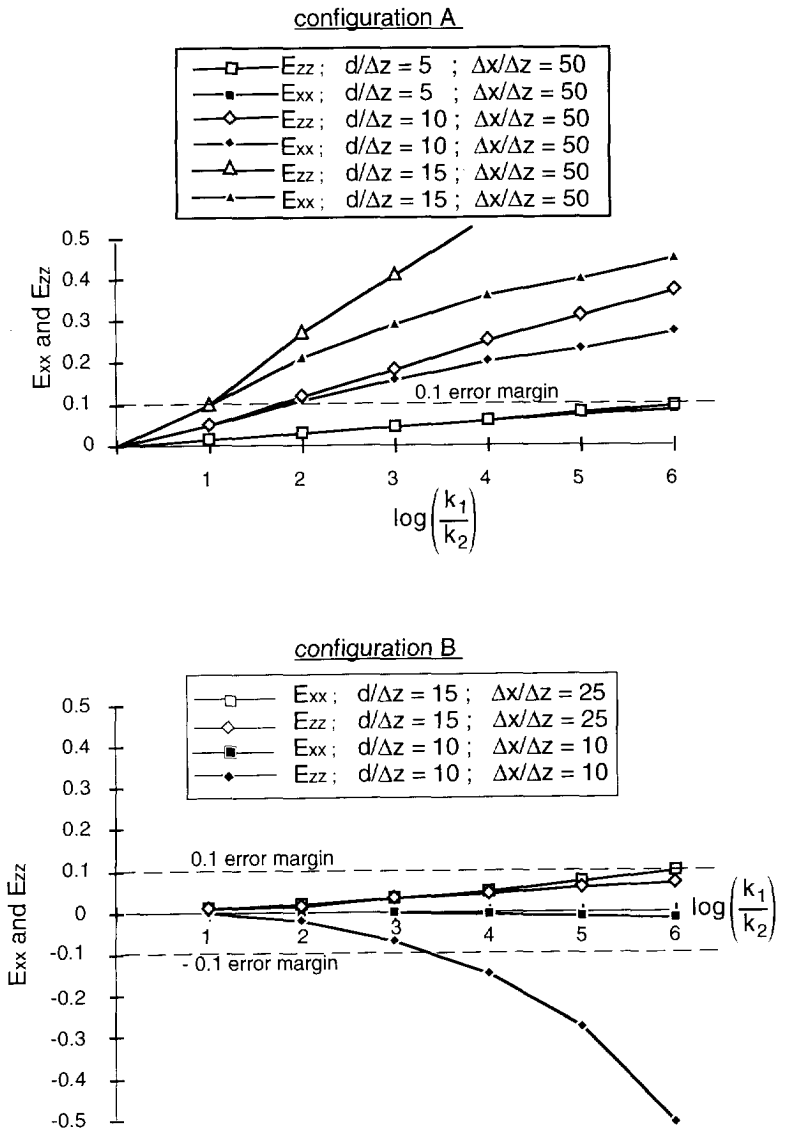

Fig A-IV.5 *Relative corrections to zero-order solutions as a function of* $\log(k_1/k_2)$ *for varying grid-block depth.*

Figure (A-IV.5) shows the relative correction of block-scale permeability in the anisotropic configuration A for an increasing grid-block depth ($d/\Delta z$) and for an aspect ratio of $\Delta x/\Delta z$=50. It can be seen that, for an anisotropic distribution, the corrections to the zeroth-order term permeabilities increase very rapidly with increasing depth, so that they can be neglected only for small permeability ratios ($k_1/k_2 < 10$). As

can be expected, further calculations show that a smaller $\Delta x/\Delta z$ will give an even more rapid increase of the correction term.

The corrections for the isotropic distribution for the smallest aspect ratios ($\Delta x/\Delta z$=25 and $\Delta x/\Delta z$=10) shown in Fig. (A-IV.5), do not increase so dramatically with depth. This again can be ascribed to the isotropic character of this particular configuration. It can be observed that, for the isotropic configuration, for a small aspect ratio ($\Delta x/\Delta z$=10) the corrections become negative with increasing grid-block depth. In other words, block-scale permeability tends to be overestimated by the zero-order term.

From this section, some guide-lines can be derived for what the dimensions of the simulator grid-blocks should be to correctly characterize stratified subsurfaces. There is no limit to the horizontal dimension over which is averaged. If heterogeneities within each layer do not have a preferential stacking, but are distributed more evenly throughout the subsurface, a block-average can be taken over a depth of 10 layers for $\Delta x/\Delta z$=10 and k_1/k_2<1000, and of 15 layers for $\Delta x/\Delta z$=25 and $k_1/k_2<10^6$. If, however, a clear preferential stacking can be identified, the depth average should not be taken over more than approximately 5 layers, unless lateral permeability contrasts are small (inferior to 10) in which case it can be taken over 15 layers. Therefore it can generally be concluded that it is more desirable to design a simulator grid with a higher resolution in the z-direction than to take more blocks in the x-direction.

Conclusions

From the foregoing, some general conclusions can be made about the limits in which the conventional averaging procedure of intrinsic permeabilities can still be applied to obtain an "equivalent homogeneous" permeability value from a small-scale distribution. This means that it is likely that a maximal error of 10% will be made if we take the following considerations in choosing block dimensions for flow simulators (they are also illustrated in Table A-IV.2):

(i) When averaging different facies permeabilities, it is of greater importance to consider the geometry of the facies (their width versus their thickness) and their distribution (whether they are spread out over the domain giving it a block-scale isotropic character) than the ratio between adjacent permeabilities.
(ii) If the facies have a thin geometry, i.e. their width Δx is many times greater than their thickness Δz (at least 50 times), a zeroth-order averaging can always be applied, even with anisotropic

permeability distributions and high permeability ratios like those that occur between clay and sand ($k_x/k_z = 10^6$).

(iii) If the facies do not have a thin geometry, a zeroth-order permeability averaging can be used only if permeability ratios are of the order 10, which occurs between very similar materials, e.g., different types of sands. In that case, the horizontal dimension of the facies still needs to be 10 times its thickness in isotropic permeability distributions, and approximately 25 times the facies thickness in anisotropic distributions.

(iv) The depth of the block over which correction terms can be neglected is also limited, and related to the number of layers over which it is taken. In the case of anisotropic distributions, the correction terms may be neglected when permeability is averaged over depths of approximately 5 layers when $\Delta x/\Delta z \geq 50$ for all permeability contrasts, and for depths of up to 15 layers for $k_1/k_2 \leq 10$. For isotropic distributions a much larger number of layers can be taken: up to 10 layers for $\Delta x/\Delta z \geq 10$ and $k_1/k_2 \leq 1000$; and up to 15 layers for $\Delta x/\Delta z \geq 25$ for all permeability contrasts.

Table A-IV.2 *Guidelines for choosing grid-block dimensions for flow simulations in relation to the aspect ratio and permeability contrast of the smaller-scale heterogeneities. This table is applicable to imperfectly-layered stratigraphies. An isotropic configuration indicates that heterogeneities are distributed more evenly through the successive layers. An anisotropic configuration represents one where heterogeneities have a preferential stacking in the sequence of layers. These limits indicate when the arithmetic mean can be used for the horizontal average permeability, and when harmonic means can be used for the vertical permeability. The maximum error by neglecting the lateral heterogeneities will be approximately 10%.*

facies	$\Delta x/\Delta z = 10$	$\Delta x/\Delta z = 25$	$\Delta x/\Delta z = 50$	$\Delta x/\Delta z = 100$
anisotropic configuration	-	$d/\Delta z \leq 5$	$d/\Delta z \leq 15$	$d/\Delta z \leq 15$
	-	$k_1/k_2 \leq 10$	$k_1/k_2 \leq 10$	$k_1/k_2 \leq 10^3$
isotropic configuration	$d/\Delta z \leq 10$	$d/\Delta z \leq 15$	$d/\Delta z \leq 40$	$d/\Delta z \leq 50$
	$k_1/k_2 \leq 10^3$	$k_1/k_2 \leq 10^6$	$k_1/k_2 \leq 10^6$	$k_1/k_2 \leq 10^6$

Appendix A: Analytical solution for special case

The analytical solution was calculated for the anisotropic configuration in the case where $k_x = k(x)$, $k_z = k(x)/A$, A is constant, and $k(x)$ is independent of z. This was used to obtain insight in the character of the expressions for the depth-averaged permeability components, and to check the numerical procedure. The analytical solutions for the combined "top flux" and "bottom flux" problems result in the following expressions:

$$\langle k_{xx} \rangle (x) = k(x) \left\{ 1 + \frac{1}{3} A d^2 \frac{\partial^2 ln\, k(x)}{\partial x^2} \right\} \qquad \text{(A-IV.a1)}$$

$$\langle k_{zz} \rangle (x) = \frac{k(x)}{A} \left\{ 1 - \frac{1}{3} A d^2 \frac{\partial^2 ln\, k(x)}{\partial x^2} \right\}^{-1} \qquad \text{(A-IV.a2)}$$

$$\langle k_{xz} \rangle (x) = \langle k_{zx} \rangle (x) = 0 \qquad \text{(A-IV.a3)}$$

Appendix B: Smoothing

The theory has been developed under the assumption that lateral permeability variations occur gradually. For computational reasons, as the program is a finite difference approach, each layer is discretized into blocks with homogeneous permeability so that permeability functions become a "step function". These steps are located at the inter-unit interfaces $x_{i+1/2}$. However, the lateral variation of the local-scale permeability should be sufficiently smooth to allow for the differentiations required by the theory presented in this paper. By differentiating these "step functions", a smoothing of the step is implicitly realized; this will be illustrated for the function Y(x) (see Figure A-IV.B1).

The smoothing of a function $Y(x)$ is given by:

$$\langle Y \rangle_{\Delta} (x) = \frac{1}{\Delta x} \int_{x-b}^{x+b} Y(x')\, dx' \qquad \text{(A-IV.b1)}$$

where b = Δx/2 and Δx is the width of the facies unit. In this way, $\langle Y \rangle_{\Delta}(x)$ is a continuous "roof" function with $\langle Y \rangle_{\Delta}(x_i) = Y(x_i)$, where x_i is the centre of the facies unit.

The derivative $\partial \langle Y \rangle_{\Delta}(x)/\partial x$, a discontinuous "step" function with its discontinuities at the unit centres x_i, is smoothed in the same way:

$$\left\langle \frac{\partial \langle Y \rangle_{\Delta}}{\partial x} \right\rangle_{\Delta} = \frac{1}{\Delta x} \int_{x-b}^{x+b} \frac{\partial \langle Y \rangle_{\Delta}}{\partial x'} dx' \qquad \text{(A-IV.b2)}$$

In this way, $\langle \partial \langle Y \rangle_{\Delta}(x)/\partial x \rangle_{\Delta}$ is a continuous "roof" function with:

$$\left\langle \frac{\partial \langle Y \rangle_{\Delta}(x)}{\partial x} \right\rangle_{\Delta} (x_{i+1/2}) = \left[\frac{\partial \langle Y \rangle_{\Delta}(x)}{\partial x} \right] (x_{i+1/2}) \qquad \text{(A-IV.b3)}$$

where $x_{i+1/2}$ is the location of the inter-unit interface. Differentiation of the first term of Eq. (A-IV.b3) leads to a discontinuous function:

$$\frac{\partial \left\langle \frac{\partial \langle Y \rangle_{\Delta}(x)}{\partial x} \right\rangle_{\Delta}}{\partial x} \qquad \text{(A-IV.b4)}$$

with the discontinuities at the inter-unit boundaries $x_{i+1/2}$.

This would mean that, numerically, a step function is first averaged, then the "smoothed" function is differentiated and finally integrated. In the theory, a smooth function is differentiated then integrated. Strictly speaking, this is not completely correct. However, if we consider that the step-function permeabilities result from discretizing lateral heterogeneities, thereby neglecting any intra-facies heterogeneity which is always present, it may be considered that a practical application of this procedure leads to correct results.

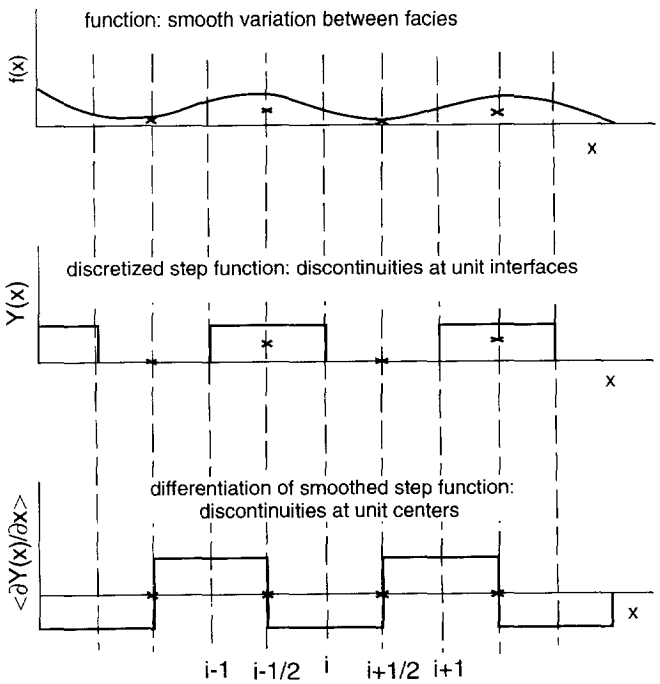

Fig A-IV.B1 *Diagram of differentiation and "smoothing" of a step function.*

Symbols

a	=	half grid-block width [m]
A	=	local-scale anisotropy factor [-]
c	=	hydraulic resistance function [m^{-1}]
d	=	grid-block depth [m]
E_{ii}	=	relative correction to the zeroth order approximation of component k_{ii} of the permeability tensor [-]
g	=	gravitational acceleration [$m \cdot s^2$]
$\underline{k}$	=	intrinsic permeability tensor [m^2]
k_h	=	local-scale permeability component in x-direction [m^2]
k_v	=	local-scale permeability component in z-direction [m^2]
k_1	=	local-scale permeability of well-conducting facies unit [m^2]
k_2	=	local-scale permeability of poorly-conducting facies unit [m^2]
$<k_{xx}>$	=	depth-averaged component of intrinsic permeability tensor in x-direction due to potential gradient in x-direction [m^2]
$<k_{xz}>$	=	depth-averaged component of intrinsic permeability tensor in x-direction due to potential gradient in z-direction [m^2]
$<k_{zx}>$	=	depth-averaged component of intrinsic permeability tensor in z-direction due to potential gradient in x-direction [m^2]
$<k_{zz}>$	=	depth-averaged component of intrinsic permeability tensor in z-direction due to potential gradient in z-direction [m^2]
q_x	=	flux component in x-direction [$m.s^{-1}$]
q_z	=	flux component in z-direction [$m.s^{-1}$]
t	=	transmissivity function [m^3]
x	=	horizontal component of position vector [m]
z	=	vertical component of position vector [m]
α	=	function [m]
β	=	function [m]
Δx	=	width of facies unit [m]
Δz	=	depth of facies unit [m]
μ	=	dynamic viscosity of the fluid [Pa·s]
ρ	=	fluid density [$kg.m^{-3}$]
ϕ	=	potential [Pa]
ψ	=	first-order correction term [-]

superscripts

'	first-order perturbation terms
"	first-order correct solution for c and t

operators

< >	depth-averaging [-]
<< >>	block-averaging [-]

References

Abbot, M.B.; Bathurst, J.C.; Cunge, J.A.; O'Connell, P.E. and Rasmussen, J., 1986a, An introduction to the European Hydrological System - Système Hydrologique Européen, "SHE", I: history and philosophy of a physically-based, distributed modelling system. Journal of Hydrology, v. 87, p.45-59.

Abbot, M.B.; Bathurst, J.C.; Cunge, J.A.; O'Connell, P.E. and Rasmussen, J., 1986b, An introduction to the European Hydrological System - Système Hydrologique Européen, "SHE", II: structure of a physically-based, distributed modelling system. Journal of Hydrology, v. 87, p.61-77.

Abramowitz, M. and Stegun, I., 1972, Handbook of mathematical functions, Dover Publications Inc., New York.

Ahlbrandt, T.S., 1974, The source of sand for the Killpecker sand-dune field, Southwestern Wyoming, Sedimentary Geology, v. 11 p. 34-57.

Ahlbrandt, T.S., 1979, Textural parameters of eolian deposits, in E.D. McKee, (Ed.), A study of global sand seas, Geological Survey Professional Paper 1052, Washington 1979, p. 21-51.

Allen, J.R.L., 1969, The paths of grains through wave-like bedforms, Geologie en Mijnbouw, v. 48(1), p.3-8.

Allen, J.R.L., 1984, Sedimentary structures their character and physical basis, Developments in Sedimentology, v 30 A and B, Elsevier, The Netherlands;

Anderson, R.S., 1987, A theoretical model for aeolian impact ripples, Sedimentology, v. 34, p. 943-956.

Anderson, R.S., 1988, The pattern of grainfall deposition in the lee of aeolian dunes, Sedimentology, v. 35, p.175-188.

Anderson, R.S., 1990, Eolian ripples as examples of self-organization in geomorphological systems, Earth Sciences Reviews, v. 29, p. 77-96.

Anderson, R.S., and Haff, P.K., 1988, Simulation of eolian saltation, Science; v. 241, p. 761-876.

Anderson, R.S., and Haff, P.K., 1991, Wind modification and bed response during saltation of sand in air, Acta Mechanica [Suppl] I, p.21-52.

Anderson, R.S., Sørensen, M and Willets, B.B., 1991, A review of recent progress in our understanding of aeolian sediment transport, Acta Mechanica [Suppl] I, p.1-20.

Arens, S.M., 1994, Aeolian processes in the dutch foredunes, Thesis University of Amsterdam.

Bagnold, R.A., 1941, The physics of blown sands and desert dunes, London. Methuen.

Bathurst, J.C., 1986a, Physically-based distributed modelling of an upland catchment using the Système Hydrologique Européen. Journal of Hydrology, v. 87, p.79-102.

Bathurst, J.C., 1986b, Sensitive analysis of the Système Hydrologique Européen for an upland catchment. Journal of Hydrology, v. 87, p.103-123.

Begg, S.H. and King, P.R., 1985, Modelling the effects of shales on reservoir performance: calculation of effective vertical permeability, Society of Petroleum Enginers Paper 13529.

Borówka, R., 1980, Present day dune processes and dune morphology on the Leba Barrier, polish coast of the Baltic. Geografiska Annaler, 62 A, p. 75-82.

Bradley, E.F., 1980, An experimental study of the profiles of wind speed, shearing stress and turbulence at the crest of a large hill, Quarterly Journal of the Royal Meteorological Society, v. 106, p.101-123.

Bridge, J.S. and Leeder, M.R., 1979, A simulation model of alluvial stratigraphy, Sedimentology, v. 26, p.617-644.

Brookfield, M.E., 1977, The origin of bounding surfaces in ancient aeolian sandstones: Sedimentology, v. 24, p. 303-332.

Cardwell, W.T., and Parsons, R.L., 1945, Average permeabilities of heterogeneous oil sands. Transactions of the American Institute of Mining, Metallurgy and Petroleum Engineering, p. 34-42

Chandler, M.A., Kocurek, G., Goggin, D.J. and Lake, L.W., 1989, Effects of stratigraphic heterogeneity on permeability in eolian sandstone sequence, American Association of Petroleum Geologists Bulletin, v. 73 (5), p. 658-668.

Clemmensen, L.B. and Abrahamsen, K., 1983, Aeolian stratification and facies association in desert sediments, Arran Basin (Permian), Scotland. Sedimentology, v. 30, p.311-339.

Clemmensen, L.B. and Blakey, R.C., 1989, Erg deposits in the Lower Jurassic Wingate Sandstone, Northeastern Arizona: oblique dune sedimentation, Sedimentology, v. 36, p. 449-470.

Cooke, R., Warren, A., Goudie, A., 1993, Desert geomorphology, UCL Press, London.

Dagan, G., 1989, Flow and transport in porous formations. Springer-Verlag.

Doe, T.W. and Dott, R.H., 1980, Genetic significance of deformed cross-bedding - with examples from the Navajo and Weber sandstones, Utah, Journal of Sedimentary Petrology, v.50, n. 3, p. 793-812.

Dubrule, O., 1989, A review of stochastic models for petroleum reservoirs, in: M. Armstrong (Ed.), Geostatistics II, Kluwer Academic Publishers, Dordrecht, p.493-506.

Ferziger, J.H., 1981, Numerical methods for engineering applications, John Wiley and Sons, United States of America, 1981.

Fisher, P.F. and Galdies, P., 1988, A computer model for barchan-dune movement, Computers & Geoscience, v. 14, n. 2, p. 229-253.

Fogg, G.E., 1986, Groundwater flow and sand body interconnectedness in a thick, multiple-aquifer system. Water Resources Research, May 1986, v. 22, no.5. p. 679-694.

Freeze, R.A., 1975, A stochastic-conceptual analysis of one-dimensional groundwater flow in nonuniform homogeneous media. Water Resources Research, October 1975, v. II, no.5. p. 725-741.

Fryberger, S.G., 1979, Dune forms and wind regime, in E.D. McKee , (Ed.), A study of global sand seas, Geological Survey Professional Paper 1052, Washington 1979, p. 137-169.

Fryberger, S.G., Al-Sari, A.M., Clisham, T.J., 1983, Eolian dune, interdune, sand sheet, and siliciclastic sabkha sediments of an offshore prograding sand sea, Dhahran Area, Saudi Arabia, American Association of Petroleum Geologists Bulletin , v. 67, n. 2, p. 280-312.

Fryberger, S.G., Al-Sari, A.M., Clisham, T.J., Rizvi, S.A. and Al-Hinai, K.G., 1984, Wind sedimentation in the Jafurah sand sea, Saudi Arabia, Sedimentology, v. 31, p.413-431.

Fryberger, S.G. and Schenk, C.J., 1981, Wind sedimentation tunnel experiments on the origins of aeolian strata, Sedimentology v. 28, p. 805-821.

Gelhar, L.W., 1986, Stochastic subsurface hydrology, from theory to application. Water Resources Research, August, 1986, v. 22, n. 9. p. 135S-145S.

Glenn, M., 1979, Glossary, in E.D. McKee , (Ed.), A study of global sand seas, Geological Survey Professional Paper 1052, Washington 1979, p. 399-407.

Glennie, K.W., 1970, Desert sedimentary environments, developments in sedimentology no.14, Elsevier Publishing Companny, Amsterdam, 1970.

Glennie, K.W., 1982, Early Permian (Rotliegendes) paleowinds of the North Sea. Sedimentary Geology, v. 34, p. 245-265.

Glennie, K.W, 1984, Lower Permian - Rotliegend, in Glennie, K.W, (Ed.), Introduction to the petroleum geology of the North Sea, Blackwell Scientific Publications, Oxford 1984, p. 120-152.

Goggin, D.J., Chandler, M.A., Kocurek, G. and Lake, L.W., 1988, Patterns of permeability in eolian deposits: Page Sandstone (Jurassic), Northeastern Arizona, SPE Formation Evaluation, June 1988.

Gong, W. and Ibbetson, A., 1989, A wind tunnel study of turbulent flow over model hills, Boundary-layer Meteorology, v.49, p. 113-148.

Haldorsen, H.H., and Lake, L.W., 1984, A new approach to shale management in field scale models. Society of Petroleum Engineers Journal, August 1984, p.447-457.

Havholm, K.G. and Kocurek, G., 1988, A preliminary study of the dynamics of a modern draa, Algodones, Southeastern California U.S.A., Sedimentology, v. 35, p. 644-669.

Horikawa, K.; Shintaro, K. and Sadakazu, K., 1983, On the sand transport rate by wind on a beach, Coastal Engineering in Japan, v. 26, p.101-120.

Howard, A.D., Morton, J.B., Gad-El-Hak, M. and Pierce, D.B., 1978, Sand transport model of barchan dune equilibrium, Sedimentology, v. 25, p. 307-338.

Howard, A.D. and Walmsley, J.L., 1985, Simulation model of isolated dune sculpture by wind, in Bandorff-Nielsen, O.E., Moller, J.T., Rasmussen, K., and Willets, B.B. (Eds.), International workshop on the physics of blown sand, proceedings, Aarhus, May 28-31 1985. Department of Theoretical Statistics, Institute of Mathematics, University of Aarhus, Memoire 8.

Hsu, S.A., 1971, Wind stress criteria in eolian sand transport, Journal of Geophysical Research, v. 26, n. 36, p. 8684-8686.

Hsu, S.A., 1973, Computing eolian sand transport from shear velocity measurements, Journal of Geology, v. 81, p. 739-743.

Hunt, J.C.R., Leibovich, S. and Richards, K.J., 1988, Turbulent shear flows over low hills, Quarterly Journal of the Royal Meteorological Society, v. 114, p. 1435-1470.

Hunter, R.E., 1977, Basic types of stratification in small eolian dunes, Sedimentology, v. 24, p. 361-387.

Hunter, R.E., 1985, A kinematic model for the structure of lee-side deposits, Sedimentology, v. 32, p. 409-422.

Illenberger, W.K. and Rust, I.C., 1988, A sand budget for the Alexandria coastal dunefield, South Africa., Sedimentology, v.35, p.513-521.

Jackson, P.S. and Hunt, J.C.R., 1975, Turbulent wind flow over a low hill, Quarterly Journal of the Royal Meteorological Society, v. 101, p. 929-955.

Jacquin, C.G. and Adler, P.M., 1987, Fractal porous media II: Geometry of porous geological structures. Transport in Porous Media 2, p. 571-596.

Journel, A.G. and Huijbregts, Ch. J., 1989, Mining Geostatistics. Academic Press.

Kasap, E. and Lake, L.W., 1990, Calculating the effective permeability tensor of a grid block. Society of Petroleum Engineers Formation Evaluation, June 1990

Kennedy, J.F., 1969, The formation of sediment ripples, dunes and antidunes, Annual review of Fluid Mechanics, 1969, p. 147-168.

Kerr, D.R. and Dott, R.H. Jr., 1988, Eolian dune types preserved in the Tensleep Sandstone (Pennsylvanian-Permian), North-Central Wyoming, Sedimentary Geology, v. 56, p. 383-402.

King, P.R., 1989, The Use of renormalization for calculating effective permeability. Transport in Porous Media, no. 4, p.37-58.

Kocurek, G., 1981, Significance of interdune deposits and bounding surfaces in aeolian dune sands, Sedimentology, v. 28 p. 753-780.

Kocurek, G. and Dott, R.H., 1981, Distinctions and uses of stratification types in the interpretation of eolian sand, Journal of Sedimentary Petrology, v. 51, no. 2, p. 579-595.

Kocurek, G., 1988, First-order and super bounding surfaces in eolian sequences- bounding surfaces revisited, Sedimentary Geology, v. 56, p. 193-206.

Kocurek, G., Townsley, M., Yeh, E., Havholm, K., Sweet, M.L., 1992, Dune and dune-field development on Padre Island, Texas, with implications for interdune deposition and water-table-controlled accumulation. Journal of Sedimentary Petrology, v. 64 n. 4, July 1992, p.622-635.

Kolm, K.E., 1982, Predicting the surface wind characteristics of Southern Wyoming from remote sensing and eolian geomorphology, in Marrs, R.W. and Kolm, K.E. (Eds.) Interpretation of windflow characteristics from eolian landforms, Geological Society of America Special Paper 192.

Koltermann, C.E. and Gorelick, S.M., 1992, Paleoclimatic signature in terrestrial flood deposits, Science, v. 256, p. 1775-1782.

Lancaster, N., 1985, Variations in wind velocity and sand transport on the windward flanks of desert sand dunes, Sedimentology, v.32 p.581-593.

Lancaster, N., 1988, Controls of eolian dune size and spacing, Geology, v.16 p.972-975.

Lettau, K. and Lettau, H., 1977, Experimental and micro-meteorological field studies of dune migration, in Lettau, K. and Lettau, H., (Eds.) Exploring the world's driest climate, University of Wisconsin, Madison.

Long. J.T. and Sharp, R.P., 1964, Barchan-dune movement in Imperial Valley, California, Geological Society of America Bulletin, v. 75 , p. 149-156.

Mason, P.J. and Sykes, R.L., 1979, Flow over an isolated hill of moderate slope, Quarterly Journal of the Royal Metereological Society, v. 105, p. 383-395.

McEwan, I.K. and Willets, B.B., 1991, Numerical model of the saltation cloud, Acta Mechanica [Suppl] I; p.123-134.

McLean, S.R., 1990, The stability of ripples and dunes, Earth-Science reviews, n.29, p. 131-144.

Mikkelsen, H.E., 1989, Wind flow and sediment transport over a low coastal dune, Geoskrifter nr. 32, Geologisk Institut Aarhus Universiteit.

Mijnssen, F.C.J., Weber, K.J., Floris, F.J.T. and Kaasschieter, E.F., 1990, Relating sedimentology to production behaviour in deltaic rocks. Society of Petroleum Engineers Paper 20946.

Mulligan, K.R., 1988, Velocity profiles measured on the windward slope of a transverse dune, Earth Surface Processes and Landforms, v. 13, p. 573-582.

Nickling, W.G., 1988, The initiation of particle movement by wind, Sedimentology, v. 35, p.499-511.

O'Brien, M.P. and Rindlaub, B.D., 1936, The transportation of sand by wind, Civil Engineering, v. 6 n.5, May 1936.

Press, W.H., Flannery, B.P., Teukolsky, S.A., and Vetterling, W.T., 1988, Numerical recipes in C, the art of scientific computing, Cambridge University Press, Cambridge, 1988.

Pugh, J.M., Glennie, K.W. and Williams, B.P., 1993, Three-dimensional modeling of an aeolian dune/interdune system: applications to hydrocarbon

production, Poster abstract for the AAPG International Conference, The Hague, October 1993.

Quintard, M., and Whitaker, S., 1987, Ecoulement monophasique en milieux poreux: effet des héterogénëités locales; Journal de Mécanique Théorique et Appliquée, v.6, no.5, p.691-726.

Reading, H.G. (Ed.), 1986, Sedimentary environments and facies, 2° edition. Blackwell Scientific Publications, Oxford.

Rikitake, T., Sato, R. and Hagiewara, Y., 1987, Applied mathematics for earth scientists, Terra Scientific Publishing Company, Tokyo, (1987).

Rubin, D.M., 1987, Cross-bedding, bedforms and paleocurrents. SEPM Concepts in sedimentology and paleontology, Volume I.

Rubin, D.M. and Hunter, R.E., 1982, Bedform climbing in theory and in nature, Sedimentology, v. 29, p.121-138.

Rubin, D.M. and Ikeda, H., 1990, Flume experiments on the alignement of transverse, oblique and longitudinal dunes in directionally varying flows, Sedimentology, v. 37, p. 673-684.

Rumpel, D.A., 1985, Successive aeolian saltation: studies of idealized collisions, Sedimentology, v. 32, p. 267-280.

Sarre, R.D., 1988, Evaluation of aeolian sand transport equations using intertidal zone measurements, Saunton Sands, England, Sedimentology, v. 35, p. 671-679

Selley, R.C., 1978, Ancient sedimentary environments, Chapman and Hall, London

Slatyer, R.O. and Mabbutt, J.A., 1964, Hydrology of arid and semi-arid regions, in Ven Te Chow (Ed.), Handbook of applied hydrology, McGraw-Hill Book Company, U.S.A., 1964.

Stam, J.M.T., Zijl,W. and Turner, A.K., 1989, Determination of hydraulic parameters from the simulation of alluvial stratigraphy, proceedings of the fourth international conference on computational methods and experimental measurements, Capri (Italy), May 1989, p.383-466

Stam, J.M.T. and Zijl, W., 1992, Modelling permeability in imperfectly layered porous media II: a two-dimensional application of block-scale permeability, Mathematical Geology, v.24, n.8, p.885-904.

Stam, J.M.T., Zijl, W. and van Dam, J.C., 1993, Proces gebaseerd modelleren van de ondergrond; een instrument voor het bepalen van stromingsparameters, H_2O v. 26, n. 8, p.216-220

Stokes, W.M.L., 1968, Multiple parallel-truncation bedding planes, a feature of wind-deposited sandstone formations, Journal of Sedimentary Petrology, v, 38, n. 2, p. 510-515

Stuyfzand, P.J., 1984, Hydrochemie en hydrologie van het duingebied tussen Egmond en Wijk aan Zee, KIWA Report SWE-85.012.

Svasek, J.N. and Terwind, J.H.J., 1974, Measurements of sand transport by wind on a natural beach, Sedimentology 21, p.311-322

Sweet, M.L., Nielson, J.; Havholm, K. and Farrelley, J., 1988, Algodones dune field of Southeastern California: a case history of a migrating modern dune field, Sedimentology 35, p.939-952.

Sweet, M.L. and Kocurek, G., 1990, An empirical model of aeolian dune lee-face airflow, Sedimentology, v. 37 p.1023-1038.

Talbot, M.R., 1985, Major bounding surfaces in aeolian sandstones - a climatic model, Sedimentology, v. 32, p. 257-265.

Tetzlaff, D.M. and Harbaugh, J.W., 1989, Simulating clastic sedimentation. Computer methods in the geosciences, Van Nostrand Reinhold, New York.

Van Veen, F.R., 1975, Geology of the Leman Gas field, in A.W. Woodland (Ed.), Petroleum and the continental shelf of Northwest Europe, London, Applied Science Publication, v. 1, p. 223-232.

Visser, W.A. (Ed.), 1980, Geological nomenclature, Royal Geological and Mining Society of the Netherlands, Martinus Nijhoff, The Hague.

Walmsley, J.L., Salmon, J.R. and Taylor, P.A., 1982, On the application of a model boundary-layer flow over low hills to real terrain, Boundary Layer Meteorology, v, 23, p. 17-46.

Warren, J.E., and Price, H.S., 1961, Flow in Heterogeneous Porous Media. Society of Petroleum Engineers, Sept. 1961, p.153-169

Weber, K.J., 1986, How heterogeneity affects oil recovery, in L.W. Lake and H.B. Carroll (Eds.), Reservoir characterization, Orlando Academic Press, p. 487-544.

Weber, K.J., 1987, Computation of initial well productivities in aeolian sandstone on the basis of a geological model, Leman Gas Field, U.K., in Tillman, R.W. and Weber, K.W. (Eds.) Reservoir Sedimentology, Tulsa, Society of Economic Paleontologists and Mineralogist Special Publication, n. 40, p.333-354.

Weber, K.J., and Van Geuns, L.C., 1990, Framework for constructing clastic reservoir simulation models. Journal of Petroleum Technology, Oct. 1990, p.1248-1297.

Weng, W.S., Hunt, J.C.R., Carruthers, D.J., Warren, A., Wiggs, G.F.S., Livingstone, I. and Castro. I., 1991, Air flow and sand transport over sand-dunes. Acta Mechanica [Suppl] 2, p.1-22.

Werner, B.T. and Haff, P.K., 1988, The impact process in aeolian saltation: two-dimensional simulations, Sedimentology, v. 35, p.189-196.

Whitaker, S., 1986, Flow in Porous Media I: A theoretical derivation of Darcy's law. Transport in Porous Media, v. 1 no.1, pp.3-25.

White, B.R., 1979, Soil transport by wind on Mars, Journal of Geophysical Research, August 10, v. 84 n.B9, p. 4643-4651.

White, C.D. and Horne, R.N., 1987, Computing absolute transmissibility in the presence of fine-scale heterogeneity. Society of Petroleum Engineers Paper 16011.

Willets, B.B., McEwan, I.K. and Rice, M.A., 1991, Initiation of motion of quartz sand grains, Acta Mechanica [Suppl] I; p.123-134.

Williams, G., 1964, Some aspects of the eolian saltation load, Sedimentology, v. 3, p. 257-287.

Williams, J.J., Buttersfield, G.R. and Clark, D.G., 1990, Rates of aerodynamic entrainment in a developing boundary layer, Sedimentology, v. 37, p.1039-1048.

Wilson, I.G., 1972, Aeolian Bedforms - Their development and origins, Sedimentology, v. 19, p.173-210.

Wipperman, F.K. and Gross, G., 1986, The wind-induced shaping and migration of an isolated dune: a numerical experiment, Boundary Layer Meteorelogy, v. 36 p.319-334.

Yang, C.S. and Nio, S.D., 1993, Application of high resolution sequence stratigraphy to the Upper Rotliegend in the Netherlands offshore, American Association of Petroleum Geologists Special Publication.

Zijl, W. and Stam, J.M.T., 1992, Modelling permeability in imperfectly layered porous media I: derivation of block-scale permeability tensor for thin grid blocks, Mathematical Geology, v. 24, n.8., p. 865-883

Summary

The general framework of this thesis is to develop simulation models of the physics of sedimentation processes, and to use them to reconstruct subsurface heterogeneities for fluid-flow simulations. The final goal is to apply these models in the exploitation and management of oil and gas reservoirs and groundwater aquifers. As a step towards this goal, this research focuses on the aeolian environment and treats the dynamics of dunes as a result of the interaction of wind and topography.

A literature review has been given of the most important studies on the aeolian environment and of the mathematical models published up to date (Chapter 2). An overview has also been given of the basic equations and of the fluid-dynamic aspects that play a role in the problem (Chapter 3). The basic equation that governs dune dynamics is the sediment-continuity equation. To solve the sediment-continuity equation, expressions need to be found for the variation of the wind velocity over a dune and for the sediment transport. By making some simplifying assumptions, solutions are obtained that show the migration and deformation of bedforms (chapter 4). These solutions help to assess the relative importance of the fluid-dynamic model and of the sediment-transport equation.

A two-dimensional model that simulates dune dynamics has been developed by combining an analytical boundary-layer model by Jackson and Hunt (1975),with Bagnold's (1941) sediment-transport formula (chapter 5). By linearizing the sediment-transport formula, analytical expressions have been developed for: the shear stress, the sediment transport, the sediment deposition, the topography and for the growth and migration of a sine-shaped dune through time. These expressions show that migration and growth are higher for higher wind velocities, higher surface roughness (with a constant shear stress), and higher wave numbers (i.e. shorter wave lengths).

A computer programme (EOLSIM) has been developed to apply this model to non-sinusoidal dunes (by means of a Fast Fourier Transform of the topography). The major problem herein is the exponential growth of the high wave numbers of the Fourier Transform of the topography. This causes the higher wave numbers to dominate the topography so that it becomes unstable. This implies that more aspects play a role in bedform stability. One of these aspects is avalanching, which occurs when the slope becomes too steep. This has been examined by developing an avalanching

routine for EOLSIM. The routine is based on geometric assumptions. The results indicate that avalanching limits bedform growth so that dunes migrate in equilibrium (i.e. maintaining their shape). Therefore it can be concluded that avalanching has a key role in bedform stability.

Chapter 7 contains the conclusions of this study and also gives some recommendations for further consideration. The conclusions are related to the model and the parameters used and also the actual results of the work. They can be summarized as follows: a) bedform growth is caused by a phase shift between the shear stress of the wind and the topography; b) migration and growth are higher for higher wind velocities, higher surface roughness, and higher wave numbers; c) smaller wave lengths have higher migration and growth rates; d) avalanching is an important process that limits bedform growth so that it migrates in equilibrium. The recommendations for further research are related to: a) improvements of the model; b) studies to determine the accuracy of the flow model; c) recommendations for experimental measurements in the field; d) model extensions to simulate the structure of aeolian deposits.

Samenvatting

Het algemene kader waar dit onderzoek in past is het ontwikkelen van simulatie modellen voor de fysica van sedimentaire processen, met als uiteindelijk doel de reconstructie van de ruimtelijke variabiliteit van de ondergrond. Dergelijke modellen kunnen hun toepassing vinden by de simulatie van vloeistofstroming van olie, gas en grondwater. Als een stap naar dit uiteindelijk doel richt dit onderzoek zich op het aeolisch milieu, en in het bijzonder op de dynamiek van duinen als gevolg van de interactie tussen wind en topografie.

Hoofdstuk 2 omvat een literatuur overzicht van studies en mathematische modellen over het aeolisch milieu. In hoofdstuk 3 wordt een overzicht gegeven van de fundamentele vergelijkingen en van de stromingsaspecten die hierbij een rol spelen. De belangrijkste vergelijking die het systeem beschrijft is de sediment-continuiteits vergelijking. Om deze op te lossen zijn uitdrukkingen nodig voor de variatie van de windsnelheid over de topografie, en voor het sediment transport. Door hiervoor eenvoudige veronderstellingen te maken, worden oplossingen verkregen die de migratie en asymmetrie van duinen verklaren (hoofdstuk 4). Deze oplossingen dienen onder meer, om het belang van het stromingsmodel ten opzichte van de sediment transport formule te bepalen.

Een twee-dimensionaal model is ontwikkeld door een analytisch grenslaag stromingsmodel van Jackson en Hunt (1975) met de sediment transport formule van Bagnold (1941) te combineren (hoofdstuk 5). Door linearisatie van de transport formule zijn analytische vergelijkingen verkregen voor: de schuifspanning van de wind, het sediment transport, de erosie en depositie, de topografie en voor de groei en migratie van een sinus-vormig duin. Deze uitdrukkingen tonen aan dat de migratie snelheid en de groei groter zijn voor hogere windsnelheden, grotere oppervlakte ruwheid (onder een constante schuifspanning) en grotere golfgetallen (kleinere golflengten).

Om dit model te kunnen toepassen op duinen van willekeurige vorm (door middel van een Fourier transformatie van de topografie), is in hoofdstuk 6 een computer programma ontwikkeld (EOLSIM). Het grootste probleem hierbij is de exponentiële groei van hogere golfgetallen van de Fourier getransformeerde van de topografie. Hierdoor overheersen de hoogste golfgetallen de topographie en wordt

deze instabiel. Dit duidt er op dat er ook andere aspecten zijn die een rol spelen in de stabiliteit en het evenwicht van duinen. Behalve de aspecten die betrekking hebben op de vloeistofmechanica en het sediment transport is een van de belangrijkste processen de afschuiving. Afschuiving van het sediment gebeurt als het talud van een duin te steil wordt. Dit is verder uitgewerkt door een afschuivingsroutine in het model op te nemen. Deze routine is gebaseerd op geometrische aannamen. De resultaten laten zien dat afschuiving de groei van duinen beperkt en het is dus duidelijk dat dit proces een belangrijke rol speelt bij het evenwicht en de stabiliteit van duinen.

Hoofstuk 7 bevat de conclusies van dit onderzoek alsmede aanbevelingen voor voortzetting van deze studie. Deze conclusies hebben betrekking op de geschiktheid van het model en van de parameters die hierin worden gebruikt, alsmede op de resultaten ervan. De voornaamste conclusies zijn: a) de groei van duinen wordt veroorzaakt door het faseverschil tussen de schuifspanning van de wind en de topografie; b) de migratie snelheid en de groei zijn groter voor hogere windsnelheden, oppervlakte ruwheid, en golfgetallen; c) kleinere golflengten hebben een hogere migratiesnelheid en groei; d) het afglijdingsproces beperkt de groei van een duin zodat dit zich in evenwicht verplaatst (dat wil zeggen met behoud van zijn vorm). De aanbevelingen voor de voortzetting van deze studie hebben betrekking op: a) de verbetering van het model; b) het bepalen van de nauwkeurigheid van het stromingsmodel; c) het uitvoeren van veldmetingen d) uitbreiding van het model om ook de structuur van eolische afzettingen te kunnen simuleren.

Resumen

El objetivo general de esta tesis es desarrollar modelos que reproduzcan la física de los procesos de sedimentación, con el fin de simular la heterogeneidad del subsuelo. Dichos modelos tienen aplicación directa en el cálculo de flujo subterráneo. Esta tesis se centra en el ambiente de depositación eólico, y más concretamente en el estudio de la dinámica de dunas como consecuencia de la interacción entre el viento y la topografía.

En el capítulo 2, se ha hecho un resumen de los estudios descriptivos y de los modelos matemáticos publicados hasta la fecha. Sigue un resumen de las ecuaciones básicas que definen el problema y de los principios de la dinámica de fluídos relativos al tema (capítulo 3). La ecuación básica que describe el sistema es la ecuación de la conservación de masa. Para resolverlo hacen falta modelos para la variación de la velocidad del viento con la topografía y para el transporte del sedimento. Haciendo simplificaciones en estas expresiones, se obtienen soluciones que describen la velocidad de migración y la asimetría de una duna. Dichas soluciones sirven para comprender la importancia del modelo de flujo con respecto a la ecuación del transporte del sedimento.

Se ha desarollado un modelo bidimensional combinando un modelo analítico de flujo en la capa límite (de Jackson y Hunt, 1975), con la fórmula de Bagnold (1941) para el tranporte del sedimento (capítulo 5). Linearizando la fórmula del trasporte, se consiguen expresiones para el esfuerzo de cizalla, el transporte de sedimentos, la depositación, la erosión, la topografía y para el crecimiento y la velocidad de migración de una duna sinusoidal. Estas expresiones señalan que el crecimiento y la migracion aumentan con la velocidad del viento, la rugosidad de la superficie (con un esfuerzo de cizalla constante) o el número de onda (es decir, disminuye con la longitud de la onda).

Un programa de ordenador (EOLSIM) ha sido desarrollado para applicar estas expresiones a dunas no sinusoidales (mediante una transformación de Fourier). El mayor problema es el crecimiento exponencial de los componentes de alto número de onda de la transformada Fourier de la topografía. Esto hace que los números de onda mas altos dominen la topografía, provocando la inestabilidad del sistema. Esto indica que hay más procesos que juegan un papel en el

equilibrio de dunas. Uno de estos procesos es el deslizamiento de la arena cuando la pendiente de la duna sobrepase un cierto límite. Para modelar este proceso se ha desarrollado una rutina para calcular el deslizamiento, basado en suposiciones geométricas. Los resultados señalan que el deslizamiento limita el crecimiento de las dunas de forma que éstas se desplazan en equilibrio (es decir, manteniendo su forma).

En el capítulo 7 vienen las conclusiones y recomendaciones de esta investigación, referentes tanto al modelo y sus parámetros, como a los resultados. Como conclusiones principales podemos señalar que: a) el crecimiento de las dunas se debe a un desfase entre el esfuerzo de cizalla del viento y la topografía; b) la velocidad de migración y de crecimiento aumentan con la velocidad del viento, con la rugosidad de la superficie o con el número de onda; c) cuanto más pequeño el número de onda mayor el crecimiento d) el deslizamiento limita el crecimiento de las dunas con lo cual surge un equilibrio y éstas migran sin cambiar de forma. Las recomendaciones se relacionan con: a) mejorías del modelo; b) comprobación de la exactitud del modelo de flujo; c) realización de medidas en el campo y d) ampliaciones del modelo para simular las estructuras de depositaciones eólicas.

Curriculum vitae

The author was born on the 7th of August 1966, in Madrid (Spain). After receiving primary education at English and French schools, she obtained her secondary education at the "Colegio San Estanislao de Kostka" in Madrid, obtaining the degrees for the Bachillerato Unificado y Polivalente (B.U.P.) in 1983, and for the Curso de Orientación Universitaria (C.O.U.) and the International Baccalaureate in 1984.

In September 1984 she started to study Civil Engineering at the Delft University of Technology, obtaining her first-year degree (Propadeuse) in 1985. The third-year specialization was chosen in hydrology and hydraulic engineering. From September 1987 to September 1989 she worked as a student-assistant for the Hydrology Section. The graduation work was done for the TNO Institute of Applied Geoscience, under the supervision of Prof. Dr ir J.C. van Dam and Prof. Dr ir W. Zijl, together with Prof. Dr A.K. Turner of the Colorado School of Mines. The subject was developing methods for averaging subsurface permeabilities of simulated alluvial stratigraphies. The degree of Civil Engineer was obtained in October 1989.

In January 1990 a research project was started at the Faculty of Mining and Petroleum Engineering of the Delft University of Technology, which resulted in this thesis. The research was carried out for the TNO Institute of Applied Geoscience and supervised by Prof. Dr ir J.C. van Dam, Prof. drs F.R. van Veen and Prof. Dr ir W. Zijl. An important part of the research was conducted at the Geomathematics Group of the Department of Applied Earth Sciences of Stanford University (California-U.S.A.), under Prof. Dr J.W. Harbaugh.